BALLISTIC EVALUATION OF CARBON NANOTUBE SHEET MATERIAL IN MULTIFUNCTIONAL APPLICATIONS

THESIS

Casey M. Keilbarth, 1st Lt, USAF

AFIT-ENY-MS-19-M-224

DEPARTMENT OF THE AIR FORCE
AIR UNIVERSITY

AIR FORCE INSTITUTE OF TECHNOLOGY

Wright-Patterson Air Force Base, Ohio

AFIT-ENY-MS-19-M-224

BALLISTIC EVALUATION OF CARBON NANOTUBE SHEET MATERIAL IN MULTIFUNCTIONAL APPLICATIONS

THESIS

Presented to the Faculty

Department of Aeronautics and Astronautics

Graduate School of Engineering and Management

Air Force Institute of Technology

Air University

Air Education and Training Command

in Partial Fulfillment of the Requirements for the

Degree of Master of Science in Aeronautical Engineering

Casey M. Keilbarth, B.S.

1st Lt, USAF

March 21, 2019

AFIT-ENY-MS-19-M-224

BALLISTIC EVALUATION OF CARBON NANOTUBE SHEET MATERIAL IN MULTIFUNCTIONAL APPLICATIONS

THESIS

Casey M. Keilbarth, B.S.
1st Lt, USAF

Committee Membership:

Maj Andrew Lingenfelter, PhD
Chair

Dr. Max Alexander, PhD
Member

Ms. Brittany Cambell
Member

Maj Ryan Kemnitz, PhD
Member

Maj Ryan O'Hara, PhD
Member

AFIT-ENY-MS-19-M-224

Abstract

Significant development of carbon nanotubes has occurred since they were first studied in the 1990's. Attempts to capture the phenomenal molecular properties in practical applications are gaining ground as new methods of producing CNTs have been developed. This thesis sought to determine if the addition of commercially produced CNT sheets to thin carbon fiber panels improved the ballistic properties of the panel. The difference between 0 and 4 CNT sheets was studied. The hypothesis was that integrating CNT sheets into the laminate would increase the projectile energy absorbed by the panel and reduce the damage to the panel incurred by the impact. Damage to the panel was assessed through delamination area and EMI shielding degradation. Projectile energy absorption was measured through residual velocity measurement and ballistic limit modeling. A gas gun shooting half inch steel ball bearings simulated high-speed debris impact on the panel. This study found that the addition of one or two CNT sheets provided a marginal increase of up to 0.7 joules of projectile energy reduction by the panel. In general it was not found that the CNT sheets significantly contributed to the ability of the panel to stop a projectile at the quantities studied. It was found that with four CNT sheets in the panel, the EMI shielding after impact at 350 ft/s was improved by as much as 40 dB compared to the panel with no CNT sheets.

Acknowledgements

This project was made possible by collaboration with the Air Force Research Lab Materials and Manufacturing Directorate through the Integrated Master's Degree Program. I didn't expect all the challenges associated with this program, but have worked to optimize the opportunities made possible through it, such as an extended timeline and access to a wider pool of talent to make this project a reality. In particular I would like to thank my advisor and thesis committee for guiding me through this project. I would also like to thank the System Support Branch for their expertise and assistance in processing the composite panels, preparing tensile specimens, conducting the ultrasonic scans of the panels and advising on matters of non-destructive inspection (NDI). Researchers in the Composite Materials Branch were of great assistance with autoclave preparation and operation in addition to analyzing panel composition. They were also instrumental in conducting the EMI shielding effectiveness testing. I would be remiss to not thank my fellow students who collaborated with me in researching the CNT material and conducting ballistic testing. Finally I would like to thank God and my family and friends who have led me to this milestone and have supported and encouraged me throughout this project.

Casey M. Keilbarth

Table of Contents

Page

Abstract iv

Acknowledgements v

List of Figures viii

List of Tables xiv

List of Abbreviations xvi

I. Introduction 1

1.1 Background 1
Carbon Nanotube History and Properties 1
Bulk Property Characteristics and Challenges 5
Ballistic Properties 7
1.2 Problem Statement 8
1.3 Thesis Overview 9
Literature Review Overview 9
Methodology Overview 10

II. Literature Review 12

2.1 Literature Review Introduction 12
Research Components 12
2.2 CNT Ballistic Testing Potential 13
2.3 Nanocomp CNT Sheet Research 19
2.4 Composite Ballistic Testing Methods 21
Types of tests 22
Methods and Calculations 22
Impact failure mechanisms and stacking sequence studies 32
2.5 Literature Review Summary 35

III. Design and Methodology 36

3.1 Introduction 36
3.2 Testing Background 36
Experimental Design 38
3.3 Materials, Equipment, and Processes 42
Panel Production Setup 42
Gas Gun Setup 47
Characterization Equipment 51
3.4 Procedures 57

Page

Panel Production . . . 57
Mechanical and EMI Testing . . . 57
Ballistic Testing . . . 60

IV. Results and Analysis . . . 62

4.1 Panel Construction and Characterization Results . . . 62
4.2 Ballistic Energy Absorption Results . . . 73
4.3 Post Impact Damage Properties . . . 84

V. Summary . . . 94

5.1 Panel Development Findings . . . 94
5.2 Ballistic findings . . . 95
5.3 Post Impact Findings . . . 96
5.4 Conclusions and Future Work . . . 96

Appendix A. Tensile Testing MATLAB Code . . . 99

Appendix B. Digital Image Correlation MATLAB Code . . . 109

Appendix C. Jonas-Lambert Method MATLAB Code . . . 114

Appendix D. Additional Images . . . 116

4.1 Tensile Specimens Images . . . 116
4.2 V50 Panel Images . . . 119
Bibliography . . . 121

List of Figures

Figure Page

1. Structure of single and multi-walled carbon nanotubes. 3

2. Orbital diagrams for sp^3 and sp^2 hybrid orbit configurations. Recreated from [15] 3

3. Orientations of carbon hexagons found in CNTs. Modified from [5] 4

4. Nanocomp Miralon carbon nanotube sheet material 6

5. High resolution SEM image of CNT sheet surface, 10 μm by 10 μm area. Used with permission. [29] 7

6. The molecular dynamics model of a carbon nanotube, (18,0) chirality, subjected to ballistic impact. Recreated from [28] 14

7. Plot of the electric conductivity (S/m) of carbon fiber and Kevlar panels with and without CNTs at a frequency of 20 Hz. Recreated from [27]. 15

8. Image of the AUTODYN ballistic impact model used by Grujicic *et al.* to study CNTs in an E-Glass composite panel. Recreated from [16] 17

9. The 7 configurations of MWCNT mats in the E-glass panels with 'T' indicating the top, 'M' indicating the middle, and 'B' indicating the bottom of the panel. The number preceding the location indicator represents the number of 50 micrometer thick MWCNT mats were placed at that location. Recreated from [16] 18

10. The resulting velocity profiles for the 7 configurations of MWCNT mats in the E-glass panels with 'T' indicating the top, 'M' indicating the middle, and 'B' indicating the bottom of the panel. The number preceding the location indicator represents the number of 50 micrometer thick MWCNT mats placed at that location. Recreated from [16] 19

11. Plot of Vo (fps) versus fragment weight (grains) with lines of constant material thickness. Recreated from [1] 25

Figure Page

12. Bending Stiffness Terms for quasi-isentropic and cross-ply, thick and thin graphite/epoxy panels. Recreated from Baig *et al.* [3] 33

13. Representation of global deformation in low velocity impact and local deformation in high-velocity impact. Adopted from [12] 34

14. Schematic representation of the shear plug damage mechanism. Recreated based on [12]. 34

15. Graphic depicting shot placement on a panel mounted in the panel holder. The labels, such as C1,R2,and L3 indicate the shot location that will be recorded in the ballistic data. 40

16. Prepreg assembly at Patz Materials and Technologies 44

17. Cure cycle for PMT-F6, cyanate ester, resin system. 44

18. Aluminum 9.5"x9.5" cutting template used to cut out carbon fiber and Miralon CNT sheet prepreg. 45

19. Diagram of panel preparation for autoclave curing 45

20. Ultrasonic scan (C-Scan) of 2"x2" samples consisting of 20 plies of CNTs, 10 plies of mixed CNT and carbon fiber plies, and all carbon fiber. 46

21. Autoclave software plot of planned cure cycle and the resulting temperature, pressure, and vacuum values from the cycle run for the PMT-F6 resin composite panels 47

22. Panel holder designed to rigidly support composite panels for ballistic testing. It includes the ability to rotate the stand in 15 degree increments to test materials at an angle. 48

23. Picture of the Phantom high-speed camera and bullet catcher with panel mounted inside for ballistic testing 49

24. Calibration picture of a scale used for determining the pixel to distance ratio of the Phantom 12.1v high-speed camera operating at 28,000 fps. 50

Figure Page

25. Snapshots from Schlieren flow visualization on the AFIT nitrogen gas gun at 1000PSI with a 1/2" diameter steel ball projectile with a .014" thick oiled shooting patch sabot. 51

26. Wet saw with diamond blade used for cutting composite panels and tabbing material 52

27. 1" wide by 8" long specimen clamped in the MTS grips with a 350 ohm strain gauge attached in the center of the 3.66" gauge section. 53

28. Water weight and dry weight scale device with thermometer to adjust the density of water value used to calculate specimen density. 54

29. Acid digestion experimental set up in a ventilated hood. Round bottom flasks with nitric acid and panel specimens placed in a heating unit and water cooled condensers attached to the top of the flask. 55

30. Focus beam tunnel with a frequency range of 2-26.5 Ghz for testing the transmission of signals through test samples placed in the opening of the system. 56

31. Wesdyne utrasonic scan equipment used to map the density of the composite panels. This was used for ensuring good consolidation of the panels from autoclave curing as well as for determining delamination area in the panels after ballistic impact. 56

32. Four panels packaged for autoclave cure. 58

33. 3.5" wide by 8" panel sections and G10 tabs, grit blasted and ready for tabbing. 58

34. Ultrasonic scan results of panel 1.1 showing fairly uniform panel density. 63

35. Ultrasonic scan results of panels 2.2 and 2.3 showing very uniform panel density represented by the white and red colors in the panel. 64

36. Carbon fibers and CNT clump after nitric acid digestion of the cyanate ester resin. 64

Figure Page

37. Tabbed sections from all five panel sets prior to cure in a vacuum table at 180°F for 90 minutes. Three 1"x8" specimens were cut out of these sections for tensile testing. 67

38. Values of Young's Modulus calculated from the strain gauge data obtained from tensile testing of the 15 1"x8" specimens obtained from the five different panel sets. 68

39. Ultimate tensile strength (UTS) in Pascals measured from the 15 tensile tests corresponding to the five different sets of panels, with the first set having no CNT sheets and the fifth set containing 4 CNT sheets. 69

40. Percent elongation at the ultimate tensile strength for the 15 tensile specimens taken from the 5 panel sets. 69

41. Fragments from an all carbon fiber specimen (Panel 1), a specimen with 2 CNT sheets (Panel 3), and a specimen with 4 CNT sheets (Panel 5). Failure for all specimens involved shear in the 45° direction and delamination flaking, but The delamination was much less pronounced in the specimens with four CNT sheets than the other specimens 70

42. Averaged plots of EMI shielding effectiveness in dB for the S12 condition defined as the measurement by port two of the signal projected from port one of the network analyzer located on the other side of the panel. 71

43. Change in projectile velocity for each panel type as measured by the three different velocity measurement methods for 640 ft/s nominal impact velocity. 73

44. Change in projectile velocity for each panel type as measured by the three different velocity measurement methods 75

45. Change in projectile velocity for each panel type as measured by the three different velocity measurement methods. 76

46. Change in projectile kinetic energy for each panel type from the three velocity measurement methods for nominal impact velocities of 640 ft/s. 76

Figure Page

47. Change in projectile kinetic energy for each panel type from the three velocity measurement methods for nominal impact velocities of 350 ft/s. 77

48. Change in projectile kinetic energy for each panel type from the three velocity measurement methods for nominal impact velocities of 180 ft/s. 77

49. Striking velocity vs residual velocity plot for each panel set based on the result of a least squared fit of the Jonas-Lambert method. 79

50. Striking velocity vs residual velocity plot for each panel set based on modeling the three sets of impact velocity data with Billon's method. 81

51. Comparison between the Jonas-Lambert method and Billon method estimates of the limit velocity for each panel configuration using both the camera software (PCC) velocities and the MATLAB digital image correlation (DIC) values 82

52. C-Scans of representative panels from each configuration after ballistic impact. 85

53. C-Scans of representative panels from each configuration after ballistic impact. 85

54. C-Scans of representative panels from each configuration after ballistic impact. 86

55. EMI shielding effectiveness measured by a focus beam tunnel in the range of 2.0-26.5GHz for the all carbon fiber panels. 87

56. EMI shielding effectiveness measured by a focus beam tunnel in the range of 2.0-26.5GHz for the panels with 1 sheets of CNTs. 88

57. EMI shielding effectiveness measured by a focus beam tunnel in the range of 2.0-26.5GHz for the panels with 2 sheets of CNTs. 88

Figure Page

58. EMI shielding effectiveness measured by a focus beam tunnel in the range of 2.0-26.5GHz for the panels with 3 sheets of CNTs. 89

59. EMI shielding effectiveness measured by a focus beam tunnel in the range of 2.0-26.5GHz for the panels with 4 sheets of CNTs. 89

60. EMI shielding effectiveness measured by a focus beam tunnel for panels of each configuration shot at 640 ft/s. 90

61. EMI shielding effectiveness measured by a focus beam tunnel for panels of each configuration shot at 350 ft/s 91

62. EMI shielding effectiveness measured by a focus beam tunnel for panels of each configuration shot at 180 ft/s 91

63. Tensile testing specimens from panel 1.1 116

64. Tensile testing specimens from panel 2.1 117

65. Tensile testing specimens from panel 3.1 117

66. Tensile testing specimens from panel 4.1 118

67. Tensile testing specimens from panel 5.1 118

68. Back-face delaminations from V50 testing of panel 1.2 119

69. Back-face delaminations from V50 testing of panel 1.2 120

70. Back-face delaminations from V50 testing of panel 1.2 120

List of Tables

Table		Page
1.	Panel shot plan for one center shot on a panel from each panel type, 0-4 sheets of CNT, at 3 velocities, 640ft/s, 350 ft/s, and 180 ft/s.	41
2.	Material properties for Nanocomp Miralon CNT product and Hexcel HM63-12k carbon fiber	42
3.	Ply stacking sequences for each of the five panel configurations.	62
4.	Specimen density values used in volume fraction determinations	65
5.	Dry fiber weights and resulting volume fraction values	66
6.	Average mass and volume fraction values for each panel set	66
7.	Thickness and width measurements used to calibrate the calculation of modulus and ultimate tensile strength provided from tensile testing the specimens.	68
8.	Striking and residual velocities obtained for the first set of ballistic tests shot between 627 and 648 ft/s.	73
9.	Striking and residual velocities obtained for the second set of ballistic tests shot between 343 and 348 ft/s.	74
10.	Striking and residual velocities obtained for the third set of ballistic tests shot between 175 and 183 ft/s.	75
11.	Jonas-Lambert method estimations of the ballistic limit for each of the panel configurations based on the three sets of striking and residual velocity obtained through ballistic testing. The norm of the residuals is also provided to indicate the fit of the model with the data.	78
12.	Billon method estimations of the ballistic limit for each of the panel configurations based on the three sets of striking and residual velocity obtained through ballistic testing.	80

Table Page

13. Results of V_{50} testing following MIL-STD-662F with exception to witness plate usage, for panels 0.2, 2.2, and 4.3. Velocity from the two chronographs located between the gun barrel and panel were recorded. Care was taken to avoid delamination overlap when determining shot placement. 83

14. Estimates of V_{50} found by averaging the highest three velocities of projectile stops and the lowest three velocities which resulted in penetration of the panel. 84

List of Abbreviations

Abbreviation		Page
CNT	Carbon Nanotube	1
MWCNT	Multi-Walled Carbon Nanotube	2
SWCNT	single-walled Carbon Nanotube	2
EMI	Electromagnetic Interference	4
AFLCMC	Air Force Life-Cycle Management Center	8
AFRL	Air Force Research Lab	8
SE	EMI shielding effectiveness	11
UHMWPE	Ultra-High Molecular Weight Polyethelene	13
UTS	ultimate tensile strength	67

BALLISTIC EVALUATION OF CARBON NANOTUBE SHEET MATERIAL IN MULTIFUNCTIONAL APPLICATIONS

I. Introduction

1.1 Background

The composite material state of the art is steadily progressing as a new age of material development surges toward stronger, lighter, higher temperature, and more producible composites. Emerging in the aerospace, defense and sports industries, advanced composites are now commonly used in numerous products. The advantages of these materials are clear: high strength-to-weight ratio, high stiffness, corrosion resistance, improved fatigue life, design flexibility, and multi-functional applications. A current material of high interest in modern materials research is the carbon nanotube.

Carbon Nanotube History and Properties.

Carbon nanotubes (CNTs) have several intruguing properties which have led to numerous research veins aimed at capitalizing on tailored uses of these revolutionizing molecueles. Before setting forth the research problem addressed in this thesis it is first necessary to describe CNTs and discuss some of their important properties.

Carbon nanotubes consist of a cylindrical hollow tube of carbon atoms in a hexagonal lattice. Individual CNTs typically have a diameter of 0.7 to 50 nanometers with lengths generally in the range of 10's of micrometers [25]. Although the first synthesis of carbon nanotubes is unknown, the first detailed observation of CNTs that was accessible to the global scientific community is credited to Sumio Iijima in 1991

[31]. The tubes Iijima observed in a scanning electron microscope are considered multi-walled carbon nanotubes (MWCNT) [19]. MWCNTs consist of overlapping CNT tubes of different diameters. The difference between the structure of single-walled CNTs (SWCNTs) and MWCNTs is depicted in Figure 1. As can be seen, the MWCNTs appear more telescope-like with the internal and external bonding between layers of nanotubes. On the other hand SWCNTs only interact with other molecules on the outside surface.

The carbon-carbon sp^2 covalent bonds that predominately make up the relatively long carbon nanotube molecules are the key to its strength [15]. These are among the strongest bonds in nature and are very stable. The sp^2 bonds are stronger than the sp^3 arrangement, seen in Figure 2, that makes up diamond. These bonds in the cylindrical molecules lead to strengths roughly 200 times that of steel of the same diameter for single-walled CNTs[30]. The hollow tubes lead to densities ranging from 1.3-2.1 g/cm^3 for SWCNTs and MWCNTs. This is significantly lower than metals including aluminum which has a density of 2.7 g/cm^3 [25].

CNTs also exhibit high electrical conductivity. This is due to their 1D character and the peculiar electronic structure of graphite. Depending on the chiral vector, a measure of molecular stacking symmetry, SWCNTs can act as either metallic or semi-conductive, with most MWCNT arrangements functioning as one dimensional conductors through electron ballistic transport. The two common arrangements for CNTs, depicted in Figure 3, are Armchair and Zigzag. The arrangement labeled 'Chiral' represents a combination of Armchair and Zigzag. Armchair configurations have the best electrical conductivity among the three, approaching the range of conductive metals [5]. One of the useful applications of the high electrical conductivity that carbon nanotubes provide is their ability to prevent electronics from being disrupted from various interfering signals. It has been found that incorporating a single sheet of

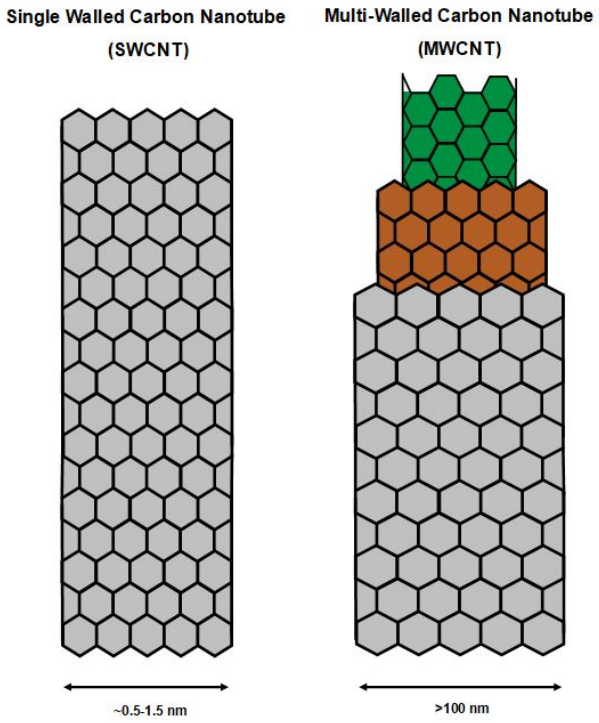

Figure 1. Structure of single and multi-walled carbon nanotubes.

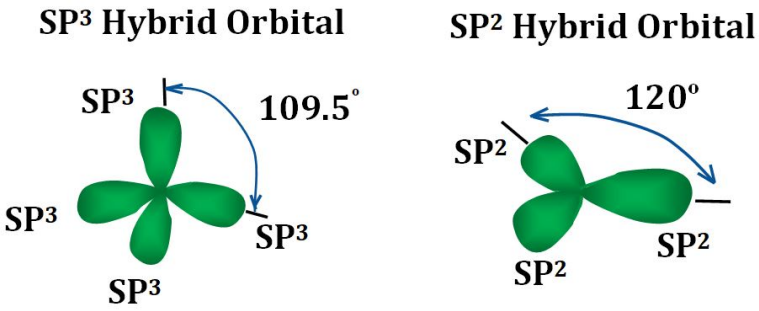

Figure 2. Orbital diagrams for sp^3 and sp^2 hybrid orbit configurations. Recreated from [15]

.

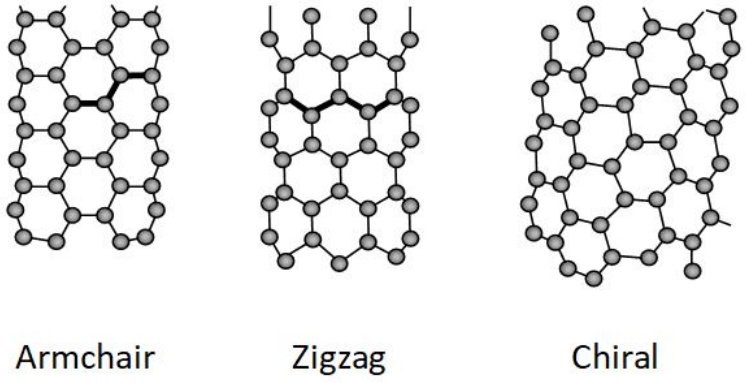

Figure 3. Orientations of carbon hexagons found in CNTs. Modified from [5]

CNTs into a composite frame theoretically provides around 46 dB of electromagnetic interference (EMI) shielding [13]. As for the use of CNTs as semi-conductors, the intrinsic carrier mobility of SWCNTs is 100,000 $\frac{cm^2}{Vs}$ versus 1,400 $\frac{cm^2}{Vs}$ for silicon oxide [38]. This demonstrates great potential for computing applications.

The thermal conductivity of CNTs is also very noteworthy with theoretical values of up to 6600 W/mK for SWCNTs. Experimental values though have been much lower ranging from 3000W/mK for MWCNTs to 3500W/mK for SWCNTs [34]. These values still supersede traditionally used metals such as copper or silver, which have values of 386W/mK and 407W/mK, respectively. The exceptional thermal conductivity results from the entire rigid CNT molecule vibrating to transfer energy which is more efficient than the electron based transfer metals use to transfer heat energy [5]. The thermal conductivity combined with the EMI shielding properties has led to research into the use of CNTs in advanced computer systems where high electrical and thermal conductivity are necessary. CNTs are inherently resistant to structural modification due to their carbon composition and strong covalent bonding. This allows them to operate with impunity in corrosive conditions like salt and moisture, as well as in some types of radiation, and to retain their mechanical properties at cryogenic temperatures [29]. With properties like these and the others surveyed it is

easy to see why there is a strong focus within materials research to understand and develop CNTs.

Bulk Property Characteristics and Challenges.

The individual nanotube molecules are extremely strong and have superb properties, but it is important to understand how the molecules interact with each other. Graphite is made up of the same carbon-carbon bonds found in CNTs and has very strong planar strength, yet it does not take much force to break it apart to write with a pencil. This occurs because the planar arrangement of the sp^2 bonds leads to only *pi*-orbitals in the perpendicular plane which produce very weak Van der Waals forces [15], short-range electrostatic attractive forces between uncharged molecules [33]. The curved nature of CNTs leads to a mixture of both *pi*-orbitals and stronger *sigma*-orbitals outside of the plane of the molecule surface and available for inter-molecule reaction [15]. These bonds are much stronger than those between layers of graphite, but they are not as strong as the sp^2 bonds that make up the molecule. This is why for MWCNTs, the weaker Van der Waals forces which make up the interlayer bonding leads to a decrease in overall strength compared with SWCNTs. This also means that bundles of SWCNTs or MWCNTs similarly experience slippage between CNTs which leads to reduced bulk properties as compared with individual tubes. Notwithstanding, the CNT bulk properties are significantly better than graphite and provide high-strength properties in bundled arrangements.

Realizing the full potential of CNTs has been a challenge because reproducibility, scale, uniformity, and cost have hindered capitalization of this exciting material. It is challenging to tightly control the formulation of CNTs and to arrange them for optimal bulk properties. Subsequently producing a product at the commercial scale is a large hurdle. One of the companies that has established a commercial CNT

product in sheet form is Nanocomp Technologies Inc. with their Miralon CNT sheet. The non-woven Miralon consists of SWCNTs and some MWCNTs, with only a few layers, and was first produced in the early 2000's [30]. The nanotubes are created in a high temperature reactor where they bind to each other and grow to be micron thick and milimeter long bundles. The nanotube "cloud" is then laid out into a mat format, as seen in Figure 4, via chemical vapor deposition. This process eliminates the need for binders or secondary processing steps [29].

Figure 4. Nanocomp Miralon carbon nanotube sheet material

Nanocomp's production process is free of toxic metals, such as nickel or cobalt, which are commonly used to form CNTs. This along with the long length of the nanotube bundles leads to a very safe product for handling as it minimizes toxicity and inhalation safety concerns. While some of the amazing properties of individual tubes are close to those in the bulk mat product, such as EMI shielding of 40dB @ 2GHz, unfortunately many of the bulk properties of Miralon do not approach the potential found in individual tubes. The thermal conductivity is only 30 W/mK, the resistivity is relatively high at 1.3 Ohms per meter, and the mechanical strength is

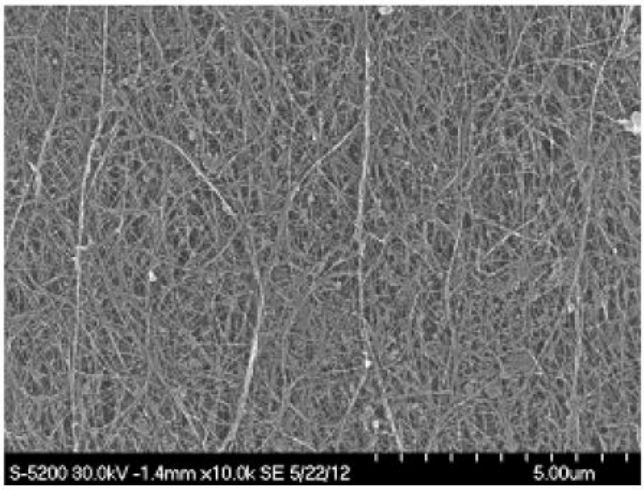

Figure 5. High resolution SEM image of CNT sheet surface, 10 μm by 10 μm area. Used with permission. [29]

around 52MPa. Despite this, Miralon sheet and tape formats have successfully been used in aerospace, electrical, and structural applications [29].

Realizing the full potential of CNT products will require extensive research and testing. Getting formulations suitable for large scale applications with consistent, controlled properties will be key for CNT development. As companies such as Nanocomp work to bridge this gap, functional evaluation for applying their products will be vital to transitioning this technology.

Ballistic Properties.

One of the areas of research which has made use of the strength and shape of CNTs and sees promise in sheet products is the area of ballistic protection. At the molecular level, the strong bonds between the carbon atoms means that it takes a good deal of energy to break it apart, and the hollow cylindrical shape means that the molecule can absorb energy by squeezing thinner and flexing its shape. Based upon these properties, researchers have tested adding raw nanotube powders to the matrix of composite panels and have seen improvements in ballistic performance. Starting

in the 2012 timeframe, companies such as Amendment II, AR500, Citizen Armor and DryWired integrated CNTs into some of their armor products [14][24][9][11]. Furthermore Nanocomp conducted tests and reported stopping a 9 mm handgun bullet with around 100 sheets of their product, which amounts to approximately 0.1 inches of material in thickness [21]. These findings are exciting for ballistic researchers, who are always seeking ways to reduce the bulk and weight of ballistic protection.

One of the potential applications of Miralon's ballistic properties is in the area of aircraft survivability. Aircraft are typically vulnerable to high-speed impact damage. The need to keep the aircraft as light as possible is balanced against the need to protect the structure, systems, and personnel from abnormal situations which could involve debris, hail, shrapnel, or even munitions, particularly in military applications. Although these events may not be frequent in many applications, cases such as the April, 2018, Southwest Airlines Flight 1248 catastrophic engine failure, which killed one person, raise questions about the ability of airframes to hold up to impact damage such as failed turbine blades. Notwithstanding its rarity in civilian applications, this is an issue military aircraft have to face head-on.

1.2 Problem Statement

The Air Force Life-Cycle Management Center (AFLCMC) and Air Force Research Lab (AFRL) recognize CNT ballistic research as a valuable branch of research to investigate. CNTs are seen as a potential solution to provide lightweight shrapnel and debris protection for passengers aboard Air Force aircraft, such as helicopters, which are vulnerable to such incidences in combat environments. Therefore, this thesis sought to determine if the addition of CNT sheets to carbon fiber panels improved the ballistic properties of the panel. The hypothesis was that integrating CNT sheets into the laminate would increase the projectile energy absorbed by the panel, and

reduce the damage to the panel incurred by the impact. This information is not available presently in academic research, and through the work presented here, a better understanding of the ballistic properties of state of the art CNT sheet material is obtained.

1.3 Thesis Overview

Given the problem statement and need for experimental testing of CNT sheet material, the goal of this thesis was to obtain application-relevant ballistic properties for CNT sheet material. The specific objectives of this thesis research are:

- Construct and characterize carbon fiber panels integrated with CNT sheets.
- Subject the panels to controlled high-speed impact conditions.
- Determine if the addition of CNT plies results in increased projectile energy absorption by the panel.
- Evaluate the contribution of CNT sheets to panel damage area and EMI shielding post high-velocity impact.

To accomplish these objectives, previous relevant research was studied to develop an experimental method. This plan was then implemented and the results analyzed. The subsequent chapters will present the work accomplished in this thesis to meet the research objectives.

Literature Review Overview.

The first step of this thesis was to conduct a literature review which surveyed the relevant studies which establish the ballistic potential of CNTs, represent the current research on CNT sheet materials, and guide composite ballistic research.

The section on the ballistic potential of CNTs presents the precedent of molecular modeling and CNT additive testing which initiated study of CNTs as a potential ballistic protection material. The second section helps characterize the results of current efforts to mass-produce CNTs and create an easily integrated sheet product which captures some of the potential demonstrated by individual CNT molecules. It also presents a thorough attempt to find what has been done with CNT sheet material and justify the thesis objective is relevant and novel. The last section is specifically important for guiding the ballistic testing methods used in this thesis to address the problem statement. Traditional impact testing is classified as low speed, high-speed, or ballistic. The primary focus based on Nanocomp's ballistic claim is on the high-speed and ballistic type impact testing. Within that type of testing there is significant variation. Projectiles can be solid, such as steel, or fracturing such as ice or lead. The firing mechanism can be a compressed gas gun, a powder cartridge gun, or an electromagnetic rail gun. Evaluation of ballistic strength can be measured as stopping velocity, V_0, 50% probability of penetration, V_{50}, or in terms of velocity and kinetic energy dissipation. With all of these types of tests it is important to assess research objectives and the available test capabilities to design a successful experiment.

Methodology Overview.

The approach taken in this study generally involved three tasks. The first task was to quantify the mechanical properties of the composite panels as prepared with a particular resin system and processing method. This involved finding the panel elastic modulus and ultimate strength. It also included finding the density of the composite as prepared and the volume fractions for the fibers and resin. Next, an understanding of the ballistic energy dissipation of the CNT sheets was pursued along with analysis

of the damage to the panel properties after impact. Investigating the ballistic energy dissipation of the panels involved experimentally finding the velocity attenuation of a projectile shot through the panels and relating this to ballistic theory. The shot parameters were designed based on high-speed debris impact mass and velocity, and various quantities of CNT sheets within the panel were studied. Damage to the panels was assessed through measuring the delamination area caused by the impact as well as through measuring the EMI shielding effectiveness SE as measured by signal attenuation through a range of frequencies. Discussion of the approach and methodology will be presented in more detail in chapter 2 and chapter 3. The results and conclusions of the experimental research will then be presented in chapters 4 and 5.

II. Literature Review

2.1 Literature Review Introduction

Chapter 2 is a review of the relevant published research which guided the present study. The review will aim to demonstrate the relevance of applied characterization and ballistic impact study of carbon nanotube (CNT) sheets. Additionally, it will present the works which guided methodology considerations for conducting composite panel ballistic research.

Research Components.

Research studies of carbon nanotubes (CNTs) have been diverse, driven by various production methods and potential applications. To scope the literature review of this multifunctional material, the review will be split into three focus areas: CNT ballistic testing potential, CNT sheet research, and composite material ballistic testing methods. CNT Ballistic Testing Potential will present works which highlight the ballistic potential of CNTs and will describe the progression of research toward ballistic testing of CNT sheet material. CNT Sheet Research will review relevant CNT sheet research, particularly research of sheet product as synthesized by Nanocomp. This will identify the need for investigating the ballistic impact characteristics of CNT sheets and present some of the research proving the Nanocomp CNT sheet material's multifunctional properties such as strength and conductivity. Composite Material Ballistic Testing Methods will review relevant literature on ballistic testing of composite panels. This review helped form the design of experiments for this thesis.

2.2 CNT Ballistic Testing Potential

The earliest application of modern composites for ballistic protection occurred during WWII, when a composite of E-glass, a type of fiberglass, and nylon were bonded in ethyl cellulose resin. This product, called Doron, was developed by the Dow Chemical Company in 1943. First adopted by the Marines, the armor became the first composite personal body armor with widespread use in the Korean War and continued use into the Vietnam War [10]. Further development of composite armor materials, often by experimental accident, led to Kevlar and ultra-high molecular weight polyethylene (UHMWPE) among others, which have proven to be great ballistic materials. The discovery of a revolutionary new high strength carbon material, carbon nanotubes, led to a push to understand their potential utilization for ballistic armor applications.

Mylvaganam and Zhang [28], set forth a molecular level ballistic model which predicts that a 600 μm thick sheet of woven CNT yarns would be able to stop a revolver bullet with an energy of 320 J [28]. As laid out in the introduction, CNTs are composed primarily of very strong sp^2 carbon bonds, which in addition to the cylindrical shape of the molecule, led to very good energy absorption characteristics in the model used by Mylvaganam and Zhang for ballistic impact [28]. Their model of the nanotube, depicted in Figure 6, describes the principle shear energy absorption which makes nanotubes suitable for ballistic protection. Energy-based analysis was utilized in their work to identify that larger radius nanotubes impacted at the midpoint between two fixed ends absorb the most energy from the projectile. They also found that the energy absorption was proportional to CNT length. With a molecular model constructed, it was extrapolated that six layers of continuous woven nanotube yarn with an area of .101 in^2 would stop a 9mm revolver bullet [28]. While the discontinuous non-woven CNT products produced today do not meet this prediction, as

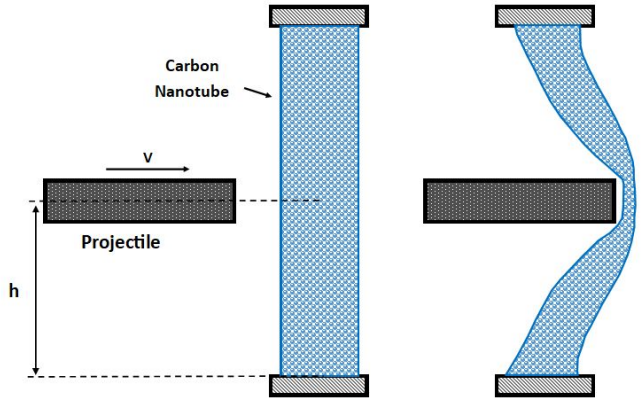

Figure 6. The molecular dynamics model of a carbon nanotube, (18,0) chirality, subjected to ballistic impact. Recreated from [28]

noted by Nanocomp's test which required around 100 layers to stop a 9mm bullet [21], Mylvaganam and Zhang's research establishes a molecular level model which identifies the potential utility of CNTs for ballistic protection.

The first attempts to utilize carbon nanotubes to improve ballistic performance of composite panels experimentally involved dispersing the nanotubes within the resin. Given that CNT "powders" were the first producible forms of CNTs, this type of testing as a resin toughener was a practical first evaluation. Researchers at Sapienza University of Rome sought to combine bidirectional Kevlar fabric, carbon fiber fabric, and epoxy mixed with CNTs to make multifunctional composites which demonstrate good impact resistance as well as provide electromagnetic shielding [27].

One of the key issues with dispersing CNTs in a resin system is keeping them from clumping together due to Van Der Waals forces, weak intermolecular forces which attract the CNTs to each other. To overcome this, the CNTs were put in an ethanol bath and evenly dispersed by ultrasonic vibrations. The sonication process was conducted at 20 kHz for 6 hours before the CNT solution was added to the resin [27]. The resin, Sika Biresin CR82, was then brushed onto both sides of each ply and the composite panel compressed at 7 bar and cured at 50°C for 16 hours followed by

80°C for 2 hours [27].

The completed panels had 6 layers of carbon fiber with 2 layers of Kevlar fabric in the middle. Panels with and without the CNTs in the resin were produced. The panels were tested for multifunctional improvement due to the addition of CNTs in the panel matrix. The three areas tested involved electrical conductivity, electromagnetic shielding effectiveness, and ballistic strength.

The first area tested was electrical conductivity. The tests of the two panels showed great improvement in conductivity in the panel with CNTs, increasing about 3000 S/m as seen in Figure 7 [27]. Increases in inductance and capacitance were also

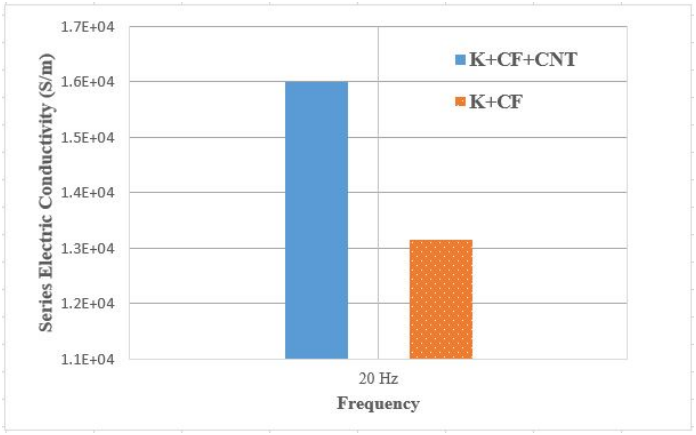

Figure 7. Plot of the electric conductivity (S/m) of carbon fiber and Kevlar panels with and without CNTs at a frequency of 20 Hz. Recreated from [27].

observed in the panel with CNTs.

Next the panels were tested for their electromagnetic shielding capability. Utilizing a reverberation chamber, the specimens were tested in the microwave range from 0.8 to 8.4 GHz to evaluate the value of adding the CNTs to the composite. The results showed that both the panels with and without CNTs closely matched the floor shielding values established by aluminum with a maximum around 80 dB at certain frequencies.

FEA modeling suggested a 5-20 dB increase in performance by the panels con-

taining CNTs with values of shielding ranging from 100 to 240 dB over the frequency range of 0.8-8.0 GHz. The researchers theorized that this increase was due to CNTs in the resin allowing "the formation of conductive multi-paths in the bulk material [27]." Because the experimental setup had a noise floor of around 80 dB, the shielding effectiveness of the panels was not adequately captured experimentally.

Having characterized the EMI shielding properties, the panels were then subjected to ballistic testing via a rail gun firing 2g aluminum projectiles. They were shot at both 400 m/s and at 1000 m/s. Both the panels with and without CNTs stopped the projectiles fired at 400 m/s, demonstrating lots of delamination and fracturing of the panels as they trapped the energy of the projectile. Neither panel stopped the 1000 m/s projectiles. To identify a difference between the panels with and without CNTs, it was observed that the damaged area in the panel with CNTs was greater for the shots fired at 1000 m/s. The authors used this to surmise that more of the energy was transfered to the panel in the specimen with CNTs. They hypothesized that the better absorption of energy was a result of the CNTs acting as a network of spring-dampers that increased the overall damping of the panel against the vibrations induced by the ballistic shock waves. Thus, the CNT reinforcement of the resin inhibited cracking of the matrix and transfered load to a larger number of fibers, resulting in more energy absorbed [27]. Residual velocities of the projectiles after impact were not recorded to provide any quantitative evidence for this theory.

Seeing that CNTs are well suited for absorbing ballistic impact at the molecular level and that they can enhance electrical and shielding properties as well as improve ballistic strength when diffused in a composite panel's resin system, it is reasonable to then expect a sheet material would lend to increasing ballistic strength in addition to practical use as EMI shielding. The primary work obtained in this topic area was the research done by Mica Grujicic *et al.* [16]. Their work published in the *Journal*

of Material Science aimed to model and validate with experimentation the inclusion of multi-walled carbon nanotube (MWCNT) reinforced poly-vinyl-ester-epoxy matrix composite material as a fiber lamina within E-glass composites designed for ballistic protection. As opposed to dispersing CNTs in the resin as was previously described, Grujicic *et al.* made a mat of randomly distributed CNTs held together with the poly-vinyl-ester-epoxy and modeled the influence the material had on ballistic properties when used in an E-glass panel. The research evaluated the importance of MWCNT mat thickness and location within the E-glass layup [16]. The researchers used the dynamics modeling software AUTODYN to model the ballistic impact events. Figure 8 depicts the model of the ballistic impact of a steel fragment simulating projectile (FSP) against the E-glass/MWCNT composite panel.

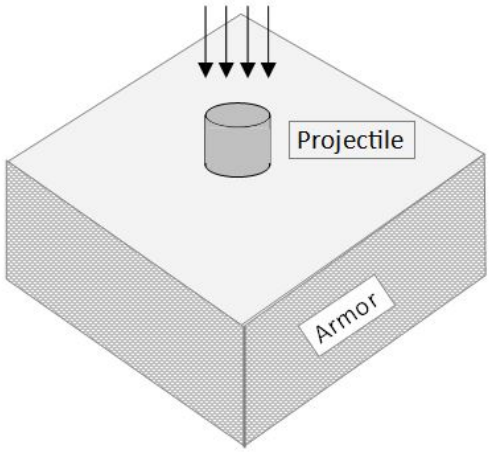

Figure 8. Image of the AUTODYN ballistic impact model used by Grujicic *et al.* to study CNTs in an E-Glass composite panel. Recreated from [16]

Using data from material characterization work on their MWCNT mat material, a variety of configurations of the mats within the E-glass compsite panels were analyzed to find the optimal placement and thickness of the mats. The various configurations can be seen in Figure 9. The software program analyzed the projectile velocity profile through the panels when .30 caliber FSPs impacted them at a velocity of 2000ft/s.

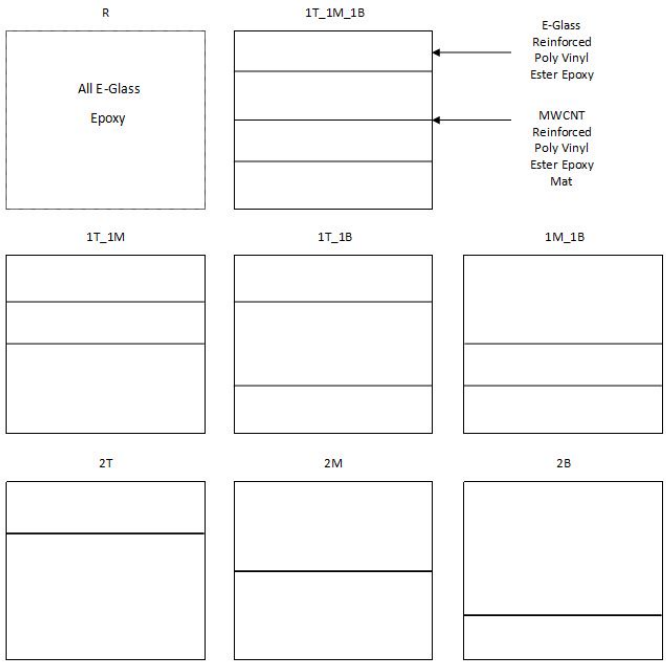

Figure 9. The 7 configurations of MWCNT mats in the E-glass panels with 'T' indicating the top, 'M' indicating the middle, and 'B' indicating the bottom of the panel. The number preceding the location indicator represents the number of 50 micrometer thick MWCNT mats were placed at that location. Recreated from [16]

The resulting velocity profiles through the panels, including the residual velocity out the back of the panel, are given in Figure 10.

This work shows that the placement of the CNT sheets near the front surface of the material had the most impact on disrupting the ballistic shock waves in the material and inhibiting shear plug formation. A detailed model depiction of the difference between the best and worst case configurations with doubled sheets, 2T and 2B respectively, depicted major delamination between the layers of both panels, but more energy being absorbed with less of a shear plug formation in the case with two sheets near the top of the panel. The decrease in residual velocity between the best CNT case and the case with all E-glass was approximately 230ft/s [16]. This research supports the idea that CNT mats can improve the ballistic performance of composite panels by disrupting shock wave propagation through a material. The

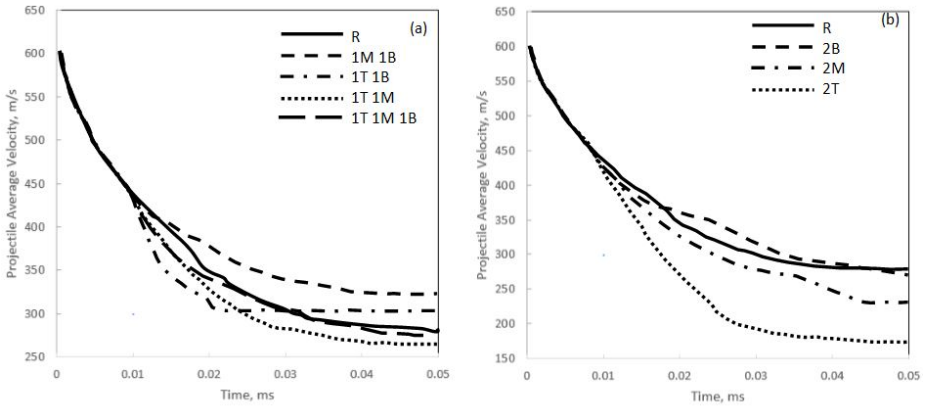

Figure 10. The resulting velocity profiles for the 7 configurations of MWCNT mats in the E-glass panels with 'T' indicating the top, 'M' indicating the middle, and 'B' indicating the bottom of the panel. The number preceding the location indicator represents the number of 50 micrometer thick MWCNT mats placed at that location. Recreated from [16]

mats used in this research were created from mixing high concentrations of short MWCNTs with some resin and do not fully represent a true fabric sheet material, but they represent the early attempts to use CNTs as a fiber reinforcement in a composite, as opposed to a resin reinforcement.

2.3 Nanocomp CNT Sheet Research

With the introduction of Nanocomp's unique millimeter long CNT non-woven sheet materials, the use of CNTs as a composite fiber material was more explicitly made possible without having to formulate a mat as was done by Grujicic *et al.* [16]. The published work done with this sheet material has not been in the realm of ballistics though. This next section of the literature review will look exclusively at the published work on the Nanocomp material to show the breadth of research on the material that was investigated.

The first research area seen in literature regards characterization of the CNT sheet material with various resin systems and looking at the effect of stretching the material to improve CNT alignment. Scientists at NASA Langely Research Center

led by Roberto Cano conducted work that showed that mechanically stretching the nonwoven Nanocomp CNT sheet material improved its mechanical tensile strength by aligning the CNT's in the stretched direction [7]. They also characterized the sheets' performance when used with four different resins, including API-60 Epoxy, LaRC PETI-9 Polyimide, RM-3010 BMI, and Ultem 1000 PEI. Stretching was conducted to 121% of the original length and was most beneficial in the BMI and PETI-9 composites' modulus values which more than doubled [7].

Another way that Nanocomp CNT sheets have been studied involves research on the thermal conductivity properties of the material. J.G. Park *et al.* utilized Nanocomp's long CNT length sheet material to study the thermal conductivity of CNT/Epoxy composites. They found that a composite with 60% CNT sheet by weight achieved roughly 55W/mK, and with 40% mechanical stretching to allign the nanotubes, the thermal conductivity jumped to over 103W/mK [34]. While this is only half the thermal conductivity for aluminum and well short of the over 3000W/mK observed for individual tubes, it is a marked improvement over the 5W/mk observed for short CNT and epoxy composites [34]. Related work involved research published in the journal of Advanced Functional Materials which utilized stretched Nanocomp CNT sheets to achieve improved properties in a CNT sheet and BMI composite. They found that the composites demonstrated a conductivity of 5500 S/cm in the aligned direction [8]. With mechanical properties similar to the best carbon fiber, IM7, and a much higher electrical conductivity, the research demonstrated that CNT products show promise for multifunctional applications combining strength and conductance [8].

Also with a more focused view towards conductance and the lightweight aspect of CNTs, Stefanie Harvey from TE Connectivity researched the suitability of CNT products to replace current copper electrical wire shielding as well as its use as a wire

core replacement [17]. Potential weight savings of over 1000 lbs on specialized aircraft such as the Lockheed Martin F-35 are possible by replacing metal cores and shielding with lightweight CNT materials. To conduct the feasibility study Harvey made wires consisting of CNT threads wrapped with CNT mat material. She found that two layers of Nanocomp CNT sheets provided 52 dB of protection at 4 GHz (supported by Estrada *et al.*[13]) which is comparable to standard copper shielding which provides 50 dB of attenuation but at 87 times the areal density of the Nanocomp material. The report notes that CNTs are suitable at shielding high frequency electromagnetic signals, but not low frequency signals, and improvements in conductance will need to be made to rival the performance of metals such as copper [17].

These research articles are representative of what is seen in current literature on the Nanocomp CNT sheet materials. The challenges in realizing molecular level properties at the macro scale is readily observed in all of these articles, and characterization of the latest advancements in CNT products is important for evaluating practical applications. As demonstrated in these articles, the research is largely found within categories looking at tensile strength, thermal properties or electrical properties, and no formal high-speed impact tests have been published. Alan Windle, a professor of materials science at the University of Cambridge, England, made the importance of sheet products clear when he said CNTs "look promising compared to commercially available fibers, but no one will really know until we make enough fiber to make a fabric and shoot a bullet at it [20]."

2.4 Composite Ballistic Testing Methods

Recognizing the scientific value in researching the ballistic properties of the Nanocomp CNT sheet material, it is important to understand from a literature review perspective the methods used to conduct ballistic testing. While CNTs are relatively

new materials, ballistic testing methods are mature and well documented. Following research practices laid out in similar works of ballistic properties will define the relevant information to collect, calculate, and report. This part of the literature review is limited to studies involving composite testing with particular focus on carbon fiber as it is a common aerospace composite material. A discussion of the two main types of ballistic testing is necessary to provide some background.

Types of tests.

There are two main research focus areas that utlilize ballistic impact tests. The first involves armor applications where what is desired is knowledge as to how well the material reduces can stop a projectile. The second involves researching residual material properties as a result of a ballistic impact. It seeks to find ways to reduce damage to the material and quantify how impact affects material characteristics and structural capability. The emphasis of this second type of ballistic testing is on understanding the resulting damage to the panel and less so on trying to evaluate the effectiveness of the composite to stop a projectile. The two research focuses are not exclusive though, and combined testing which seeks to identify projectile stopping capability as well as to characterize material properties after impact are found in literature such as the work done by Resnyansky and Katselis to evaluate composite helicopter skin material [37], and work by the Avco Corporation with other materials [32]. Keeping the two types of tests in mind, relevant literature to the current study will be reviewed.

Methods and Calculations.

Starting back with early composites, Doron composite ballistics information is found in a 1963 report from the Ballistics Analysis Laboratory at John Hopkins Uni-

versity [1]. In this report seven different nonmetallic materials were subjected to ballistic testing. The materials included bonded and unbonded Nylon, Lexan, stretched and as-cast Plexiglass, Doron, and Bullet Resistant Glass. The tests were conducted to provide information for vulnerability analysis of body-armor, transparencies such as aircraft windshields, and special function materials such as a packed parachute[1]. The primary results of the study include estimating the ballistic limit, V_0, and plotting V_0 relative to material or fragment properties. The study limited it's scope to data sets with steel projectiles.

This 1963 report states that one of the findings from an earlier report on small projectiles was that when a projectile remains essentially intact after impact, its performance seems to be directly related to the weight and the presented area of the entire projectile [1]. This is used to reasonably assume that the differences in impactor shape do not influence correlations as much as these two parameters. The data collected for each impact included material thickness, fragment weight, obliquity, striking velocity, residual velocity, residual weight and hole area. These variables are important due to the fact that in a ballistic impact, kinetic energy, which is related to projectile mass and velocity, is absorbed by the material through breaking the chemical bonds holding the panel together. Therefore the amount of material impacted is important for determining how many bonds are affected by the impact event. Thus, the projectile area as well as the panel thickness and relative angle to the projectile velocity are important in understanding the energy change in a penetrating projectile. In order to capture all of these experimental variables, the authors created the exponential equation presented here in Equation 1:

$$V_r = V_s - 10^c (eA)^\alpha m_s^\beta (sec\theta)^\gamma V_s^\lambda \tag{1}$$

where V_r is the fragment residual velocity. V_s is the fragment striking velocity which

becomes V_0 when V_r equals zero. The target thickness, e, can be changed to areal density, E, for better comparison between materials. A is the average presented area of the fragment, which can be ignored if similarly shaped fragments are used. Here m_s is the weight of the original projectile, θ is the angle between the trajectory of the fragment and the normal to the target. Finally c,α,β,γ, and λ are constants determined experimentally for each material. This equation intuitively relates residual velocity, the area of the target material interacting with the projectile and the striking kinetic energy. The exact contribution of each component to the residual velocity is material specific and determined through the exponential constants. The constants are found by using a least squares fitting method and the logarithmic version of the residual velocity equation as shown in Equation 2:

$$log(V_S - V_r) = c + \alpha log(eA) + \beta log(m_s)\gamma log(sec\theta) + \lambda log(V_s) \tag{2}$$

which clearly delineates the contributions from each experimental variable on the velocity change of the projectile. The report notes that a projectile mass change is more likely with metal-on-metal impacts than with the nonmetallic materials impacted in their study, and their results support this conclusion [1].

The results of this research provided several different sets of plots. These plots related V_0 calculations to other variables such as material thickness, fragment weight and areal density. Figure 11 represents one of these plots for Doron. Overall, this paper provided useful information on the fundamentals of conducting ballistic impact tests of composites and methodology for useful calculations of the ballistic limit velocity, V_0, when enough data sets are available.

Within ballistic testing aimed at stopping the projectile, another parameter, besides ballistic limit prevalent in research is V_{50}, the velocity at which a projectile has a 50 percent probability of penetrating the material. Standard testing for this

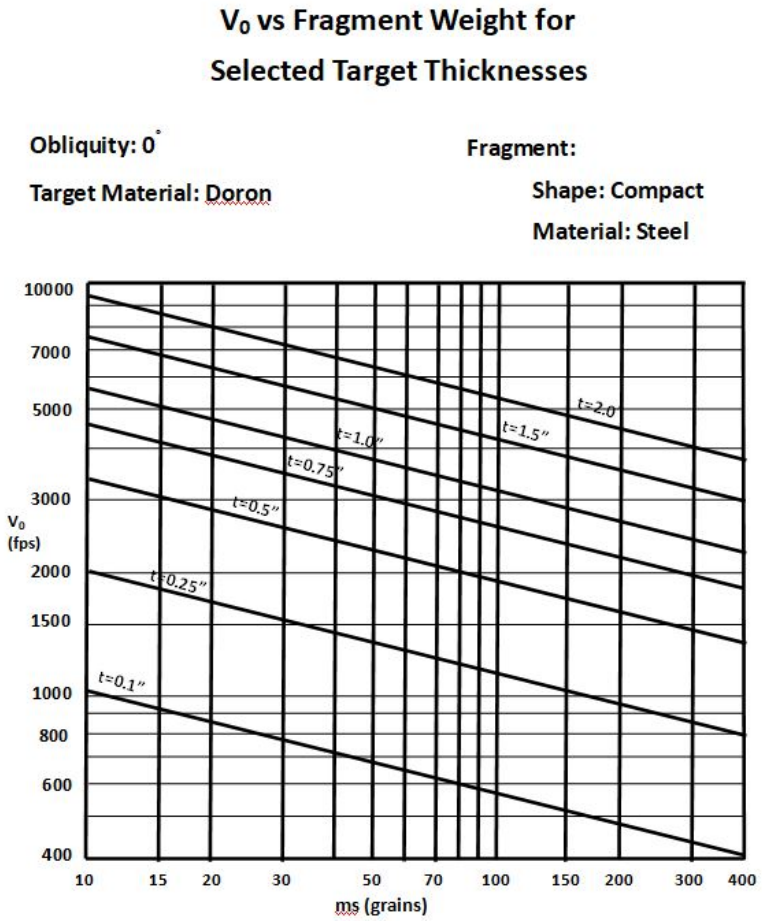

Figure 11. Plot of Vo (fps) versus fragment weight (grains) with lines of constant material thickness. Recreated from [1]

parameter is outlined in MIL-STD-662F, the Department of Defense test method standard for V_{50} ballistic test for armor [41]. The V_{50} evaluation consists of shooting the test item at varying velocities until an equal number of complete and partial penetrations (minimum of 2 each) have been recorded within a velocity range, typically set between 60 and 125ft/s. To distinguish between penetrations, a witness plate, consisting of a 0.02" thick 2024 T3 aluminum plate is placed 6 in. behind the test item. If light from a 60W, 110V light bulb can be seen through a puncture of the witness plate, then it is considered a complete penetration. If no light penetrates the witness plate it is a partial penetration. This military standard is used for ballistic

acceptance testing in addition to research and development of new ballistic materials for small arms projectile protection [41]. As a commonly used test standard, V_{50} is a good metric for comparison between materials for ballistic applications. While the standard test procedures are useful for many materials, additional consideration of shot placement is needed for composite materials. Kinsler and Collins [22] compared V_{50} results for ultra-high molecular weight polyethylene (UHMWPE) composites shot following MIL-STD-662F. They found appropriate spacing of shots is needed to prevent delamination overlap [22]. In their testing, specific to UHMWPE, they found V_{50} increased over the first three to four sets of V_{50} shots on a single panel with delamination overlaps and decreased significantly from the max to the fifth and final set of data.

Kinsler and Collins suspected that conducting multiple V_{50} experiments on the same panel might lead to an overestimate of the V_{50} as compared to traditional acceptance testing, which would use fewer shots on the same target. While the specific trends seen in their data may not be relevant for carbon fiber and CNT composites, the findings prove the importance of identifying the true area damaged by the impact for determining shot placement for multi-hit testing. This is helpful for planning shot placement on panels for testing CNT ballistic properties.

In general, V_{50} testing is most useful when testing a panel designed to meet a specific threat. It answers the question of the projectile type and velocity this panel can protect against fifty percent of the time. Conducting V_{50} testing requires careful control of the shot velocity. Another challenge with the V_{50} method is that due to the witness plate, finding residual velocities can be challenging and the binary penetration data may have limited applicability beyond finding V_{50} values. The basis behind ballistic testing is understanding how much energy a specimen can absorb from a given projectile. Therefore a more direct method to examine the data is through

evaluating projectile velocity attenuation. When striking and residual velocity data is collected for ballistic testing, there are a few different ways to analyze the data and evaluate results. The residual velocity can be plotted against impact velocity and compared. Additionally, the kinetic energy of the projectile before and after impact can be calculated and provide a means of comparison. The V_0 method outlined earlier demonstrates one way that impact and residual velocity data can be used to asses the energy absorption of a panel and predict the ballistic limit of the panel. Although the particular form presented was best suited for comparing data with significant variability of test parameters, other methods exist based upon the same data. These analysis options have led many researchers exploring new materials to evaluate ballistic protection capability through velocity attenuation of penetrating shots [36][16][35][37].

Researching a new material or layup through residual-velocity energy methods is most meaningful when a baseline and the new panel are manufactured and tested together comparatively. While some studies compare to other published research data for their baseline, tests against a co-produced baseline are common practice. For example Micheli *et al.* made panels with and without CNTs in the resin and Grujicic studied the difference between all E-Glass panels and ones with layers of CNTs within the panel [27][16]. Testing against a co-produced baseline helps eliminate the influence of panel processing, material batch variability, and ballistic test conditions among other variables on the comparison study.

Methods for calculating the ballistic limit, V_0, from velocity attenuation data have been developed for cases with limited test variables and non fragmenting projectiles. The mathematical relationships developed by Jonas and Lambert, and related work by Billon were used as more specific forms of the previously discussed ballistic limit method [23][4]. While these methods aren't exact, they are reasonable estimates

which gain fidelity with increasing data sets, as does V_{50} testing. These methods also allow for quantified comparison of material ballistic performance in terms of ballistic limit velocity.

The estimate for V_0 developed by Lambert and Jonas, the so called Jonas-Lambert method, is based on the conservation of energy with constants to account for error [23], as seen in Eq. 3:

$$\frac{1}{2}M_s V_s^2 = \frac{1}{2}M_r V_r^2 + \frac{1}{2}M_L V_L^2 \tag{3}$$

where the s subscript terms refer to the striking kinetic energy, the r subscript terms the residual kinetic energy, and the L subscript terms the ballistic limit conditions. From here the Jonas-Lambert method assumes that the mass of the projectile does not change at any point. Equating all mass terms and rearranging Eq. 3 leads to:

$$V_r = (V_s^2 + V_L^2)^{\frac{1}{2}} + \varepsilon. \tag{4}$$

There is an error term, ε, added because some of the assumptions used for the cancellation of the masses are not exact. The Jonas-Lambert method also changes the exponent of the velocity terms to a variable, p, and includes an alpha term to also help describe error, as shown in Eq. 5:

$$V_r = \alpha(V_s^p - V_L^p)^{\frac{1}{p}} + \varepsilon \tag{5}$$

where the unknowns of α, p and V_L can be found via a least-squares fitting method assuming that at least three shots of data are recorded, although more data will improve the accuracy.

Following the work of others along the vein of the Jonas-Lambert method, Billon, developed a method for finding a best estimate of V_0, called V_a, that starts with the

conservation of energy in terms of kinetic energy analysis [4]. This is seen in Eq. 6:

$$\frac{1}{2}M_iV_a^2 = \frac{1}{2}M_iV_i^2 - \frac{1}{2}M_rV_r^2 \tag{6}$$

where the i subscript terms refer to the the impact conditions, r subscript terms to residual terms and V_a represents the ballistic limit velocity. To account for projectile and panel mass loss upon impact, Billon utilizes a positive constant, k, to keep track of the mass ratio, leading to Eq. 7:

$$V_a = (V_i^2 - kV_r^2)^{\frac{1}{2}} \tag{7}$$

where k is defined in Eq. 8 as:

$$k = \frac{M_r}{M_i}, \tag{8}$$

which keeps track of both projectile and panel-related mass changes due to projectile impact. Now it can be assumed that the Va value can be calculated for each case, m, which ranges between 1 and N (the total number of data sets). Further, assuming the the initial and residual mass values are fairly constant then the following relationship, Eq. 9, is true:

$$(V_a^m)^2 = (V_i^m)^2 - k(V_r^m)^2 \tag{9}$$

where k is assumed to be constant for all m. The velocity terms can be redefined as seen in Eq. 10:

$$A_m = (V_i^m)^2; B_m = (V_r^m)^2; C_m = (V_a^m)^2 \tag{10}$$

which leads to a simplified form of Eq. 10

$$C_m = A_m - kB_m. \tag{11}$$

Billon goes on to mathematically solve for an explicit solution of the equation. If the average of Eq. 11 is taken, the following equation results:

$$\overline{C_m} = \overline{A_m} - k\overline{B_m} \tag{12}$$

where the average is the sum from 1 to N of the term divided by N. In order to meet the objective of minimizing the sum of the squared deviations from the mean value of C_m, S must be minimized as seen in Eq. 13

$$S = \Sigma_{m=1}^{N} C_m^2 - N\overline{C_m^2} \tag{13}$$

which can be expanded with the expressions for C_m and $\overline{C_m}$ and further expanded from the squared terms to give a full expression for S:

$$S = \Sigma_{m=1}^{N}[A_m^2 - 2kA_mB_m + k^2B_m^2] - N(\overline{A_m}^2 - 2k\overline{A_mB_m} + k^2\overline{B_m}^2). \tag{14}$$

Taking the derivative of this equation with respect to k and setting equal to zero, results in Eq. 15, an expression for k

$$k = \frac{\Sigma_{m=1}^{N} A_mB_m - N\overline{A_mB_m}}{\Sigma_{m=1}^{N} B_m^2 - N\overline{B_m^2}} \tag{15}$$

which can be solved with known quantities: $\overline{A_m}$, $\overline{B_m}$, $\Sigma_{m=1}^{N} B_m^2$, and $\Sigma_{m=1}^{N} A_mB_m$ to provide an explicit calculation of k. Billon goes on to prove that the second derivative of Eq. 14 is positive and therefore the value of S calculated from the k value is a minimum. Finally, the square root of C_m results in V_a without requiring the iterations of a least squares fit.

The direct calculation developed in this method is useful and provides a good estimate of ballistic limit without much mathematical manipulation. So both the

Jonas-Lambert and Billon methods estimate ballistic limit values helpful for defining ballistic properties in addition to simple velocity and energy comparisons. In comparing an example data set, Billon uses in his method to the results from using that data with the Jonas-Lambert method, the difference in resulting Vo estimation is within 1 m/s [4]. These methods were critical for developing a plan for testing and evaluating the thesis objectives with regards to ballistic testing. Additional discussion and application of these methods are presented in both the Design and Methodology chapter and the Results and Analysis chapter.

Projectile type and velocity.

With an understanding of a few models used to understand ballistic impact properties of materials, such as V_0 and V_{50}, it is important to recognize the firing parameters useful for conducting such a study. Studies focused on armor testing tend to use powder accelerated projectiles such as actual bullets their material might encounter. This method directly validates the ability of a material to stop a specified firearm threat, but it presents challenges for material research studies. The range needed to conduct such tests is complex and costly to obtain. It can also be difficult to adjust the velocity of the projectile, as it must be adjusted by changing the powder used in the shot, as demonstrated in the work by Pineda *et al.* [35]. Further, since most firearm projectiles are lead, finding residual velocities is difficult due to projectile fragmentation. Therefore for many scientific studies, a more controlled set-up is preferred. Ballistic testing by Loikkanen *et al.* of Boeing is representative of this type of controlled testing which uses a gas gun, a device that launches projectiles through a barrel with compressed gas [26]. This study involved panels of 8 to 32 plies of Boeing carbon fiber layed up in a quasi-isotropic arrangement. The projectiles used were half inch diameter steel spheres and steel cylinders. These two projectiles are common in

literature, with cylinders being utilized extensively to develop modeling simulations as presented in Micheli's work [27]. Loikkanen *et al.* fired projectiles at velocities of 100ft/s to 900 ft/s representing a high-speed jet engine fragment impacting composite targets [26]. The energy absorbed per ply was found through measuring the initial and exit velocity of the projectile. This study formed a basis for the present work in the choice of ballistic testing with a gas gun and half inch steel spheres to simulate high-speed debris impacts. Projectile velocities of hundreds of feet per second were also validated as being representative of high-speed debris by Stojadinovic *et al.* who modeled flyrock velocity from rock blasting [39]. They found that rock debris velocity from over 900 blasts was as high as 778 ft/s and averaged 240 ft/s [39].

Impact failure mechanisms and stacking sequence studies.

In addition to predicting the ballistic limit, it is also important to evaluate ballistic impact damage. Thus it is necessary to understand how composites typically fail and what panel production considerations can impact the results. One of the panel properties to consider is the stacking sequence of the material, especially when unidirectional material is utilized. Unidirectional material use is common practice for many composite materials, including carbon fiber. Carbon fiber is extensively used in aircraft fuselages and wings, such as in the Boeing 787 Dreamliner [40]. Baig *et al.* [3] studied the effects of ballistic impact on graphite/epoxy composites to develop models and understand the influence of laminate characteristics including stacking sequence and thickness [3]. His research focused on understanding the residual properties of the composite after impact. His work found that larger, slower projectiles produce more damage in the composite compared to faster, more pointed, smaller projectiles. He utilized both quasi-isotropic and cross-ply stacking sequences and noted that the quasi-isotropic panels had less damage due to less rigidity as compared with

the cross-ply panels as seen in Figure 12.

Baig [3] also studied the natural frequencies of different stacking sequences and found that the high-speed bullets with smaller ballistic damage had little impact on the natural frequencies of cross-ply panels, while it generally decreased the frequencies in the quasi-isotropic panels. For the higher damage tests the frequencies were reduced for both layups in the lower frequencies, and slight increases in some higher frequencies were observed.

In addition to experimental data, Baig put forward additional considerations for modeling the failure regions of the composite. He explains that composite failure is primarily caused by material deformation and the creation of new surfaces. The new surfaces take the form of delamination, fiber failure, and matrix cracking [3]. Delamination occurs when the layers of the composite material, or lamina, separate from each other. Fiber failure is characterized by the breaking of the fiber material from tensile or shear forces. Matrix cracking occurs when the resin matrix cracks independent of the fibers.

These failure modes can play out differently for different tests. For instance, it is important to understand the difference between low velocity and high-velocity failure responses. Ellis [12] in his work on graphite-epoxy ballistics, outlines the

Stacking Sequence	D_{11} N-m
$(0/90/\pm45)_s$	8
$[(0/90/\pm45)_2]_s$	52
$[(0/90)_4]_s$	62
$[(0/\pm45/90)_7]_s$	1990
$[(0/90)_{14}]_s$	2380

Figure 12. Bending Stiffness Terms for quasi-isentropic and cross-ply, thick and thin graphite/epoxy panels. Recreated from Baig *et al.* [3]

major mechanisms of composite failure for both low and high-speed impacts. In low speed impact, the material has time to bend, which engages the whole material, while high-speed impact has a localized effect on the material as illustrated in Figure 13.

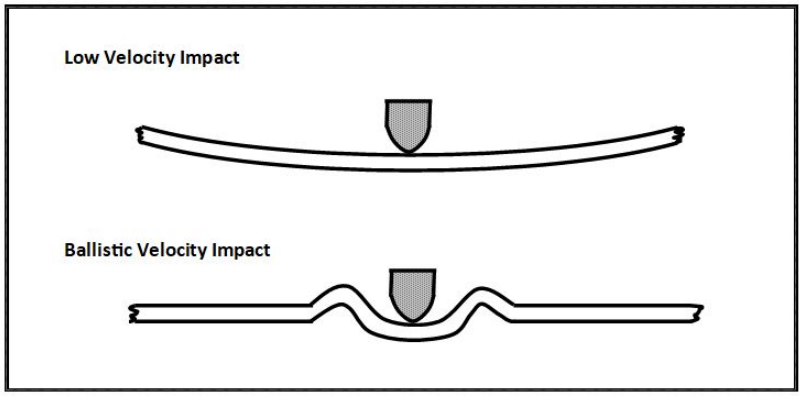

Figure 13. Representation of global deformation in low velocity impact and local deformation in high-velocity impact. Adopted from [12]

If the velocity is high enough, then the failure can be characterized as shear-plug type failure. Due to the high stresses created at the point of impact, the material around the perimeter of the projectile is sheared and pushed foreword causing a hole or "plug" slightly larger than the diameter of the projectile and increases as it penetrates the composite as seen in Figure 14 [12]. Understanding composite failure mechanisms is important for designing ballistic testing experiments and analyzing the results. The published works in this section on ballistic experimentation were valuable for setting up and evaluating the experiments conducted in this thesis.

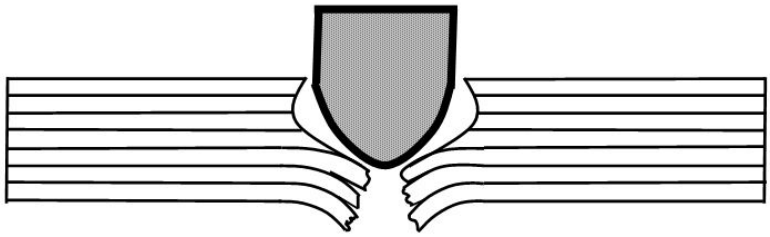

Figure 14. Schematic representation of the shear plug damage mechanism. Recreated based on [12].

2.5 Literature Review Summary

The preceding review of literature relevant to this thesis served to present the case for studying the ballistic properties of Nanocomp's CNT sheet product. Molecular level theories led to explorations of CNTs as resin reinforcements, followed by CNT mats being integrated into ballistic composites. The testing of the Nanocomp sheets thus far has focused on the electrical and thermal characteristics of the material, yet despite its appearance in commercial products, ballistic testing has not been published. This sets the stage for the current work, and additional literature review of ballistic testing of composite materials was conducted to form the basis for designing tests to adequately conduct initial testing of the hypothesis of this thesis. The objective of this thesis is to formally test the hypothesis that adding Nanocomp sheet material to carbon fiber panels, in addition to increasing the panel's electromagnetic shielding, will also improve the ballistic performance of the panel. The test methods used to evaluate this hypothesis will be laid out in the Methodology chapter based upon principles presented in the literature review.

III. Design and Methodology

3.1 Introduction

Upon conducting a literature review, the need to conduct experiments to further understanding of Carbon Nanotube (CNT) sheet material ballistic properties was exposed. The approach of this thesis will focus on evaluating the CNT sheet material as part of a typical carbon fiber composite panel that might incorporate a few sheets of CNT material for EMI shielding, thermal conductivity, or strength purposes as this is a realistic current application where the contribution to ballistic performance of the panel by the CNTs is unknown. This will primarily be accomplished by identifying changes in estimated V_0 values as well as projectile residual energy values for different configurations of CNT sheets within a thin carbon fiber composite panel. Material characterization of tensile properties, EMI shielding before and after impact, and damage region will also be conducted to further evaluate the influence of the CNT sheets on the panel properties.

3.2 Testing Background

From the literature review of methods it was found that for the purposes of our initial research investigations, a combined approach for the ballistic testing was suitable. This approach would involve comparing residual velocities of the projectile, estimating V_0 values using residual velocity results following the calculations developed by Lambert *et al.* [23] and Billon [4], as well as conducting V_{50} testing per MIL-STD-662F except without the witness plate. Having multiple methods of comparison available is helpful for validating results. The data provided from these tests then provides the ability to quantify the influence of adding CNT sheet material to thin, quasi-isotropic, carbon fiber composite panels.

The design for the composite panels to be used for testing the research hypothesis was then determined. Based on the high cost of the CNT sheet material and the research of Micheli *et al.* [27] and Grujicic *et al.* [16], it was decided that the research panels would consist of a relevant composite panel incorporating a few CNT sheets. It was determined that since quasi-isotropic carbon fiber is a common aerospace composite panel type, it would make a good test bed for integration of the CNT sheet material. As pointed out by Baig *et al.* [3], the quasi-isotropic orientation of the panels, plies in the 0,+/-45 and 90 degree orientations, should have less panel damage from ballistic impact than if a crossply orientation, only 0 and 90 degree plies, was used. This allows for closer shots on the panels. The carbon fiber used was laid up in a quasi-isotropic orientation following the stacking sequence, [45,0,-45,90—90,-45,0,45], resulting in 8 plies of carbon fiber. The CNT sheet material was placed in the middle to avoid panel warping and to allow for balanced scaling up of the CNT layer. Grujicic showed theoretically that CNT mats at the middle of an E-Glass panel performed well, only bested by having the CNTs near the front surface [16]. Additionally, the small thickness of the panel reduces the size of the damage area due to less shear plug damage [12]. A thin panel also keeps the ballistic limit within a velocity range obtainable with available test facilities at AFIT and lowers material costs.

The ballistic range utilized for this experiment consists of a gas gun which fires projectiles using compressed nitrogen at a pressure of up to 1800 psi. The projectiles used were 1/2 inch steel spheres. The spherical shape was chosen so as to minimize the experimental variables, since spheres will impact more consistently than fragment simulating projectiles, and the hard material will not break apart upon impact so that residual energy calculations do not lose accuracy due to trying to track a fragmented object. The gas gun set-up cannot accelerate projectiles fast enough to model most

firearms, but it does model high-speed debris, which can have a greater damaging impact on composite panels than supersonic bullets as noted by Baig *et al.* [3].

Experimental Design.

Having decided upon a host panel construction and ballistic profile for the projectile, it was necessary to define a test matrix that would provide appropriate data to test the research hypothesis. The first factor determined was how much CNT to put in the panels. Based on research for EMI sheilding, a single sheet of Miralon is sufficient for attaining over 40dB of attenuation. From the study conducted by Grujicic, 100μm of CNTs demonstrated significant improvement in ballistic properties for an E-Glass panel. Since Miralon has a typical thickness of 25μm, this would amount to four plies of the CNT product. Due to the high cost of material, limiting the study to these bounds, from one to four sheets was practical and sufficient to experimentally evaluate the material. The ballistic methods discussed benefit from having several sets of data, but at a minimum three sets are needed for the V_0 calculations. Based on the work of Baig, it was clear that secondary shots are not independent of the first shot, so in order to reduce sources of error, a minimum of three panels of each test case were needed for V_0 ballistics evaluation so that three independent center shot tests could be conducted. Additional shots could then be made on the panels used for V_0 estimation to collect data for estimating V_{50}. Multiple shots on a panel is expected per the Mil-Standard for V_{50} testing with care to keep shots outside of delamination regions necessary. In addition to the three panels required for V_0 and V_{50} testing, one panel per panel type was needed for mechanical testing and analysis. This brought the total to four panels per type needed to conduct the testing. As a margin of safety, a fifth panel per set made sense to have as a backup, and to provide additional data if needed after the initial testing. Based on this information a test

plan with 25 panels, consisting of 5 CNT sheet variations with 5 panels per variation, was suitible for obtaining sufficient data and optimizing cost.

The next factor to determine in the experimental design was the general shot pattern for multiple shots on the panels. Although the panel design elements of stiff carbon fiber material and a quasi-isotropic stacking sequence help lower the size of the damage area compared to other materials or stacking sequences, it was still important to estimate how big the damage area might be so that it can be determined how many shots on the panel can be taken. A 0.089" thick quasi-isotropic panel of IM7 carbon fiber prepregged with Cycom 5250-4 resin was used to provide an estimate of the damage area obtained from impact with the half-inch steel ball bearings at representative velocity. The center panel test shot resulted in a damage area of roughly $1.7in^2$ with 3/8 inch wide delamination along the fibers in the 45 degree ply on the back of the panel. Based on this estimate and the V_{50} procedures which dictate at least 2 projectile radii of separation between shots, it is reasonable that several shots could be made to the panels with potential shot locations as indicated in Figure 15 without damage overlap. This design allows for an initial center shot to be made followed by up to 8 shots around it to provide V_{50} data points while avoiding delamination overlap. The locations with double circles indicate the locations that are most spread out. The remaining four shots require careful attention to avoid delaminated zones from previous shots. With a plan for shot location established it was then important to determine the projectile velocities to be used one the panels. The models discussed for estimating V_0 require some variation in projectile striking velocity and benefit from shots fired much faster than the ballistic limit, as well as near the ballistic limit. Based on the literature review of projectile type and velocity, velocities in the hundreds of feet per second are relevant for simulating high-speed debris impact. With a 5 ft barrel, the AFIT gas gun can achieve 640 ft/sec at 1000

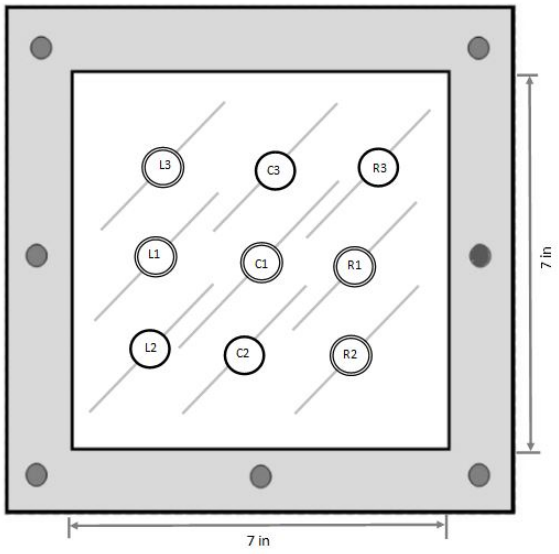

Figure 15. Graphic depicting shot placement on a panel mounted in the panel holder. The labels, such as C1,R2,and L3 indicate the shot location that will be recorded in the ballistic data.

psi with the half inch steel ball bearing. With this as a higher bound, the V_{50} of the 16 ply carbon fiber panel, which was found to be 352 ft/s, serves as a midpoint velocity where penetration of the thinner test panels is ensured. For the low velocity shots 180 ft/s was chosen. This was determined after the first two sets of data were collected and the residual velocities at 350 ft/s indicated significant residual energy. Assuming constant energy absorption by the panels, as used by Lambert and Billon, a guess for the limit velocity of the panels around 140 ft/s was determined, and a 40 ft/s increase was used to ensure penetration but still approach the limit velocity [23] [4]. The randomized testing order for the panels at the three velocities is presented in Table 1.

The information collected for the V_0 testing included included: projectile mass, impact velocity and residual velocity of the projectile. Because the high-speed tests should cause the smallest damage area to the panels, the panels with zero, two, and four sheets of CNTs shot at 640 ft/s, 1.2, 3.2, and 5.3 respectively, were selected to conduct more shots to estimate the V_{50} of the panels. The shot placement was

Table 1. Panel shot plan for one center shot on a panel from each panel type, 0-4 sheets of CNT, at 3 velocities, 640ft/s, 350 ft/s, and 180 ft/s.

Vimpact = 640 ft/s		Vimpact = 350 ft/s		Vimpact = 180 ft/s	
Shot #	Panel #	Shot #	Panel #	Shot #	Panel #
1	1.2	6	3.4	11	4.2
2	3.2	7	5.4	12	2.4
3	2.3	8	2.2	13	1.5
4	5.3	9	4.3	14	3.5
5	4.4	10	1.3	15	5.2

determined following Figure 15. The information collected for the V_{50} testing included projectile mass, impact velocity, and whether the projectile penetrated the panel. With a shooting plan formulated, the ballistic testing plan for determining the energy absorption of the panels is set.

The remainder of the test plan involved characterizing the panel and how the CNT sheets affect the panel damage area, and EMI shielding. These methods are well-established and are laid out in detail in the following sections. They are not dependent on the ballistic test plan and therefore were not critical considerations of experimental design outside of ensuring one panel per set could be used for physical property testing. Physical property testing involved making 3 tensile specimens from a panel of each type to be tested in an MTS machine using a strain gauge to measure the elastic modulus and ultimate strength of the laminates. It also involved cutting out smaller specimens which were put through an acid digestion process to determine the resin and fiber content of the panels. Additional testing conducted before and after ballistic testing included ultrasonic scans of the panels, to visualize impact damage area, and measuring the shielding effectiveness (SE) of the panels in a focus beam tunnel from 2-26.5 GHz.

In summary, a test plan consisting of five sets of five panels was constructed with each set having zero to four CNT sheets. The test shot plan to find the residual velocity relationships, V_0 and V_{50} estimations was developed to work with the 25 panel

production plan. Testing for material characterization and panel properties before and after ballistic impact was also presented. With this in place, the experiment was executed and conclusions made regarding whether adding the CNT sheets improved the ballistic performance of the panels by reducing projectile energy as well as by improving post-impact damage and EMI shielding characteristics.

3.3 Materials, Equipment, and Processes

Panel Production Setup.

With the experimental design established and the methods broadly outlined for conducting this research into CNT sheet ballistic properties, the specifics of the materials and equipment used will now be discussed.The panels were composed of Hexcel HM63 unidirectional carbon fiber and Nanocomp Miralon CNT sheet. The properties of both materials can be seen in Table 2.

Table 2. Material properties for Nanocomp Miralon CNT product and Hexcel HM63-12k carbon fiber

	Miralon CNT	HM63
FAW (gsm)	15	120
Thickness (μm)	25	100
RC (%)	65	35
TS (Mpa)	21-35	4688
p (g/cm³)	0.3-0.5	1.83

The materials were pre-impregnated with PMT-F6 resin by Patz Materials and Technologies. The Patz prepreg machine shown in Figure 16, applies a precise amount of resin to the material and rolls it up on a backing material. It is then kept at sub 10°F temperatures and shipped in dry ice. Kept at very low temperatures, the prepreg material is good for 12 months. The date of manufacture for both materials was 23 October 2018 and the lot numbers were PP18326-1 for the carbon fiber and PP18326-

2 for the Miralon CNTs. Due to the unavailability of 12" wide Miralon product, the material used for this project was 9.5" wide for both the CNT sheet and the Hexcel carbon fiber prepregs.

PMT-F6 is a cyanate ester resin system with a cure temperature of 350 °F and a glass transition temperature, Tg, over 550 °F. The cure cycle for the PMT-F6 resin provided by the company is depicted in Figure 17. This type of resin was chosen due to its excellent integration with Miralon CNT sheet product as a prepreg resin and prevalent use in aerospace applications. One reason for the good integration is that the resin doesn't use a particulate catalyst hardener which may get filtered out through the CNT mat. To cut the material, razor blades were used along with a cutting template, as seen in Figure 18, to ensure consistent cuts. A 45° measuring triangle was used to align the template for cutting the 45° plies.

After being cut and stacked, the material was compacted together using a vacuum table. The Heatcon Composite Systems vacuum table applies around 27 psi of vacuum. The stacks of material are placed between sheets of non-porous Teflon with a sheet of porous teflon and polyester breather on top so the pump can pull vacuum through the entire table area. The table also has temperature control, a feature used when tabbing the tensile test specimens.

For preparing the panels for curing in an autoclave, tacky tape, porous and non-porous Teflon sheets, polyester breather and bagging film were used to prepare the panels for autoclave processing as depicted in Figure 19.

This layup was deemed appropriate as it is a common autoclave arrangement for composite material curing, particularly when resin content is controlled (as in a prepreg material) and not much needs to be bled out of the panel. The CNT sheets are prepared more resin rich than the carbon fiber due to their thinness and to ensure resin coverage through the random distribution of CNTs that make up the mat. In

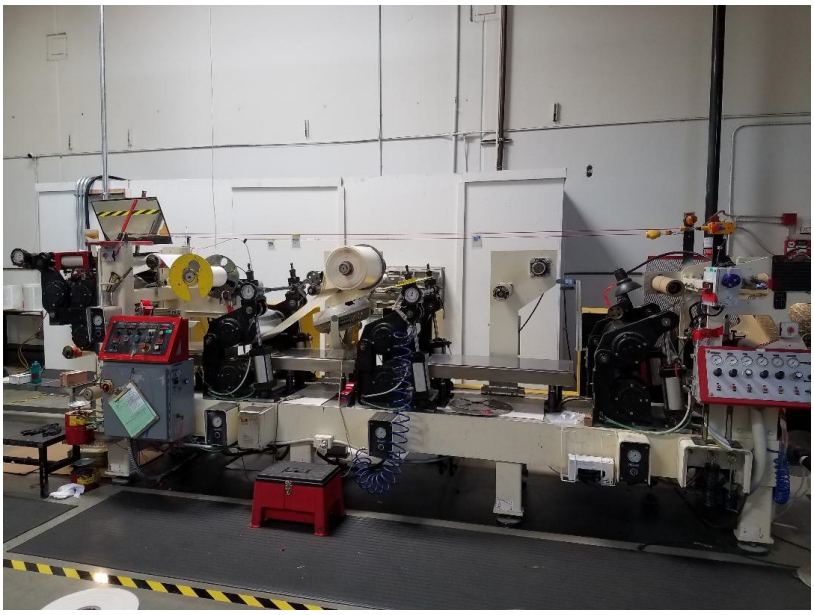

Figure 16. Prepreg assembly at Patz Materials and Technologies

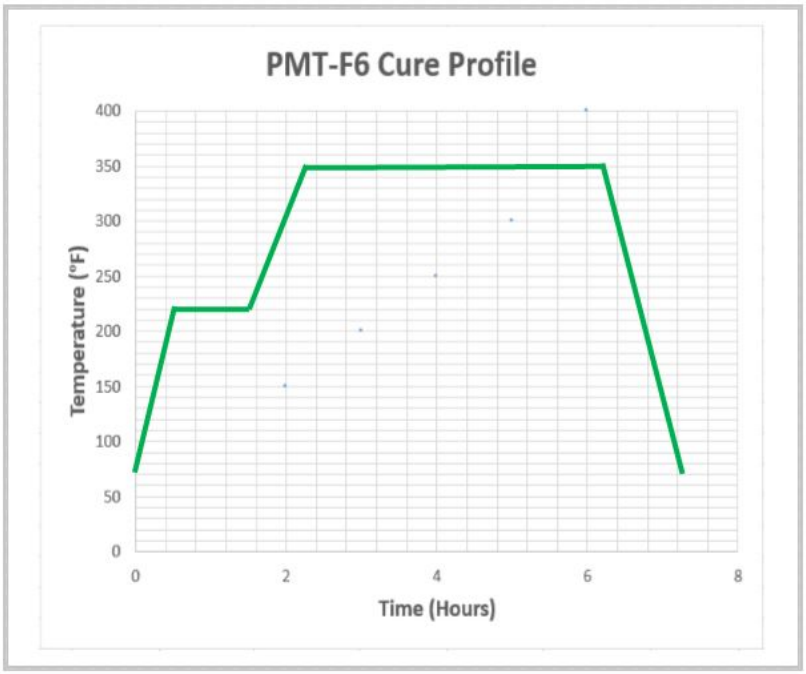

Figure 17. Cure cycle for PMT-F6, cyanate ester, resin system.

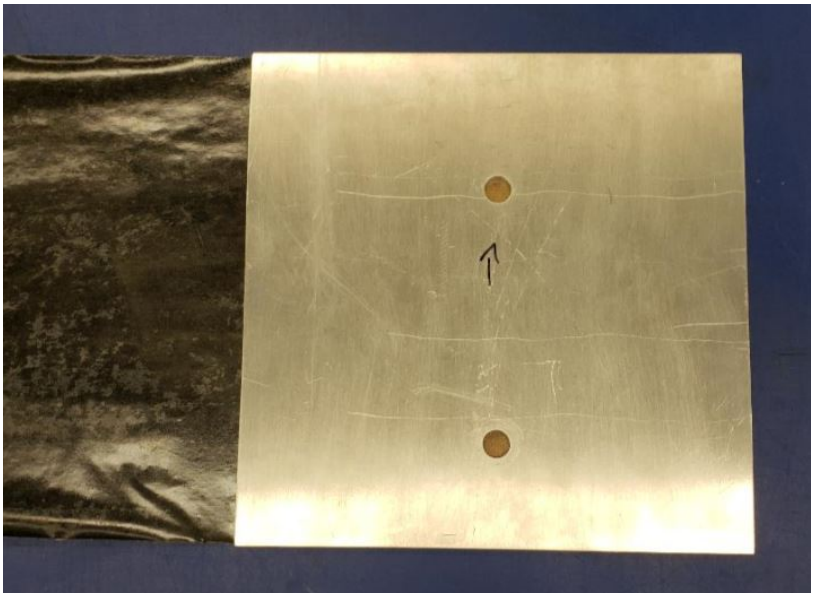

Figure 18. Aluminum 9.5"x9.5" cutting template used to cut out carbon fiber and Miralon CNT sheet prepreg.

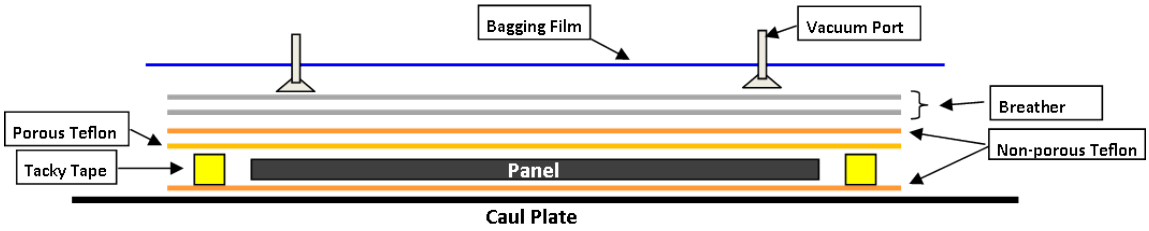

Figure 19. Diagram of panel preparation for autoclave curing

order to determine if bleeder cloth was needed to remove some of the CNT resin, three 2"x2" test samples were processed to ensure adequate curing and resin content. One sample was 20 plies of carbon fiber, the next was 20 plies of CNTs, and the final one consisted of a mixture of 10 plies with six plies of carbon fiber and four plies of CNTs. The samples were arranged in a symmetric crossply (0/90) arrangement for simplicity. The samples were checked for good processing by visual inspection and C-Scan results, which indicated uniform density (outside of the edges) without any measurable regions of voids or resin richness as seen in Figure 20.

The tacky tape used smeared over the edge of the thinner all-CNT and mixed panels causing larger edge effects compared to the thicker carbon fiber panel which

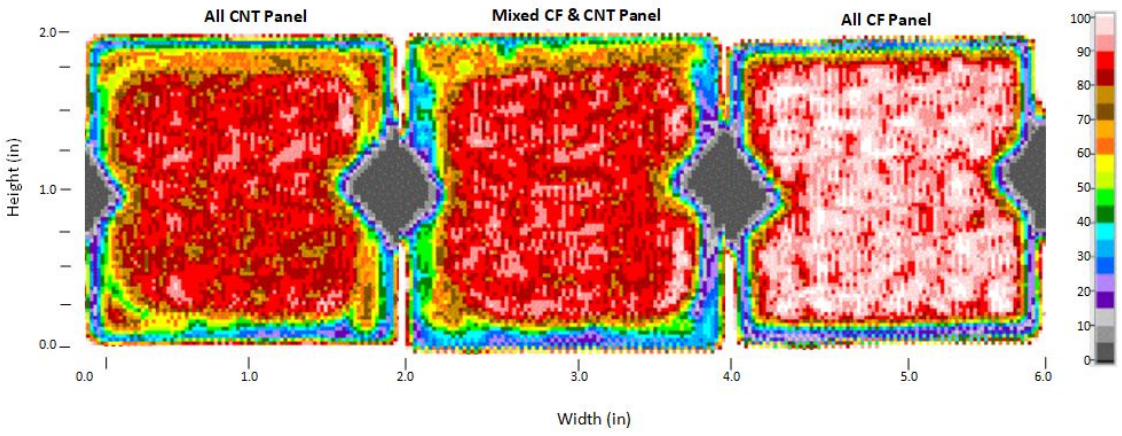

Figure 20. Ultrasonic scan (C-Scan) of 2"x2" samples consisting of 20 plies of CNTs, 10 plies of mixed CNT and carbon fiber plies, and all carbon fiber.

was closer to the thickness of the tape. For final panel production a more rigid tacky tape was used to reduce edge effects.

The autoclave used for all of the panel processing was an ASC Process Systems Autoclave, which can fit specimens up to 30"x36" in area. The autoclave can apply controlled pressure, temperature, and vacuum to cure composite resin systems. Within the autoclave, four prepared panels could be fit in a square pattern on a 30"x30" steel tool plate covered with a sheet of Kapton, a high temperature resistant film material. A single vacuum port was utilized and 2 thermo-couples, with J-type plugs, were placed near the panels to measure the part temperatures which guide the autoclave operation. Due to high humidity levels, around 46% relative humidity, during the material cutting process, an extra hour at 100°C was added to the autoclave cycle to bake out moisture prior to curing the resin. The final cure cycle with representative results can be seen in Figure 21. This concludes the materials and equipment used to make the panels for this research.

Figure 21. Autoclave software plot of planned cure cycle and the resulting temperature, pressure, and vacuum values from the cycle run for the PMT-F6 resin composite panels

Gas Gun Setup.

The ballistic range gas gun consists of a pressure tank, valve, and barrel. The barrel is made with a half inch inner diameter smooth-bore steel tube. The the gun has an air tank which is pressurized by a standard industrial nitrogen tank that holds 330 cubic feet of nitrogen at 2500 PSI. A Sensotec PPG/E981-05-01 pressure transducer, with a range up to 2500 PSIG, provides pressure values within the gun's air tank. The voltage values from the transducer are read through a National Instruments USB data aquisition system, NI USB-6210, to a laptop which uses LabView software with the appropriate conversions to read out the pressure. A Marotta MV74 solenoid valve is used to fill the gun air tank, which is rated to 1800 psi. Another Marotta MV74 valve is incorporated at the gun tank to release pressure if needed. The valve used for firing the gun is a Circle Seal Controls type SV430 solenoid valve. This valve can hold up to 3000PSI, has a valve coefficient (Cv) of 0.80, and has a verticle stroke length of .032". All of these valves are wired to a 24V power supply and to an electronic safety.

While the gas gun had been developed for prior research, a bullet catcher and test panel holder was developed as part of this project. The main frame utilizes 80/20 products consisting of 1.5 inch square aluminum tubing, aluminum brackets, and 3/4" long 3/8" diameter hexhead screws. The walls of the test frame are made of 1/2 inch thick polycarbonate sheets. The backing for stopping projectiles consists of a box of sand, 9 inches deep, followed by two 3/8 inch thick panels of marine grade plywood coated with Herculiner (TM by Old World Industries, LLC) truck bed liner. Finally, behind this is a 1/2 inch thick steel plate. The panel holder was designed based on engineering concepts and previous literature, such as the work done by Resnyanski and Katselis who utilized two metal frame pieces which were bolted together around the test panel and then bolted into a stand which could rotate to allow for testing at angles[37]. The final design, constructed out of 1/4 inch thick steel, is shown in Figure 22. For measuring the velocity of the projectile before and

Figure 22. Panel holder designed to rigidly support composite panels for ballistic testing. It includes the ability to rotate the stand in 15 degree increments to test materials at an angle.

after impact, three Caldwell Ballistic Chronographs are used. These chronographs are accurate to within 0.25% which means about 1.5 ft/sec of uncertainty for a shot fired at 600ft/sec. They were also equipped with an IR light attachment to aid in preventing errors due to fluorescent lighting in the range. The chronographs are used in conjunction with a Phantom v12.1 high-speed camera. The camera was set to a pixel window of 512x830 and a frame rate of 28,000 fps. The camera provides visual information about the impact behavior and a reliable calculation of projectile velocities through digital image correlation. A picture of the bullet catcher set up can be seen in Figure 23. In order to scale the camera pixels to a distance, a 90°

Figure 23. Picture of the Phantom high-speed camera and bullet catcher with panel mounted inside for ballistic testing

angle measuring device was taped to a test panel just bellow the impact area of the projectile. The inches per pixel could then be calculated based on images taken of the

scale. With the frame rate of the camera known, the velocity of the projectile could then be calculated by dividing the distance traveled by the time interval between frames. Calculating the velocity this way was done both through a MATLAB code and through the Phantom Camera Control software. Using the camera's software proved to be accurate to within 3.34 ft/sec when the distance traveled was measured over 14 frames. Figure 24 shows the picture of the scale used to calibrate the camera pixel measurements. The projectiles fired from the gas gun were 1/2 inch spherical

Figure 24. Calibration picture of a scale used for determining the pixel to distance ratio of the Phantom 12.1v high-speed camera operating at 28,000 fps.

steel ball bearings from McMaster-Carr. The ball bearings were fired in conjunction with an oiled .014 inch thick cotton shooting patch, produced by Ox-Yoke Originals, often used in muzzle-loading firearms. The shooting patch was used to seal the ball bearing in the barrel and not let the air blow out past the projectile. In order to validate the patch fit, the Schlieren method was used to visualize gas flow out of the barrel when the gas gun is fired. Figure 25 presents three pictures taken from the Schlieren video of a test firing of the gas gun. This test showed that the patch and projectile create a good seal in the barrel and don't allow significant amounts of gas to leak during firing.

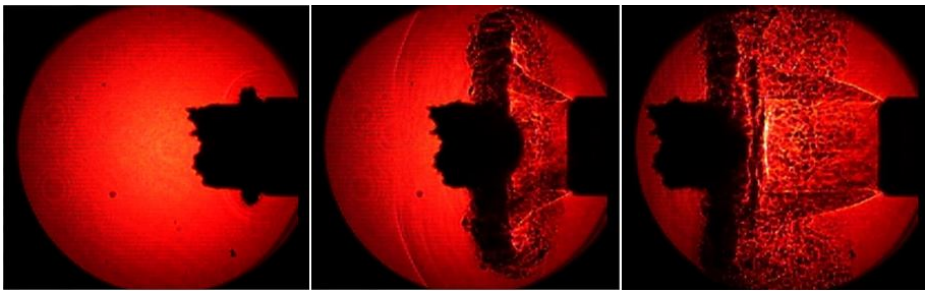

Figure 25. Snapshots from Schlieren flow visualization on the AFIT nitrogen gas gun at 1000PSI with a 1/2" diameter steel ball projectile with a .014" thick oiled shooting patch sabot.

Characterization Equipment.

In order to characterize the mechanical properties of the panels produced, one of the panels from each set of five was designated to be used for characterization of the panels. Each panel had a three and a half inch wide by eight inch section cut out in order to make three one inch wide by eight inch long specimens for tensile testing according to ASTM D3039 [2]. The panels were cut out using a diamond bladed wet saw, depicted in Figure 26. The tabs for the tensile test specimens were made out of 0.062" thick G-10, a fiberglass and epoxy composite commonly used in composite tabbing. Both the tabs and the tabbing area of the specimens were cleaned with acetone and grit blasted to prepare the surfaces for bonding. The bonding agent used was Loctite EA 9394 AERO, batch number JH6MAA2680. This two-part structural paste adhesive is mixed with a ratio of 100 to 17 for Part A and Part B respectively and has a pot life of 90 minutes. It provides 4,200 psi of tensile lap shear strength at room temperature and performs well at temperatures up to 350°F where it still holds up to 1,200 psi [18]. Scrim cloth was used when adhering the tabs to the specimens to control the bond thickness. In order to protect the panel and tabs from extra adhesive the unbonded surfaces were covered in flash breaker tape. Additionally the tape was used to keep the tabs aligned during curing. While the adhesive can be cured at room temperature for seven days, a much faster cure can be obtained at an elevated

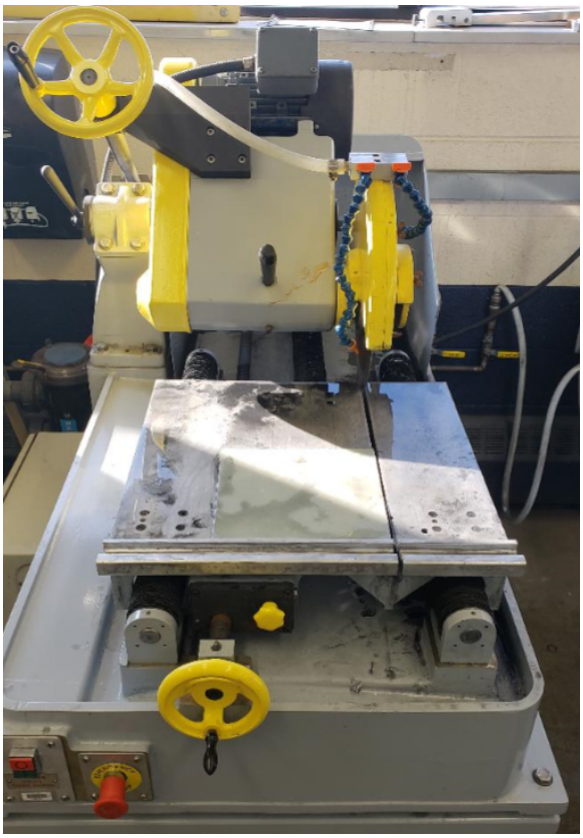

Figure 26. Wet saw with diamond blade used for cutting composite panels and tabbing material

temperature [18]. Therefore the tabbed specimens were placed in a temperature controlled vacuum table and held at 180°F for 90 minutes while remaining under vacuum for 24 hours.

The tabbed panels were then cut into 1" wide specimens using the diamond blade wet saw and strain gauges, 350 ohm gauges from Vishay Precision Group with a Gage Factor of 2.105, were attached in the center of the gauge section as seen in Figure 27. The specimens were then clamped into an MTS model 810, a 22 KIP servo hydraulic material testing machine. The strain gauge was then connected to a P3 data recorder and balanced. The test involved loading the specimen at a strain rate of $10^{-}3$ in/min until failure. The recorded data from the P3 strain gauge data recorder provided the material elastic modulus and ultimate tensile strength through a MATLAB code

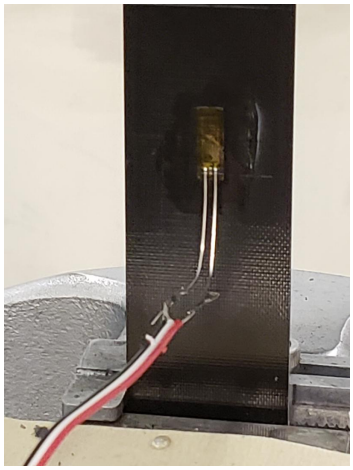

Figure 27. 1" wide by 8" long specimen clamped in the MTS grips with a 350 ohm strain gauge attached in the center of the 3.66" gauge section.

attached in the Appendix. These values could then be plotted and compared for all five test cases.

Another characterization test used in this study was an acid digestion to determine the fiber and resin volume fractions in the completed panel types. In order to do this, three half inch by three quarter inch specimens were cut out from the mechanical properties panels. First the weight and density of the specimens were found using a scale and a water based density measuring scale device pictured in Figure 28.

The specimens were then dried out in an oven at 101°C overnight. After this the resin and fibers were separated using nitric acid. The acid digestions were conducted in a ventilated hood. 30-40mL of acid was mixed with the specimens in round bottom flasks. The flasks were then placed in a heating system and a water cooled condenser was attached to the top of the flasks as seen in Figure 29. The flasks were heated and left for six hours to dissolve the resin in the specimens. The fibers were filtered out of the acid, which was discarded properly, and rinsed with distilled water. The fibers were then baked at 101°C for 24 hours before being weighed and put back in the oven. The fiber weight was measured two subsequent times in 24 hour intervals for each sample to ensure all the moisture had been baked out and all that was left

Figure 28. Water weight and dry weight scale device with thermometer to adjust the density of water value used to calculate specimen density.

was fiber. This information allowed the volume fractions of fiber and resin to be calculated given the resin and fiber density values.

The other main piece of equipment to be used to characterize the panels is an AFRL focus beam tunnel which is used to evaluate electromagnetic shielding. The device shown in Figure 30 consists of frequency horns enclosed in aluminum frame on either side of an opening for placing materials to test the transmission of signals through the sample. The focus beam tunnel has a sound floor of approximately -80 dB and has a frequency range of 2-26.5 GHz. This was used to get values, in dB, of signal attenuation, and thus EMI shielding, before and after impact to help understand multifunctional damage to the panels from the ballistic impacts.

In order to measure the damage area in the panels due to impact and confirm good autoclave curing of the panels, C-Scan equipment will be used to provide a density map of the panel through ultrasonic wave propagation through the material. The system used was manufactured by Wesdyne and consists of a water tank and

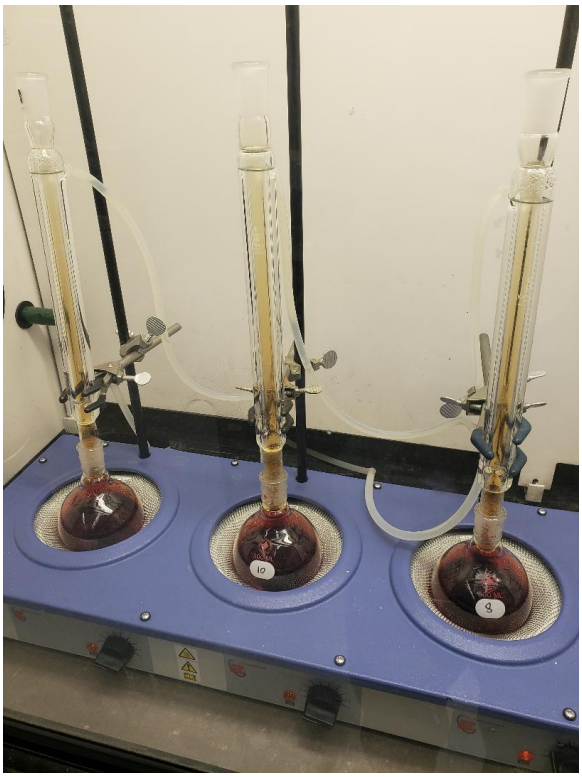

Figure 29. Acid digestion experimental set up in a ventilated hood. Round bottom flasks with nitric acid and panel specimens placed in a heating unit and water cooled condensers attached to the top of the flask.

a measurement arm with a 5 Ghz ultrasonic probe which scans across the part and provides a density map scaled to the highest density observed in the scan. The C-Scan test equipment can be seen in Figure 31.

This section has discussed the main materials and equipment used for accomplishing the goals of this research. Additional information on the materials or equipment can be obtained by contacting the author.

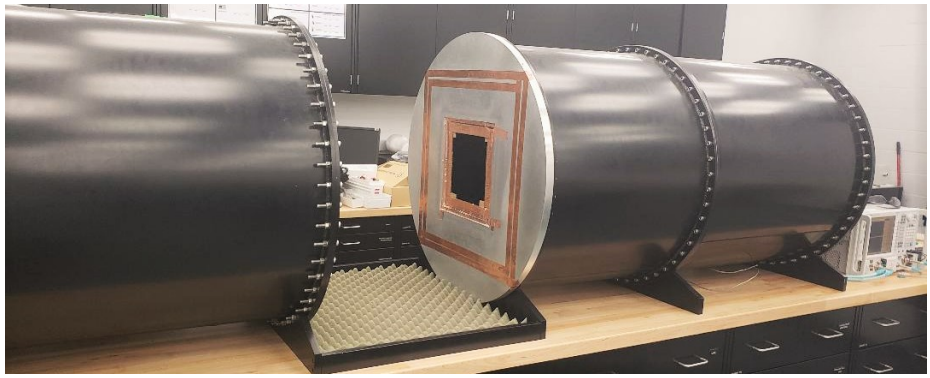

Figure 30. Focus beam tunnel with a frequency range of 2-26.5 Ghz for testing the transmission of signals through test samples placed in the opening of the system.

Figure 31. Wesdyne utrasonic scan equipment used to map the density of the composite panels. This was used for ensuring good consolidation of the panels from autoclave curing as well as for determining delamination area in the panels after ballistic impact.

3.4 Procedures

Having discussed the equipment, materials and processes, the order and procedure for conducting the present research will be laid out.

Panel Production.

The material was hand cut using razor blades into 100 sheets of 0/90 orientation carbon fiber, 100 sheets of +/-45 orientation carbon fiber, and 50 0/90 Miralon CNT sheets to make the 25 panels. After being cut, the material was stacked, in groups of 4 plies and put in the vacuum table at 20-30 psi for 15-20 minutes.The pressed stacks of four are then stacked together (along with the required sheets of CNTs) and vacuumed together.

The panels were then prepared, four at a time, for the autoclave using the diagram in Figure 19. Figure 32 shows the panels on the tool plate as cured in the autoclave. The panels were cured in the autoclave following the cycle shown in Figure 17 for four hours at 350°F and cooled before being removed and trimmed on the diamond saw to exactly 9x9 inches. In total, 25 panels were made according to the test plan. Five groups of five panels with each group containing panels with 0-4 CNT sheets.

Mechanical and EMI Testing.

Once all of the panels were prepared, ultrasonic scans were conducted to provide baseline plots of the panel density. Each panel was submerged in the water tank and the 5GHz measurement head traversed the panels via computer controlled servo-electric motors to create two dimensional plots of the material density. Next one panel from each set had a 3.5" wide by 8" long section cut out making tensile testing specimens. The gauge section was tapped with flash breaker tape, and the tabbing area was cleaned and grit blasted to prepare for tabbing as seen in Figure 33. The

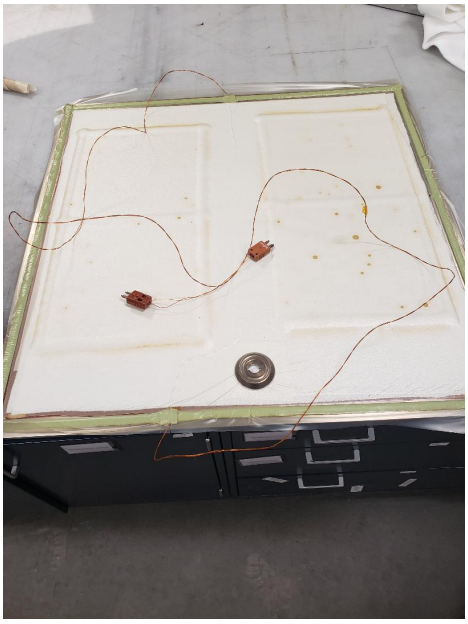

Figure 32. Four panels packaged for autoclave cure.

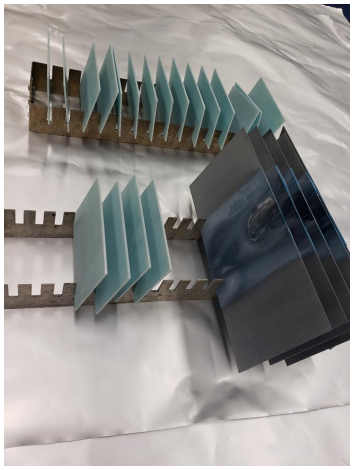

Figure 33. 3.5” wide by 8” panel sections and G10 tabs, grit blasted and ready for tabbing.

tabs were then adhered to the specimens and cured. Three one inch wide specimens were then cut out of the panel sections. Strain gauges were attached to the middle of the gage section on the specimens. The specimens were then mounted in the 22 KIP MTS machine. The bottom of the specimen was clamped, then the top, and the strain gauge attached to the P3 data recorder. The specimens were then pulled until fracture.

For the volume fraction measurements, three 1/2" inch by 3/4" specimens were cut out from the panel used for the tensile specimens. The thickness of the specimens was measured and they were weighed, both dry and in distilled water. From these measurements, the specimen density was calculated by relating the density of water to the change in weight of the specimen between the two weight measurements as seen in Equ. 16

$$D_s = \frac{W_d}{W_d - W_w} * D_w + D_a \tag{16}$$

where D_s is the specimen density, D_w is the density of the water, D_a is the density of air, and W_d and W_w are the dry and wet masses of the specimens respectively. Following this, the specimens were dried out in an oven at 101 °C for 24 hours. The specimens were then dissolved in the nitric acid in a heated round bottom flask for 6 hours, before the fibers were filted out and dried in an oven for 24 hours. At the completion of 24 hours of drying, the fibers were weighed on a scale. Two more times, the fibers were dried for 24 hours and reweighed to ensure complete drying. Given the weight of the fibers, the density and weight of the original specimen, and the published densities of the resin (1.199 g/cm^3) and fibers (1.83 g/cm^3), the volume fractions were determined.

The remaining four panels from each panel set, not used for material property specimens, were tested in the focus beam tunnel across the frequency range, 2-26.5 GHz, to establish the EMI shielding for each panel set. The system was calibrated

for air with a 9"x9" opening and then a panel was sealed into the opening with copper tape. It was then subjected to a signal sweep over the frequency range and the residual signal was recorded and processed to provide the dB of signal attenuation observed. With all of these characterization tests accomplished, the panels were then ready for ballistic testing.

Ballistic Testing.

Prior to ballistic testing, 3-4 test shots would be fired through the gas gun to help ensure consistent shot velocity and that all systems were operating properly. The panels were then mounted in the panel holder in the order of the test plan using 16, 1/4" diameter hexhead bolts, tightened to a comfortable hand tightness. The panel holder was then bolted to the test frame using 7 1/2" diameter hexhead bolts. The 1/2" diameter steel ball bearing was then pushed with a firing patch sabot from the muzzle back against the valve. The gas gun tank was then pressurized to the prescribed pressure. The high-speed camera was then triggered and the shot fired. The three chronograph velocities were recorded, the high-speed camera video saved, and pictures of the damage to the panel were taken. The panels were then removed from the test frame and panel mount.

Following the initial ballistic testing of one shot per panel, the panels were tested again in the focus beam tunnel to determine the EMI shielding post impact. Once the EMI shielding testing was completed, ultrasonic scans were conducted to visualize the damage area in the panels. With this data collected, the three panels to be used for V_{50} testing, 1.2, 3.2, and 5.3, were shot eight additional times in the locations specified by Figure 15. The impact velocities from the two chronographs in front of the specimen were recorded as well as whether the shot penetrated the material. The velocities shot were adjusted during testing in order to achieve at least three penetrating and

three non-penetrating results. The V_{50} testing concluded the experimental work done for this research.

This chapter has provided the necessary information used to design and implement the research experiments. It allows project repeatability as it details the materials, processes, and information that was collected and analyzed to evaluate the influence of CNT sheets on the ballistic performance of carbon fiber composite panels.

IV. Results and Analysis

The goal of this chapter is to present the results and analysis obtained following the experimental methods outlined in the previous chapter. The goal of these experiments was to explore the hypothesis that the integration of CNT sheet materials would improve upon the ballistic properties of carbon fiber panels subjected to high-speed debris type impact. The three primary categories of experimentation included panel construction and characterization, projectile energy reduction for varying numbers of CNT sheets between one and four, and finally the resulting delamination area and changes in EMI shielding caused by the high-speed impact.

4.1 Panel Construction and Characterization Results

Based upon the experimentation plan, 25 panels were produced. All of the panels consisted of a base panel of carbon fiber with a quasi-isotropic stacking sequence of eight plies arranged as follows: [45/0/-45/90|90/-45/0/45]. The five sets of panels contained 0-4 plies of Nanocomp Miralon CNTs at the mid-plane of the laminate. The resulting panel ply sequences are depicted in Figure 3. The panels were labeled in the form of "A.B" where "A" ranges from 0-4 representing the number of CNT sheets in the panel, and "B" ranges from 1-5 indicating the panel number within the set of panels established by "A".

Table 3. Ply stacking sequences for each of the five panel configurations.

Panel Set CNT Sheets	Ply Stacking Sequence
0	[45 / 0 / -45 / 90 | 90 / -45 / 0 / 45]
1	[45 / 0 / -45 / 90 / CNT(0) / 90 / -45 / 0 / 45]
2	[45 / 0 / -45 / 90/ CNT(0) / CNT(0) / 90 / -45 / 0 / 45]
3	[45 / 0 / -45 / 90 / CNT(0) / CNT(90) / CNT(0) / 90 / -45 / 0 / 45]
4	[45 / 0 / -45 / 90 / CNT(0) / CNT(90) / CNT(90) / CNT(0) / 90 / -45 / 0 / 45]

The first panel, 0.1, was cured in the autoclave by itself to validate the autoclave procedures. The panel appeared properly cured from visual inspection, but to ensure that regions of large voids or resin over-saturation did not exist, the panel was ultrasonically scanned resulting in the two dimensional plot of panel density seen in Figure 34. This scan showed a fairly uniform panel density with only the top left corner indicating poor properties. This may have occurred due to the panel not being flush against the backing plate in that corner of the ultrasonic test fixture, allowing a gap to exist. After reviewing the scan, the rest of the panels were processed in groups of four. The subsequent C-Scans of the panels showed very uniform density results. Figure 35 is representative of the rest of the panel scans.

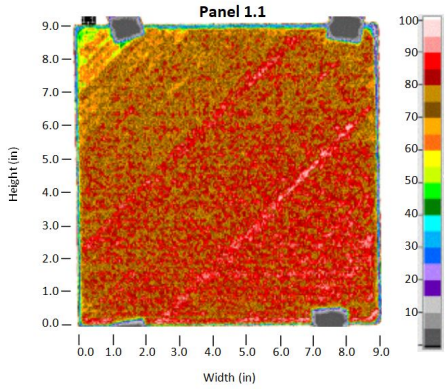

Figure 34. Ultrasonic scan results of panel 1.1 showing fairly uniform panel density.

To further characterize the panels, the volume fractions of resin and fiber were measured through acid digestion. The 1/2" by 3/4" specimens were weighed both dry and in $68-73$°F distilled water. The dry weight, wet weight and calculated specimen densities are listed in Table 4. Nominally, the resin has a density of 1.199 g/cm^3, and the fiber has a density of 1.83 g/cm^3. Upon completion of the acid digestion process, the fibers were filtered out using distilled water and placed into aluminum specimen trays. Interestingly, while the carbon fibers split up as a result of the acid digestion, the CNTs remained bundled together as seen in Figure 36.

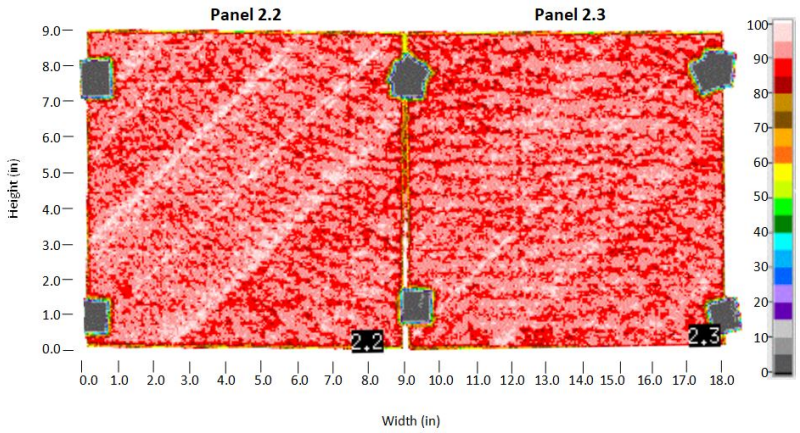

Figure 35. Ultrasonic scan results of panels 2.2 and 2.3 showing very uniform panel density represented by the white and red colors in the panel.

Figure 36. Carbon fibers and CNT clump after nitric acid digestion of the cyanate ester resin.

Once all the specimens were dried out and weighed three times the volume fractions were calculated out with the results tabulated in Table 5. From these values the average mass fraction and volume fraction values for each panel set was determined, as seen in Table 6. The nominal resin percentage by weight of the carbon fiber prepreg was 35%, so it follows that the cured panels with no CNTs would have a resin content by weight slightly lower than this value due to bleed off of resin into the layup materials. For the all carbon fiber samples the weight percent of resin was 31.79%, indicating that a small fraction of the resin bled out during curing as

Table 4. Specimen density values used in volume fraction determinations

Panel - Sample number	Thickness Measurement 1 (mm)	Thickness Measurement 2 (mm)	Dry Weight (g)	Wet Weight (g)	Water Density (g/cm^3)	Air Density (g/cm^3)	Sample Density (g/cm^3)
0.1 - 1	0.948	0.964	0.3316	0.1178	0.99814	0.0012	1.5493
0.1 - 2	0.958	0.972	0.3388	0.1220	0.99813	0.0012	1.5610
0.1 - 3	0.975	0.975	0.3410	0.1206	0.99813	0.0012	1.5455
1.1 - 1	0.996	1.011	0.3453	0.1225	0.99760	0.0012	1.5473
1.1 - 2	1.017	1.000	0.3498	0.1261	0.99800	0.0012	1.5618
1.1 - 3	1.012	1.015	0.3490	0.1251	0.99802	0.0012	1.5568
2.1 - 1	1.002	1.002	0.3454	0.1234	0.99804	0.0012	1.5540
2.1 - 2	1.040	1.001	0.3565	0.1281	0.99805	0.0012	1.5590
2.1 - 3	1.018	1.017	0.3496	0.1244	0.99806	0.0012	1.5506
3.1 - 1	1.071	1.081	0.3694	0.1308	0.99808	0.0012	1.5464
3.1 - 2	1.092	1.088	0.3784	0.1336	0.99809	0.0012	1.5440
3.1 - 3	1.085	1.097	0.3794	0.1330	0.99811	0.0012	1.5381
4.1 - 1	1.067	1.081	0.3755	0.1330	0.99811	0.0012	1.5467
4.1 - 2	1.108	1.115	0.3827	0.1333	0.99813	0.0012	1.5328
4.1 - 3	1.067	1.090	0.3758	0.1274	0.99813	0.0012	1.5113

expected. The final fiber volume ratio of 57.85% matches well with desired results for typical carbon fiber reinforced composite panels of 57-60% volume ratio of fibers [6]. Due to the high resin content in the CNT sheet material, 65% by weight, it also makes sense that the panel resin content would increase with increasing numbers of CNT sheets in the panel. Thus the increase in resin mass percentage from 31.79% to 37.04% is expected and reasonable. To minimize the effects of the high resin content in the CNT sheets, thin fiberglass bleeder sheets placed on top of the panel can draw out additional resin from the laminate during curing. It is the opinion of the author this might easily lead to over-extraction of resin from the carbon fiber plies and thus hinder ply bonding and introduce regions with significant voids if not carefully designed.

While the percentage seems to increase by about 2% for each sheet of CNTs, that is not the case in panels with 2 sheets of CNTs. In this case, the resin content by weight increased by only 0.19% from the panel with one ply. The value is not alarming, but it does represent that the panel must have had more resin bleed off than the other panels in the autoclave. This may be due to extra space between the

Table 5. Dry fiber weights and resulting volume fraction values

Panel - Sample number	Dry Fiber Weight 1 (g)	Dry Fiber Weight 2 (g)	Weighing Pan Dry Weight (g)	Mass Fraction Fiber	Mass Fraction Resin	Volume Fraction Fiber	Volume Fraction Resin	Volume Fraction Void
0.1 - 1	0.2272	0.2272	2.5924	0.6852	0.3148	0.5801	0.4068	0.0131
0.1 - 2	0.2298	0.2301	2.6346	0.6792	0.3208	0.5793	0.4177	0.0030
0.1 - 3	0.2324	0.2326	2.5543	0.6821	0.3179	0.5761	0.4098	0.0142
1.1 - 1	0.2303	0.2302	2.7244	0.6667	0.3333	0.5637	0.4302	0.0062
1.1 - 2	0.2350	0.2350	2.6445	0.6718	0.3282	0.5733	0.4275	-0.0008
1.1 - 3	0.2342	0.2340	2.7186	0.6705	0.3295	0.5704	0.4279	0.0017
2.1 - 1	0.2306	0.2306	2.6809	0.6676	0.3324	0.5669	0.4308	0.0023
2.1 - 2	0.2384	0.2381	2.6238	0.6679	0.3321	0.5690	0.4318	-0.0008
2.1 - 3	0.2335	0.2335	2.7150	0.6679	0.3321	0.5659	0.4295	0.0046
3.1 - 1	0.2396	0.2395	2.6819	0.6483	0.3517	0.5479	0.4535	-0.0014
3.1 - 2	0.2441	0.2436	2.6679	0.6438	0.3562	0.5432	0.4587	-0.0019
3.1 - 3	0.2425	0.2421	2.6652	0.6381	0.3619	0.5363	0.4642	-0.0005
4.1 - 1	0.2397	0.2394	2.7066	0.6375	0.3625	0.5389	0.4676	-0.0064
4.1 - 2	0.2408	0.2406	2.6862	0.6287	0.3713	0.5266	0.4747	-0.0013
4.1 - 3	0.2344	0.2340	2.6803	0.6227	0.3773	0.5142	0.4756	0.0102

Table 6. Average mass and volume fraction values for each panel set

Panel	Avg. Mass Fraction Fiber	Avg. Mass Fraction Resin	Avg. Volume Fraction Fiber	Avg. Volume Fraction Resin	Avg. Volume Fraction Void
0.1	0.6821	0.3179	0.5785	0.4114	0.0101
1.1	0.6697	0.3303	0.5691	0.4285	0.0024
2.1	0.6678	0.3322	0.5673	0.4307	0.0020
3.1	0.6434	0.3566	0.5424	0.4588	-0.0013
4.1	0.6296	0.3704	0.5266	0.4726	0.0008

tacky tape and panel when it was prepared for autoclave curing or due to lower resin content in those specific plies of CNTs. Outside of this minor anomaly, the results of the acid digestion demonstrate that the panel bagging process and autoclave curing resulted in appropriate values of resin content in the finished products.

The characterization of the mechanical properties of the panels was completed through tensile testing samples from each of the panel types. The 3.5" by 8" sections were cut out of the characterization panels with the wet saw and the G10 tabs were cut using a shear, followed by fine trimming using the wet saw down to their final dimensions of 3.5"x 2.165". The width of the tabs was allowed to be a bit oversized since it was trimmed of in the end. The length of 2.165" was cut with a tolerance

of +/−0.001” to help ensure a gauge section of 3.661” +/−0.002”. Additional G10 was cut to the size of gauge section so that during tabbing it was used as a guide as well as prevent specimen bending during vacuum table curing. Figure 37 shows the tabbed specimens prior to elevated temperature curing in the vacuum table. After

Figure 37. Tabbed sections from all five panel sets prior to cure in a vacuum table at 180°F for 90 minutes. Three 1”x8” specimens were cut out of these sections for tensile testing.

curing, three 1”x 8” specimens were trimmed from the specimens. The dimensions of the specimens are given in Table 7

The specimens were then strain gauged, mounted in the MTS, and pulled at a constant rate of 10^{-3} in/min until the specimen fractured. The resulting stress strain curves produced from the strain gauge data was then processed using a MATLAB code, found in the Appendix, to determine the modulus of elasticity, percent elongation, and ultimate tensile strength (UTS). The values for Young’s Modulus were compared with predicted values obtained from a MATLAB code which uses composite material laminate theory to estimate panel strength. The results of the tensile tests are presented in Figures 38, 39, and 40.

Table 7. Thickness and width measurements used to calibrate the calculation of modulus and ultimate tensile strength provided from tensile testing the specimens.

	Width (in.)			Thickness (in.)		
Panel-Sample Number	Top	Bottom	Average	Top	Bottom	Average
0.1-1	1.0040	1.0060	1.0050	0.0380	0.0390	0.0385
0.1-2	1.0060	1.0030	1.0045	0.0390	0.0390	0.0390
0.1-3	1.0010	0.9980	0.9995	0.0380	0.0380	0.0380
1.1-1	0.9960	1.0000	0.9980	0.0400	0.0395	0.0398
1.1-2	0.9980	1.0040	1.0010	0.0400	0.0400	0.0400
1.1-3	0.9975	1.0005	0.9990	0.0390	0.0400	0.0395
2.1-1	1.0040	1.0020	1.0030	0.0400	0.0400	0.0400
2.1-2	1.0060	1.0050	1.0055	0.0400	0.0400	0.0400
2.1-3	1.0005	1.0020	1.0013	0.0395	0.0400	0.0398
3.1-1	1.0020	1.0065	1.0043	0.0430	0.0430	0.0430
3.1-2	1.0055	1.0050	1.0053	0.0415	0.0415	0.0415
3.1-3	1.0050	1.0020	1.0035	0.0425	0.0425	0.0425
4.1-1	1.0055	1.0065	1.0060	0.0430	0.0420	0.0425
4.1-2	1.0045	1.0050	1.0048	0.0435	0.0440	0.0438
4.1-3	1.0060	1.0020	1.0040	0.0435	0.0440	0.0438

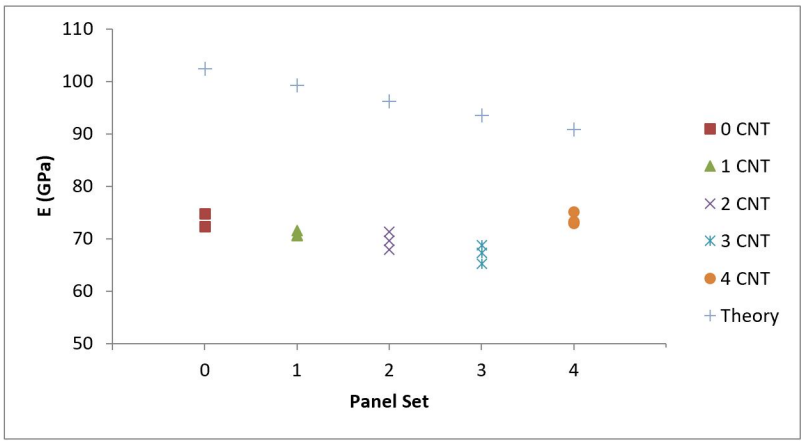

Figure 38. Values of Young's Modulus calculated from the strain gauge data obtained from tensile testing of the 15 1"x8" specimens obtained from the five different panel sets.

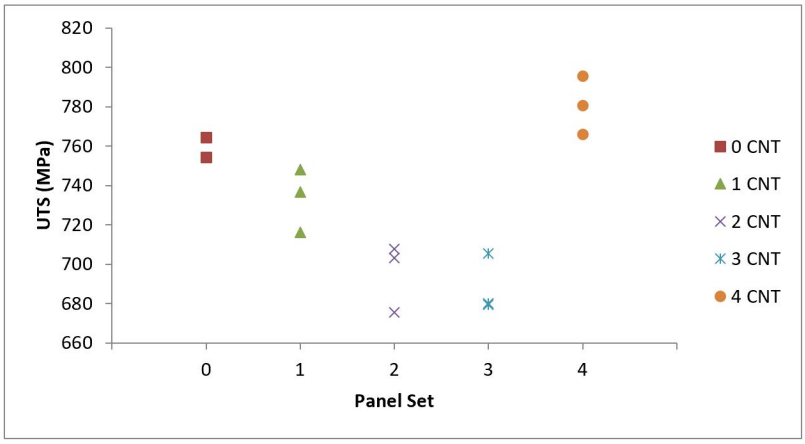

Figure 39. Ultimate tensile strength (UTS) in Pascals measured from the 15 tensile tests corresponding to the five different sets of panels, with the first set having no CNT sheets and the fifth set containing 4 CNT sheets.

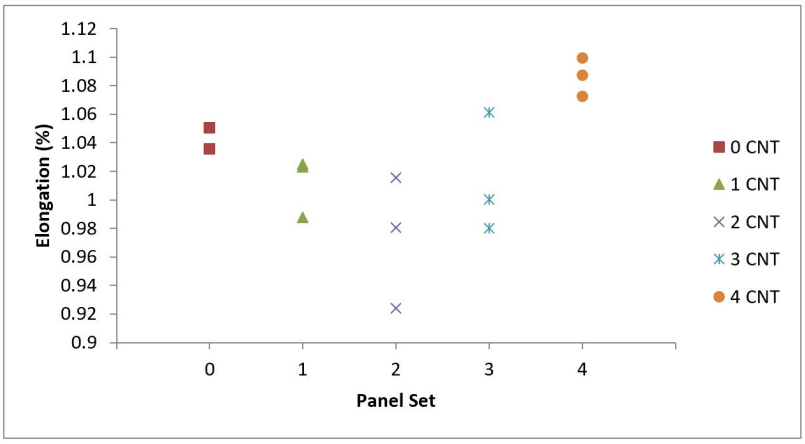

Figure 40. Percent elongation at the ultimate tensile strength for the 15 tensile specimens taken from the 5 panel sets.

As seen in Figure 38, the values calculated for modulus of elasticity were much lower than the predicted values, although they mostly followed the downward trend. The model used to estimate the values does not account for the additional shearing in the laminate induced by the 45° plies which make up half of the carbon fiber plies in the panels. This inter-laminar shearing was clearly evident in the way that the specimens failed. The specimens failed primarily through delamination of the plies. This was evidenced by the splitting of the laminate along the central ply boundary which occurred in all of the specimen tests to some degree, including the specimens with no CNT sheets. It was in fact most pronounced in the specimens with no CNT sheets and least evident in the specimens with four CNT sheets. Figure 41 shows the fragments from a specimen with no CNT sheets, two CNT sheets and four CNT sheets. The fragments show the delamination splitting characteristic of the failure mechanism observed in these tests.

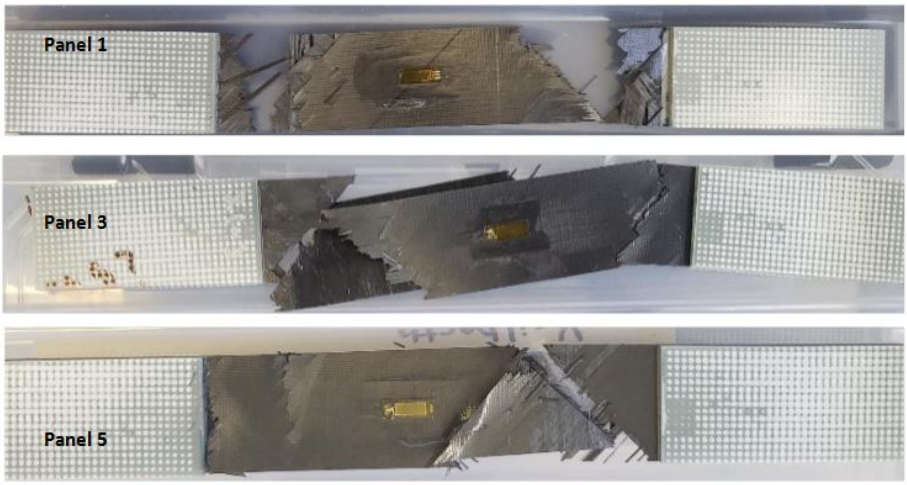

Figure 41. Fragments from an all carbon fiber specimen (Panel 1), a specimen with 2 CNT sheets (Panel 3), and a specimen with 4 CNT sheets (Panel 5). Failure for all specimens involved shear in the 45° direction and delamination flaking, but The delamination was much less pronounced in the specimens with four CNT sheets than the other specimens

These tests demonstrate that the CNT sheets generally decrease the panel stiffness and ultimate tensile strength up until the case of four CNT sheets. The case of four

CNT sheets demonstrated a similar modulus to the all carbon fiber specimens, but it allowed for increased strain which increased the ultimate tensile strength of these specimens. It was observed after testing that the 0° and 45° plies were switched in the ply stacking order, resulting in the two 0° plies being near the center of the panel. This may have resulted in the observed trend anomaly.

The final test element involved in characterizing the panels was to establish baseline EMI shielding properties for the panels prior to ballistic impact. The signal attenuation results were obtained for the condition defined as S12, the measurement of the horizontal signal from horn one by horn two. The results for the panels of the same configuration were averaged together and the S12 results plotted together as seen in Figure 42. These results show that regardless of how many CNT sheets are in

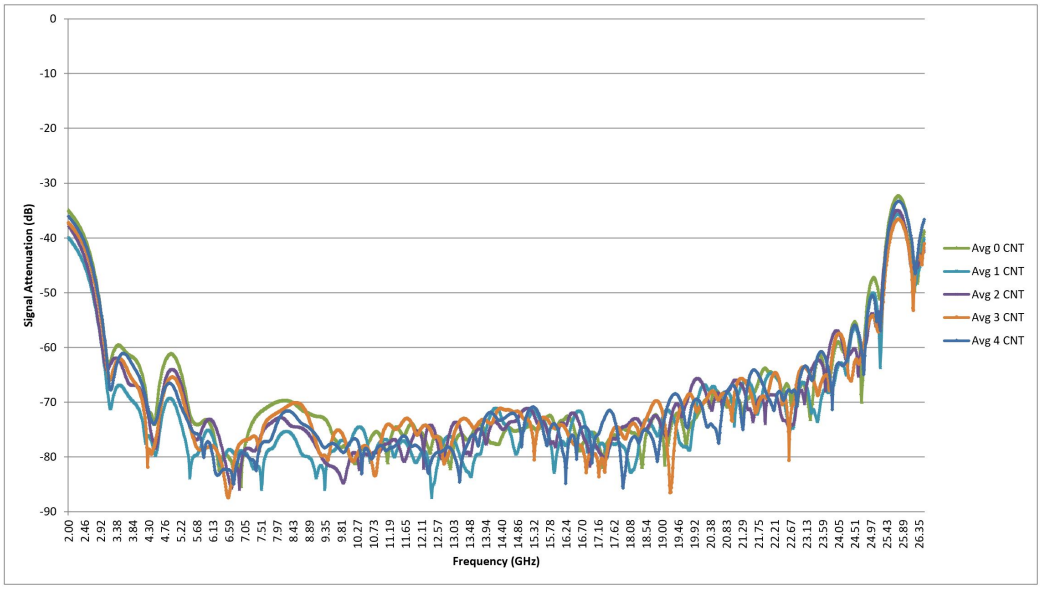

Figure 42. Averaged plots of EMI shielding effectiveness in dB for the S12 condition defined as the measurement by port two of the signal projected from port one of the network analyzer located on the other side of the panel.

the panel, the shielding effectiveness closely matches the noise floor values of the test equipment. Similar issues were experienced in the work done by Micheli *et al.* where the presence of carbon fiber in the panel provided a degree of conductivity adequate

to match the noise floor of the experimental set up [27].

A few points of interest on the plot include 2 GHz, 5 GHz, and 8 GHz. At these frequencies there is a bit of delineation seen between the panel sets. The case at 2 GHz shows an increasing shielding from -35 dB down to -40 dB for the panel with no CNT sheets at the top and the panel with four CNT sheets at the bottom. At the other two frequencies the case of one CNT sheet performs the best, roughly 8 dB lower than the no CNT case at 5 GHz and 5 dB at 8 GHz. Most likely these differences are caused by signal variance of the noise floor, and so definite conclusions were not determined, but it was generally observed that the panels with CNT sheets demonstrate better shielding than the all carbon fiber panels. If the full extent of shielding effectiveness was desired, experiments using equipment capable of increased power or reduced noise floor would be necessary.

The testing results presented and analyzed thus far served to accomplish the first thesis objective of constructing and characterizing carbon fiber panels containing Miralon CNT sheet material. The C-Scans and acid digestion data served to prove the manufacturing process resulted in a well bonded hybrid composite panel. The tensile tests and EMI shielding helped to characterize properties of the panels. Decreasing strength and modulus of elasticity were observed as the number of CNT sheets increased up until the test condition with four CNT sheets. Four CNT sheets resulted in increased UTS and percent of elongation. The signal attenuation measurements of EMI shielding indicated that the CNT sheets improved the shielding provided by the panel, but since the results for all cases appear to follow the noise floor of the focus beam tunnel, higher power testing or a lower noise floor is required to determine the true shielding improvement trends offered by the CNT sheets in the panel.

4.2 Ballistic Energy Absorption Results

The ballistic testing of the panels was conducted using the AFIT gas gun set up in accordance with the ballistic test plan. The first five panels were shot at an average velocity of 637 ft/s. The impact and residual velocities were recorded from the chronographs, and through the high-speed camera footage which was analyzed using a MATLAB code in addition to measurement software built in to the camera control system. This first round of testing resulted in the data presented in Table 8. Comparing the change in projectile velocity for each panel among the three velocity measurement sources provides the following set of plots shown in Figure 43.

Table 8. Striking and residual velocities obtained for the first set of ballistic tests shot between 627 and 648 ft/s.

	Phantom Camera DIC Data			Chronograph Data			Matlab DIC Data		
Panel #	Vin	Vout	ΔV	Vin	Vout	ΔV	Vin	Vout	ΔV
0.2	649.744	634.667	15.077	644	error		648.2406	634.1018	14.1388
1.3	628.205	612.500	15.705	628	606	22	627.1490	613.8655	13.2835
2.2	637.778	623.137	14.641	636	616	20	636.6119	624.1669	12.4450
3.4	633.889	618.333	15.556	632	612	20	633.2133	619.8353	13.3780
4.3	637.778	621.250	16.528	633	615	18	637.2117	624.0003	13.2114

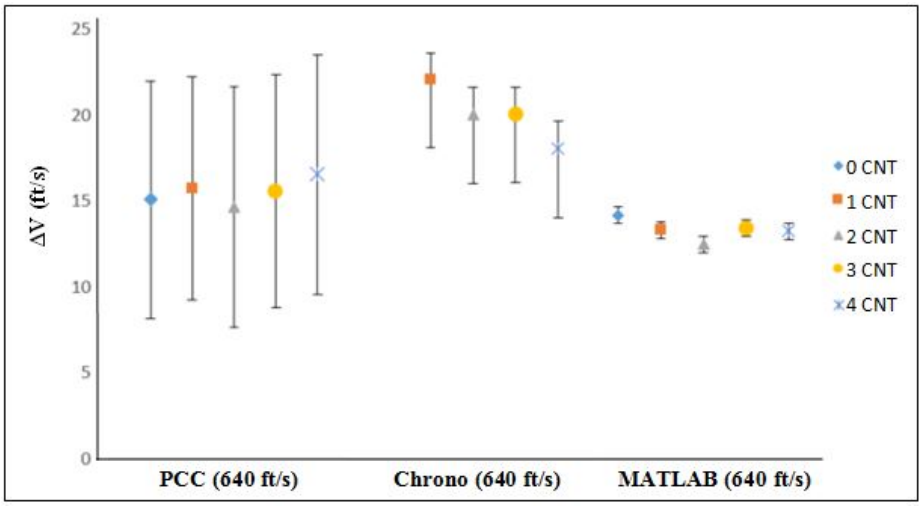

Figure 43. Change in projectile velocity for each panel type as measured by the three different velocity measurement methods for 640 ft/s nominal impact velocity.

These initial results were very close together with less than a 5 ft/s variation between the highest and lowest velocity attenuation values. Therefore it was determined that a slower speed should be chosen for shooting the next set of panels in order to increase the velocity attenuation observed. This occurs due to the fact that a panel will cause the largest change in velocity at its limit velocity, wherein all of the projectile energy is absorbed by the panel. The new impact velocity was chosen to be 350 ft/s. This velocity was selected based on the experimentally determined V_{50} of a 16 ply carbon fiber panel which was found to be 352 ft/s. By basing the value on the limit of a much thicker panel, penetration of the test panels was ensured. The next set of ballistic data is presented in Table 9. The striking velocities for these five

Table 9. Striking and residual velocities obtained for the second set of ballistic tests shot between 343 and 348 ft/s.

	Phantom Camera DIC Data			Chronograph Data			Matlab DIC Data		
Panel #	Vin1	Vout	ΔV	Vin1	Vout	ΔV	Vin1	Vout	ΔV
2.4	346.957	321.010	25.947	347	317	30	348.1593	322.7944	25.3649
4.4	348.985	322.291	26.694	347	318	29	348.3051	323.8149	24.4902
1.2	346.956	316.768	30.188	347	312	35	346.8959	318.0811	28.8148
3.3	342.222	315.000	27.222	345	310	35	343.2515	315.0684	28.1831
0.3	347.879	320.833	27.046	348	error		348.7424	320.7536	27.9888

shots were very consistent with only a 3-6 ft/s variation in speed depending on the velocity measurement method. The resulting change in projectile velocities for each velocity measurement system is presented in Figure 44

A greater change in velocity was observed in these tests, and a trend was identified in which the panels with only a single sheet of CNTs appear to outperform the other test cases. In order to get test shots even closer to the ballistic limit of the panels, a third velocity of 180 ft/s was selected. The first two shots were fired at too low of a pressure which resulted in non-penetrating shots on the panels with 1 and 3 CNT sheets. The pressure was then adjusted and the remainder of the shots fired very

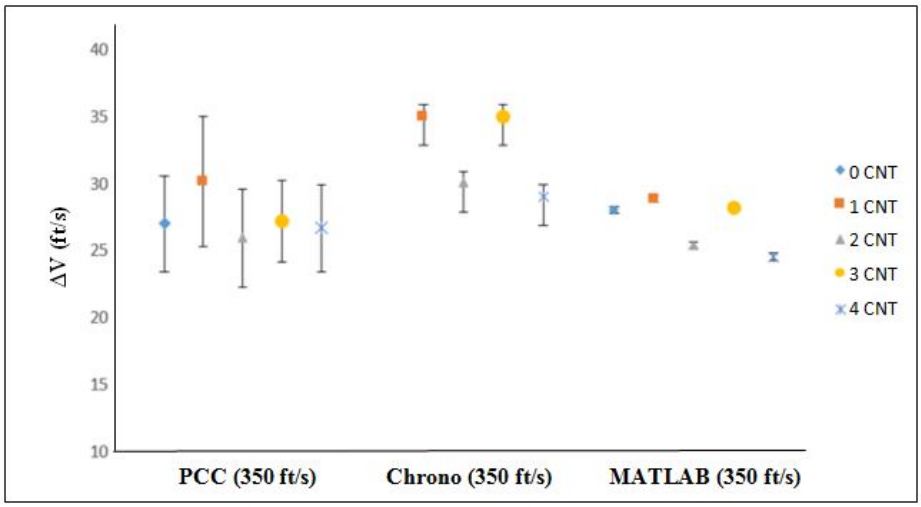

Figure 44. Change in projectile velocity for each panel type as measured by the three different velocity measurement methods .

close to 180 ft/s, varying by ±4 ft/s. To get a full set of data, the fifth panel from the sets with 1 and 3 CNT sheets were added to the test series and shot at 180 ft/s. The recorded velocity data is presented in Table 10. As seen in the table, no imaging

Table 10. Striking and residual velocities obtained for the third set of ballistic tests shot between 175 and 183 ft/s.

	Phantom Camera DIC Data			Chronograph Data			Matlab DIC Data		
Panel #	Vin	Vout	ΔV	Vin	Vout	ΔV	Vin	Vout	ΔV
3.2	error	error		154	N/A		error	error	
1.4	error	error		153	N/A		error	error	
0.5	181.364	113.344	68.020	181	113	68	179.0506	114.2617	64.7889
2.5	176.061	95.832	80.229	177	95	82	175.8889	96.1467	79.7422
4.2	185.555	127.778	57.777	185	127	58	183.8828	127.7617	56.1211
1.5	176.296	95.444	80.852	177	95	82	175.7334	95.7061	80.0273
3.5	error	error		183	117	66	error	error	

based velocities were calculated for the panels with 3 CNT sheets. This was due to a camera triggering error. The projectile velocity change was then plotted for each of the velocity measuring methods as seen in Figure 45.

Figure 45 clearly shows that the panels with one and two CNT sheets performed the best at reducing projectile velocity. From the velocity data collected over the

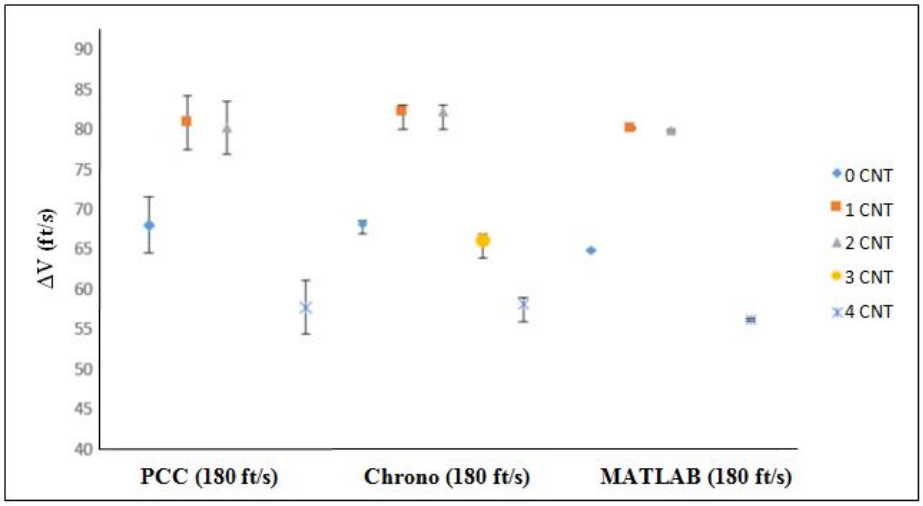

Figure 45. Change in projectile velocity for each panel type as measured by the three different velocity measurement methods.

three sets of panels, the kinetic energy absorption was compared. Figures 46, 47, and 48 show the kinetic energy reduction across the three test velocities for each velocity measurement method. These plots show similar trends to the plots of change in

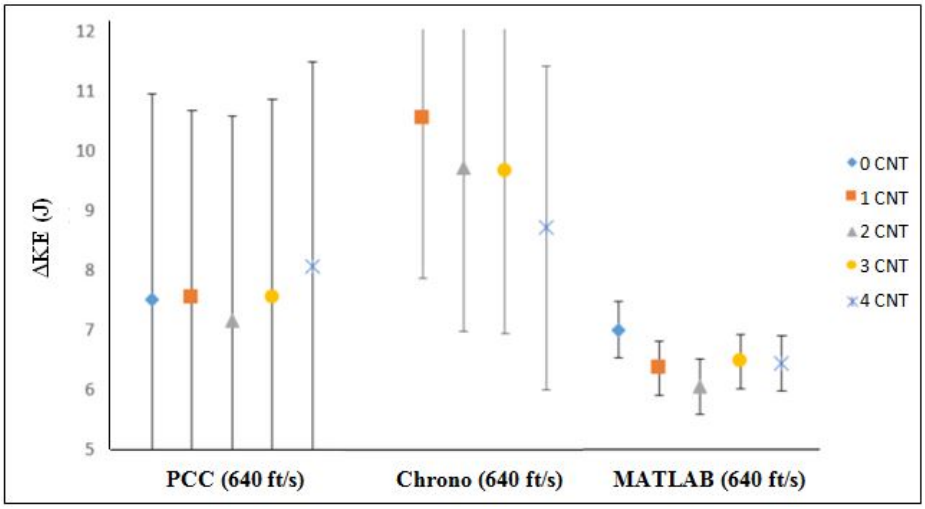

Figure 46. Change in projectile kinetic energy for each panel type from the three velocity measurement methods for nominal impact velocities of 640 ft/s.

velocity. This logically follows since the kinetic energy is related to the velocity squared. The energy approach shows that the amount of kinetic energy absorbed by a panel is fairly constant across the range of velocities tested, only varying between 6-

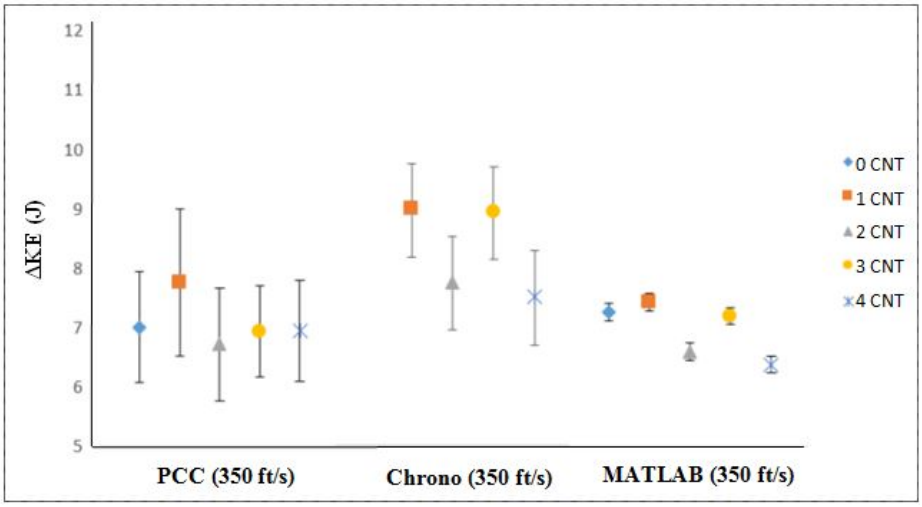

Figure 47. Change in projectile kinetic energy for each panel type from the three velocity measurement methods for nominal impact velocities of 350 ft/s.

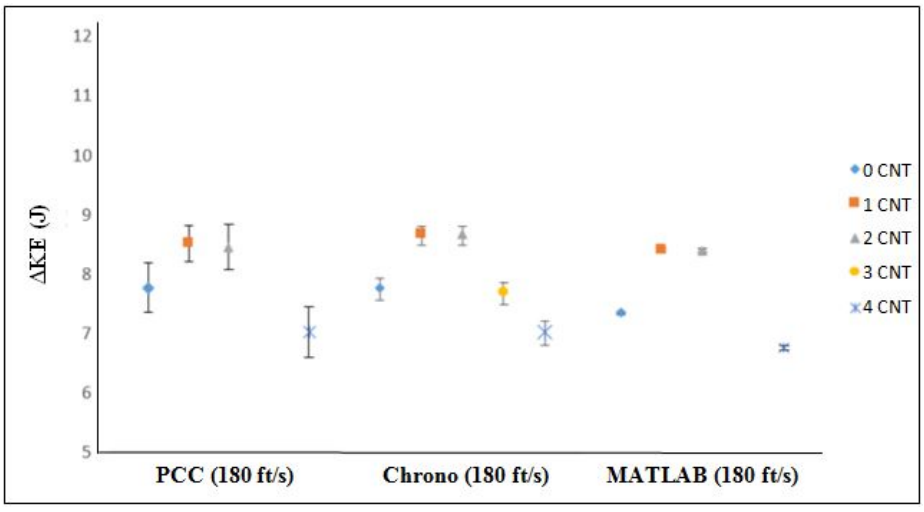

Figure 48. Change in projectile kinetic energy for each panel type from the three velocity measurement methods for nominal impact velocities of 180 ft/s.

9 J. This agrees with the assumption of constant energy absorption made by Lambert and Billon in their estimations of ballistic limit [23][4].

Now that three sets of impact and residual velocities have been obtained for each panel configuration, the estimations for ballistic limit were calculated. The Jonas-Lambert method was implemented using the MATLAB code attached in the Appendix. The three sets of data were input and the initial guess for α and P from Equation 5 was modified until a good fit of the data was achieved by the least squares method. The results for the Jonas-Lambert method are presented in Table 11

Table 11. Jonas-Lambert method estimations of the ballistic limit for each of the panel configurations based on the three sets of striking and residual velocity obtained through ballistic testing. The norm of the residuals is also provided to indicate the fit of the model with the data.

	PCC Velocities				Matlab DIC Velocities			
Panel Set	α	P	V0	R-Norm	α	P	V0	R-Norm
0	0.9945	2.1992	148.0511	2.75E-23	1	2.024	138.8038	5.46E-02
1	0.9984	2.1224	151.7216	1.46E-20	1	2.1587	151.9827	4.41E-01
2	0.9924	2.3621	156.574	9.38E-17	0.9972	2.311	155.3698	1.59E-16
3	0.99	2.22	147.9	1.71E-19	1	2.0985	144.5064	2.45E-01
4	0.9939	2.1095	138.3082	2.91E-14	0.9977	2.1125	136.6838	3.36E-12

Using the coefficients and predicted limit velocity from the Jonas Lambert method, a plot of striking velocity vs residual velocity can be produced for each panel set. The results of this are shown in Figure 49. From the mathematical estimates of V_0 from implementing the Jonas-Lambert method it is seen that the best performing panels are the sets with one and two plies of CNT sheet material. The panels with four and five sheets performed worse than these two, although all four cases with CNT sheets had V_0 estimates higher than the all carbon fiber panels.

The next method used to calculate V_0 developed by Billon, was then used to model the data set. Because Billon's model has an explicit solution, the process was accomplished using an Excel spreadsheet. The results of applying Billon's model

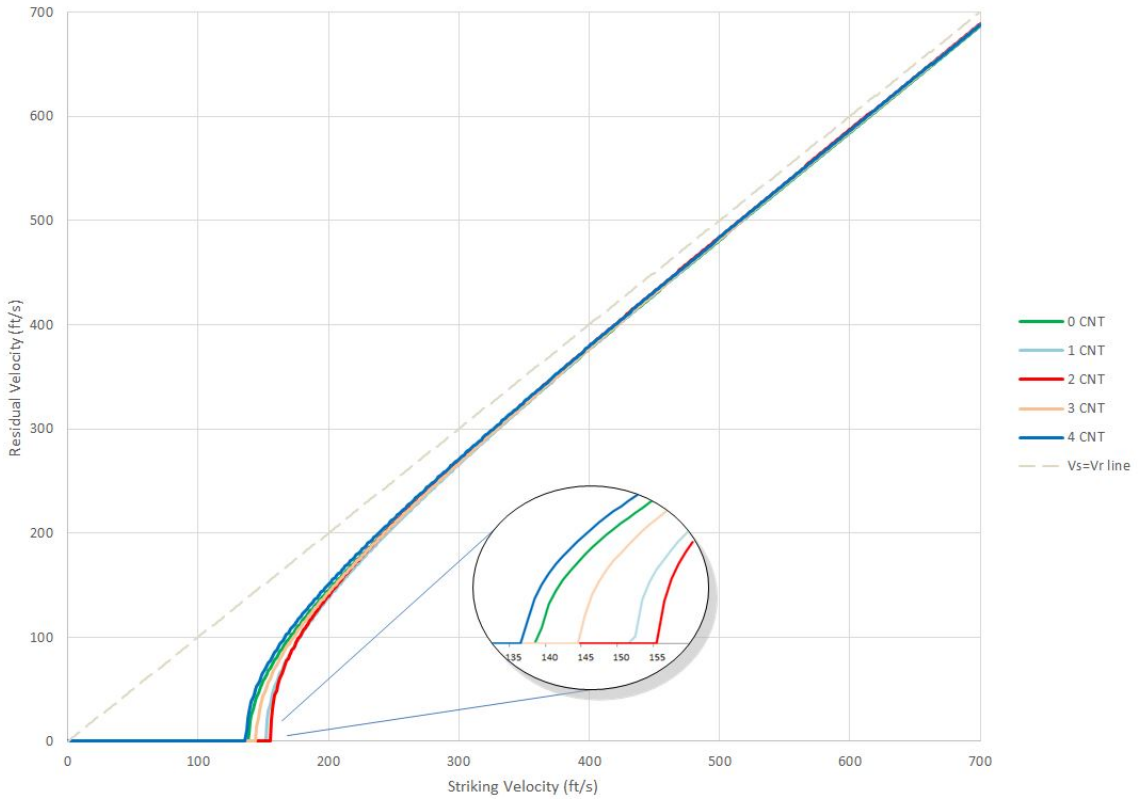

Figure 49. Striking velocity vs residual velocity plot for each panel set based on the result of a least squared fit of the Jonas-Lambert method.

to the shot information is presented in Table 12. Using the values of k and the V_0 estimates with Equation 15, a plot of striking velocity vs residual velocity was created for each panel set. The plot is displayed in Figure 50. As seen in this figure, Billon's model estimates a higher V_0 for the panels with one CNT sheet than the others, with the four CNT sheet panels performing worse than the all carbon fiber ones. The difference between the panels quickly diminishes the higher the striking velocity of the projectile. This follows with what was observed in the raw test data. The curves produced for both methods are based on constant kinetic energy absorption by the panels. The Jonas Lambert method allows the exponent to vary from 2 as well as account for mass changes through α, the constant term. The mass change term, k, is the primary factor accounted for in Billon's method. A comparison of the two

Table 12. Billon method estimations of the ballistic limit for each of the panel configurations based on the three sets of striking and residual velocity obtained through ballistic testing.

	PCC Velocities		Matlab DIC Velocities	
Panel Set	k	V_0	k	V_0
0	0.999766	138.5864	0.99781	137.8487
1	0.994318	146.3396	0.9868	145.83
2	0.994145	142.053	0.987872	142.4598
3	1.000754	137.5951	0.992285	140.1811
4	1.008038	132.6191	0.998498	130.868

methods against each other in terms of predicted limit velocity is seen in Figure 51. This figure shows that the Jonas-Lambert method predicted higher limit velocities than the Billon method. It also favored test case 3, which had 2 CNT sheets, while the Billon method identified the best performer as test case 2, consisting of only one CNT sheet. Both models indicate that the higher numbers of CNT sheets fail to perform significantly better than the baseline carbon fiber panels.

The trend of improved ballistic energy absorption for only one or two CNT sheets is seen in the velocity attenuation data, kinetic energy attenuation data, and by the two methods of estimating the ballistic limit velocity of the panels. This finding is very interesting. It goes against the hypothesis that more CNT sheets would lead to more ballistic energy absorption by the panel. A consideration in evaluating these results is the velocity measurement method. The three methods, chronographs, Phantom Camera Control software, and MATLAB digital image correlation, were used so that the results of one method could be weighed against the information obtained by the other methods. Based upon the velocity measurement precision, the MATLAB code was generally trusted the most. By including data from the other methods, it is seen that the results at high velocity do not lead to distinction of results due the number of CNT sheets in the panel. It is only in the low velocity case, 180 ft/s, that all three methods showed the same trend of one or two sheets providing a greater reduction in velocity and kinetic energy. It is also this case where the measurement error is small

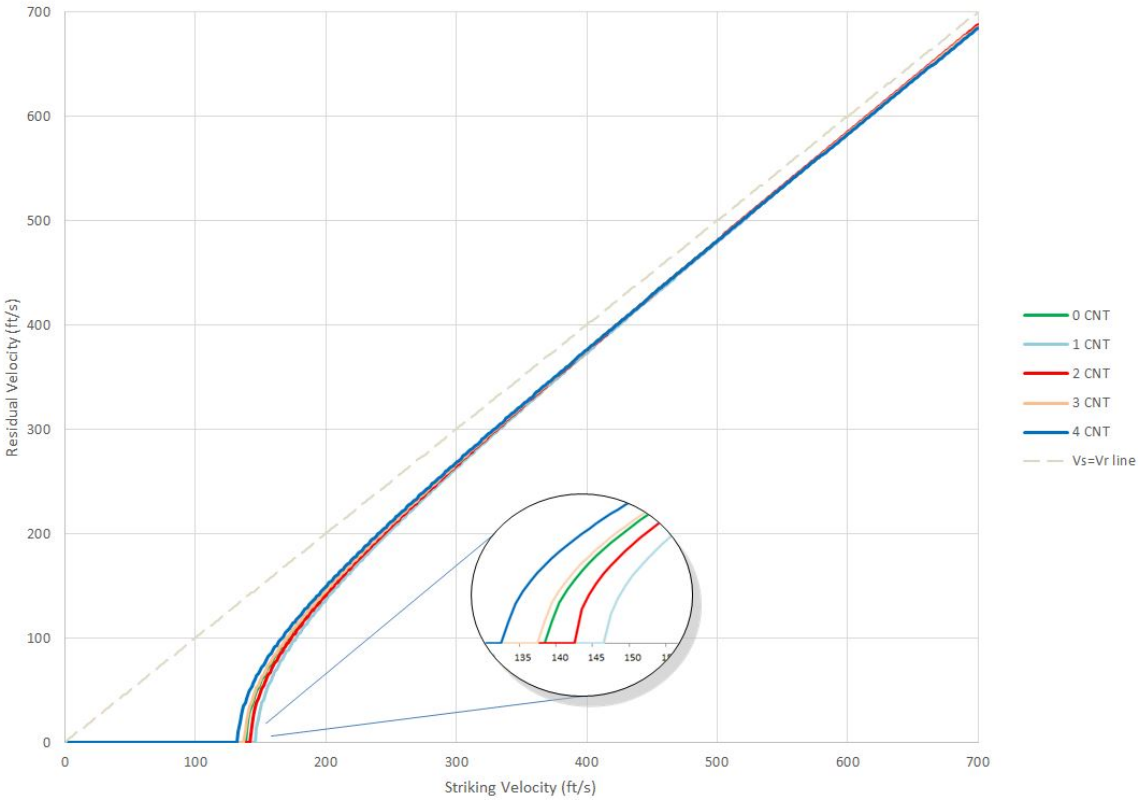

Figure 50. Striking velocity vs residual velocity plot for each panel set based on modeling the three sets of impact velocity data with Billon's method.

enough to state that the difference between the test cases is significant. The fact that the two ballistic limit velocity estimation methods resulted in the same trends while using the data from all three test velocities further indicates that this observed trend has merit.

These findings contradict Micheli's results which indicated that a larger CNT layer improved ballistic energy absorption in his panels while thinner layers did not improve performance [27]. The exact causes of these results are likely complex and multifaceted. The thorough exploration of these causes was outside the scope of this project, but some thoughts are presented here. One explanation of the reverse trend considered focused on the mechanical nature of the host panels used in both experiments. Micheli used E-Glass as the material the CNT layers were embedded

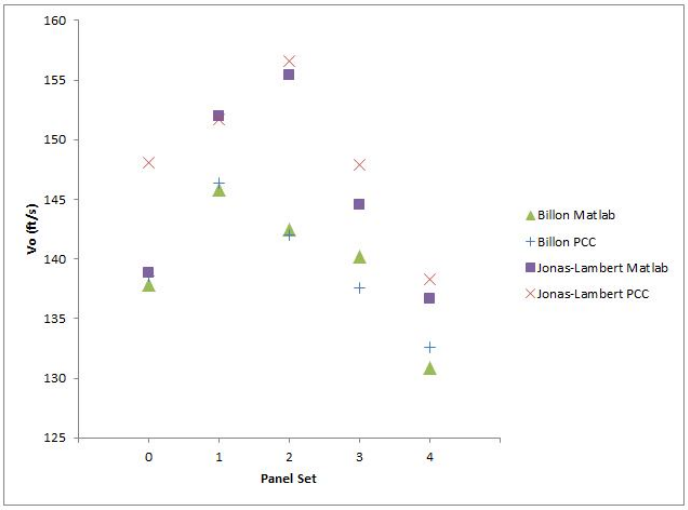

Figure 51. Comparison between the Jonas-Lambert method and Billon method estimates of the limit velocity for each panel configuration using both the camera software (PCC) velocities and the MATLAB digital image correlation (DIC) values

in. E-Glass has a lower modulus of elasticity and can undergo more elongation prior to failure than carbon fiber. The difference between the materials also impacts the ways that shock waves travel through the material. Therefore it is not unreasonable to expect different trends to appear for CNTs in a carbon fiber panel than for CNTs in an E-Glass panel.

While material differences may account for the difference between Micheli's results and the present work, the fact that Nanocomp stopped a 9mm bullet with around 100 sheets of the Miralon CNT product indicates that the trend should show improved ballistic properties for increasing numbers of CNT sheets. The results of this study may be interpreted to show that this relationship is not linear. A nonlinear relationship could explain an increase followed by a dip in performance before larger increases in ballistic performance at even higher numbers of CNT sheets. Following this idea of a nonlinear relationship between the number of CNT sheets and the ballistic attenuation of a projectile, a study consisting of higher numbers of CNT sheets in the panel would be valuable for determining the nature of the trend.

A related factor which may be influencing this trend is the thickness of the panels.

Only eight plies of carbon fiber were used in this research. The thinness of the panels means that there is not much time for the impact shockwaves to interact with the panels and render the CNT sheets ineffective at disrupting the ballistic shocks and absorbing projectile energy. Increasing the panel thickness

Finally, as an additional metric of ballistic performance. Three panels were selected to have multiple impacts designed to determine the V_{50} of the panels. Panels 0.2, 2.2, and 4.3 were selected since they were shot with the highest velocity projectile. The higher velocity impacts resulted in smaller damage area than the the slower velocity impacts. By using these panels, the area available for additional shots was maximized. The 8 additional shots on each panel were kept within a velocity range of 40 ft/s which is well within the minimum frequently used velocity span limit of 60 ft/s identified in the Mil-Std [41]. The gun pressure was changed slightly between shots to achieve at least 3 penetrations and 3 nonpenetrations. The results of this testing for the three panels are shown in Table 13. From these data points, the lowest

Table 13. Results of V_{50} testing following MIL-STD-662F with exception to witness plate usage, for panels 0.2, 2.2, and 4.3. Velocity from the two chronographs located between the gun barrel and panel were recorded. Care was taken to avoid delamination overlap when determining shot placement.

Panel 0.2				Panel 2.2				Panel 4.3			
Location	Vin (ft/s)	Vin2 (ft/s)	Penetrate	Location	Vin (ft/s)	Vin2 (ft/s)	Penetrate	Location	Vin (ft/s)	Vin2 (ft/s)	Penetrate
R1	146	147	N	R1	146	147	Y	L1	error	152	N
L1	145	146	N	R2	140	141	N	R1	168	165	Y
L2	151	153	N	L1	159	161	Y	R3	154	error	Y
R3	145	147	N	L2	error	144	N	L2	153	155	Y
C3	150	151	Y	R3	147	148	Y	L3	error	130	N
R2	165	167	Y	L3	148	149	Y	R2	154	155	Y
L3	151	152	Y	C2	error	141	N	C2	150	151	N
C2	153	154	Y	C3	145	147	Y	C3	134	135	N

three penetrations were averaged with the highest three projectile stops to estimate the V_{50} of the panels. The results are shown in Table 14. The values of V_{50} obtained indicate the cases of two sheets of CNTs and four sheets of CNTs do not improve the ballistic performance of the panels. These single panel tests are not sufficient to

Table 14. Estimates of V_{50} found by averaging the highest three velocities of projectile stops and the lowest three velocities which resulted in penetration of the panel.

V50 Test Results	
Panel #	V50 (ft/s)
0.2	150.6667
2.2	144.6667
4.3	150.5000

statistically draw detailed conclusions from, but they serve to show that there is not a meaningful difference between the ballistic resistance of the panels. The accuracy of the three shot averaging method is not capable of characterizing the small difference observed between the panel sets without a larger number of samples which is outside the scope of this present work.

Based upon the results of the ballistic experiments it was determined that the benefit of adding a few CNT sheets to thin carbon fiber composite panels is minimal. Some improvement of about 0.7 joules of energy absorption was observed for the cases of one or two sheets of CNTs when shot at 180 ft/s. Three and four sheets of CNTs did not show potential for further improvement of energy absorption by the panel. Based on the high cost of the CNT material it does not appear to be the best candidate for improving the ballistic performance of the thin carbon fiber panels.

4.3 Post Impact Damage Properties

Prior to conducting the V_{50} testing of panels 0.2, 2.2, and 4.3, all of the shot panels were C-Scaned to visualize the damage areas in the panels caused by the shots in the center of the panel. The results of the C-Scans are presented in Figures 52, 53, and 54. From these figures the damage area in the panels shot at 350 ft/s show the largest damage area. This is an interesting result since it was expected that more damage would occur in the panel the slower the projectile. The panels shot at 180 ft/s show damage regions very similar in size to the panels shot at 640 ft/s. This trend

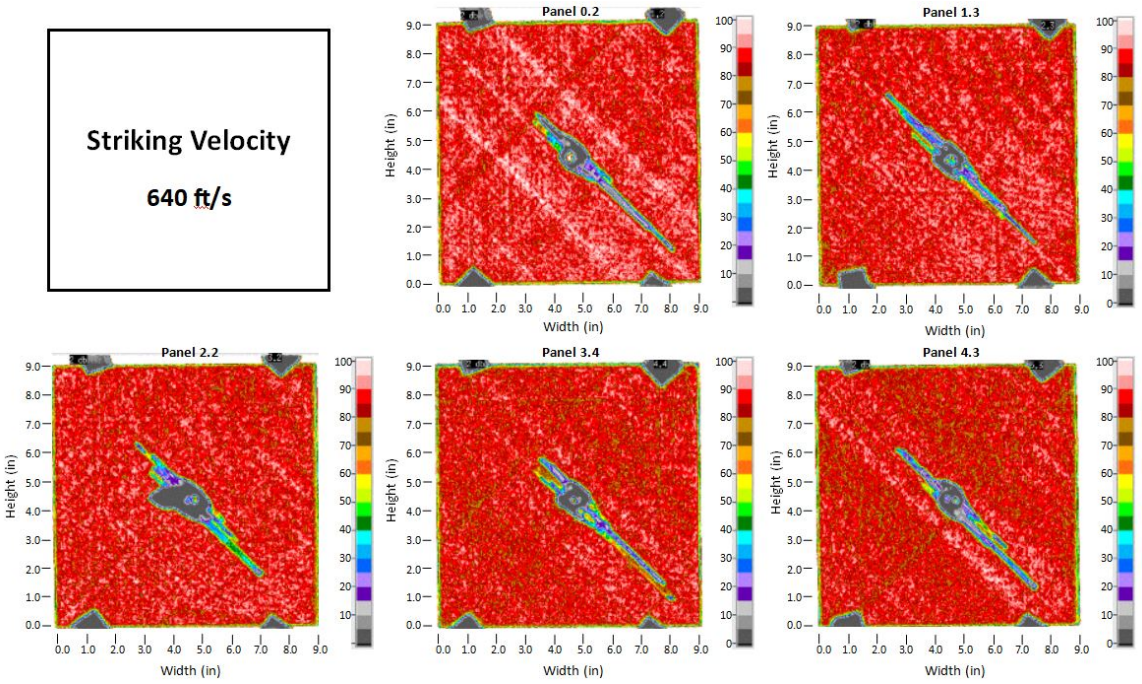

Figure 52. C-Scans of representative panels from each configuration after ballistic impact.

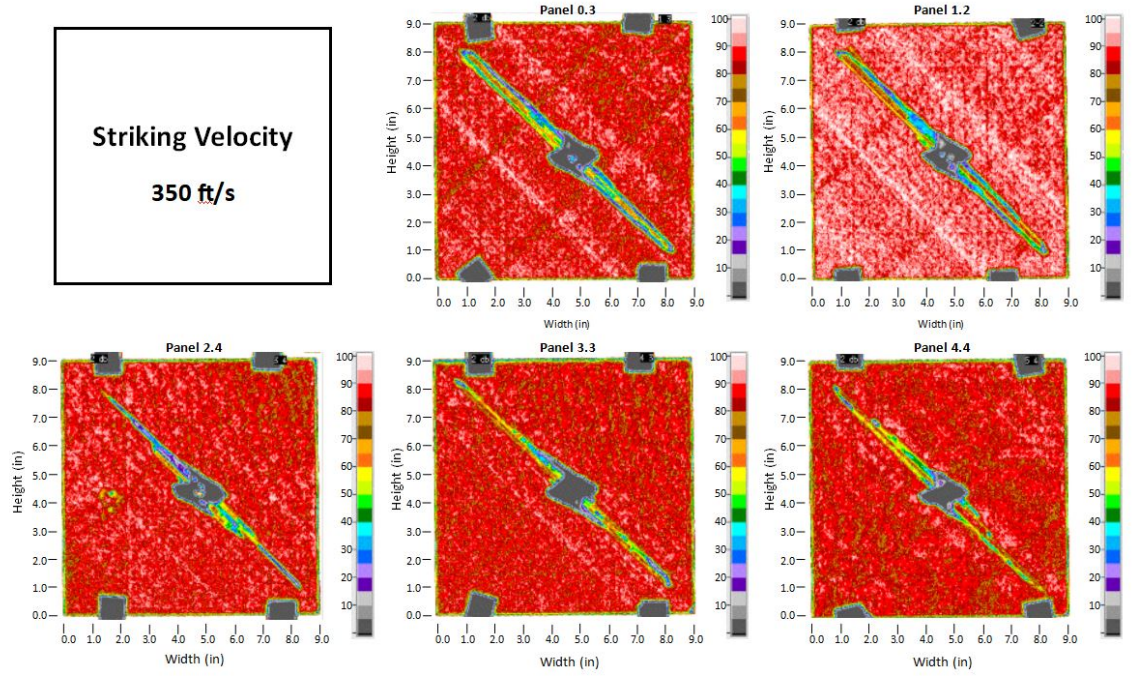

Figure 53. C-Scans of representative panels from each configuration after ballistic impact.

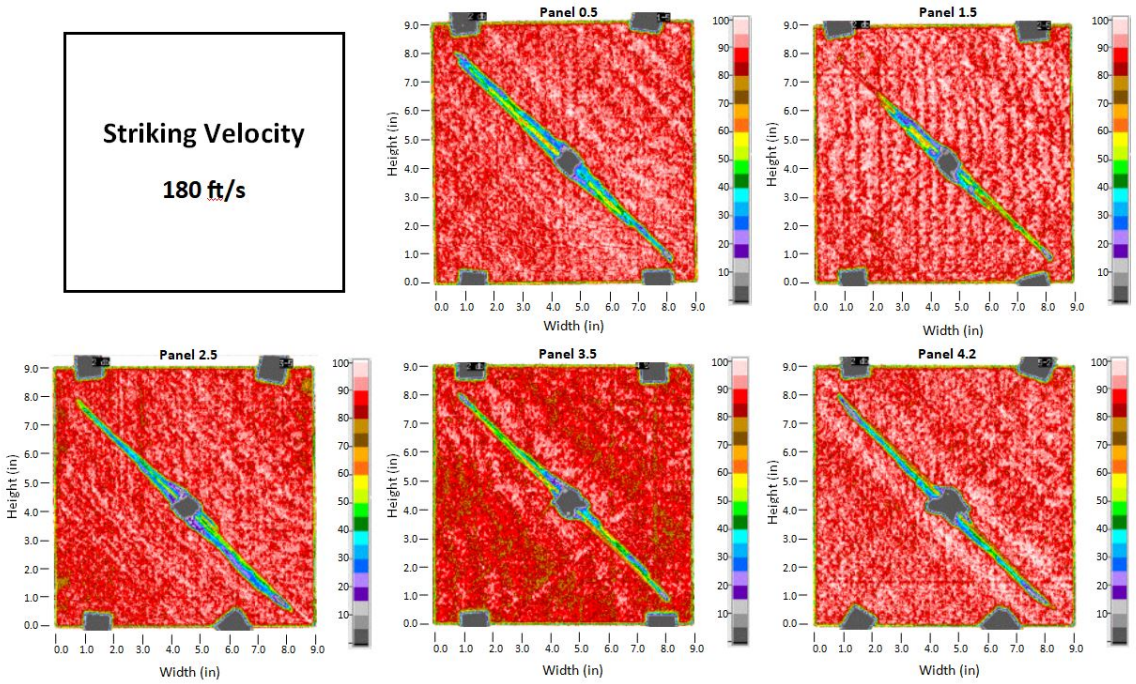

Figure 54. C-Scans of representative panels from each configuration after ballistic impact.

was independent of whether CNT sheets were in the panel or not. This indicates that the impact shock waves for the shots at 350 ft/s may have resulted in increased wave interaction along the 90° plies at the midplane of the panels. This could result in the larger damage area in the 90° direction, as seen by the increased width of the damage area in the panels shot at 350 ft/s. The only individual anomaly is the panel shot at 640 ft/s with two sheets of CNTs. This panel shows a significantly larger damage region in the panel than all the other panels shot at that velocity. Because this panel didn't show improved energy absorption compared to the other panels, this may have occurred due to a flaw in the panel near the point of impact which allowed an increased region of delamination.

Another observation was that the C-Scan images correspond with visual examination of the panels with regards to the amount of shearing at the projectile penetration point. It was seen that the more CNT sheets were in the panels, the less the projectile

was able to form a shear plug straight through the panel. There appears to be more frayed fibers touching across the puncture region in the panels with higher amounts of CNTs. This is clearly seen in the C-Scans for the panels struck at 350 ft/s. Here the panels with 3 and 4 CNT sheets do not show a distinct puncture hole in the panel, indicating the presence of significant fiber overlap across the puncture hole. While the delamination region around the impact zone does not vary significantly with the number of CNT sheets in the panel, the behavior around the penetration site seems to support that the CNTs help to some degree.

The impacted panels were also tested in the focus beam tunnel to measure the signal attenuation provided by the panel after impact. The results for each of the panel configurations is presented in Figures 55, 56, 57, 58, and 59. These results show

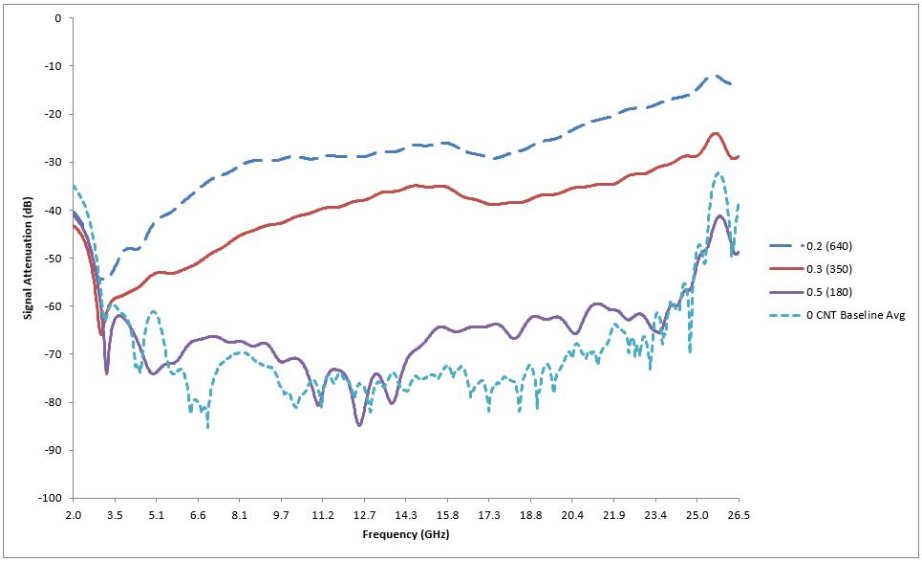

Figure 55. EMI shielding effectiveness measured by a focus beam tunnel in the range of 2.0-26.5GHz for the all carbon fiber panels.

that as the velocity of impact increased, the electromagnetic shielding effectiveness decreased, particularly in the higher frequency range. This trend makes sense because the faster projectiles created more of a shear plug through the panels than the shots at slower speeds. Remaining frayed fibers in the area of the projectile impact allow

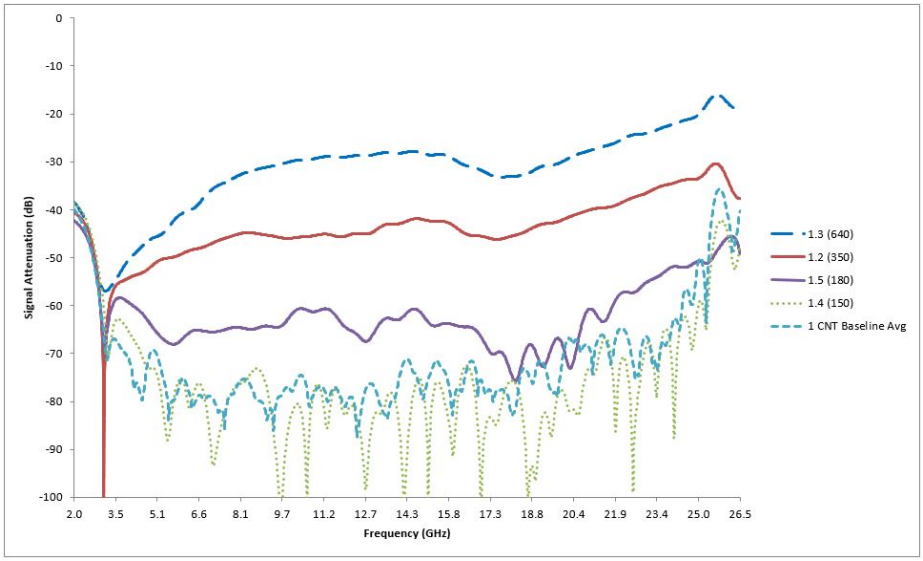

Figure 56. EMI shielding effectiveness measured by a focus beam tunnel in the range of 2.0-26.5GHz for the panels with 1 sheets of CNTs.

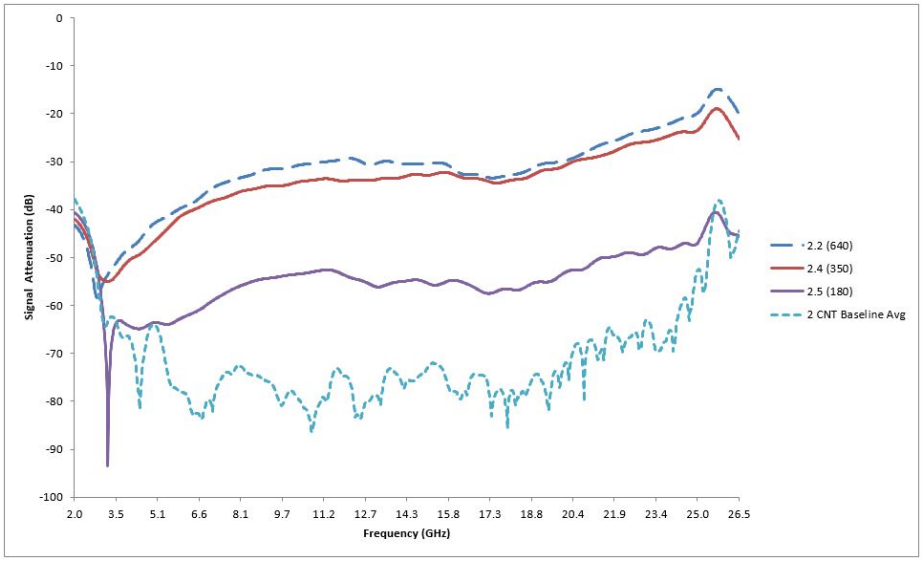

Figure 57. EMI shielding effectiveness measured by a focus beam tunnel in the range of 2.0-26.5GHz for the panels with 2 sheets of CNTs.

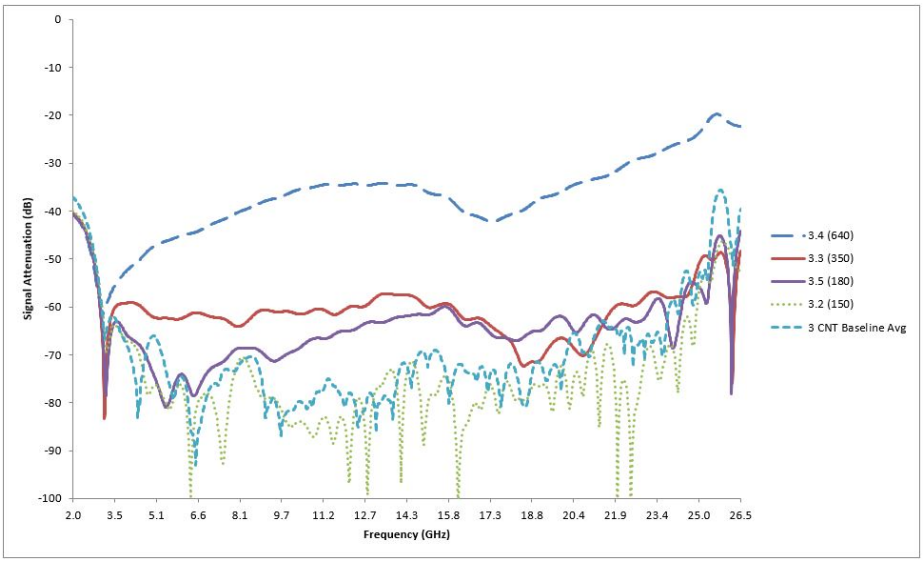

Figure 58. EMI shielding effectiveness measured by a focus beam tunnel in the range of 2.0-26.5GHz for the panels with 3 sheets of CNTs.

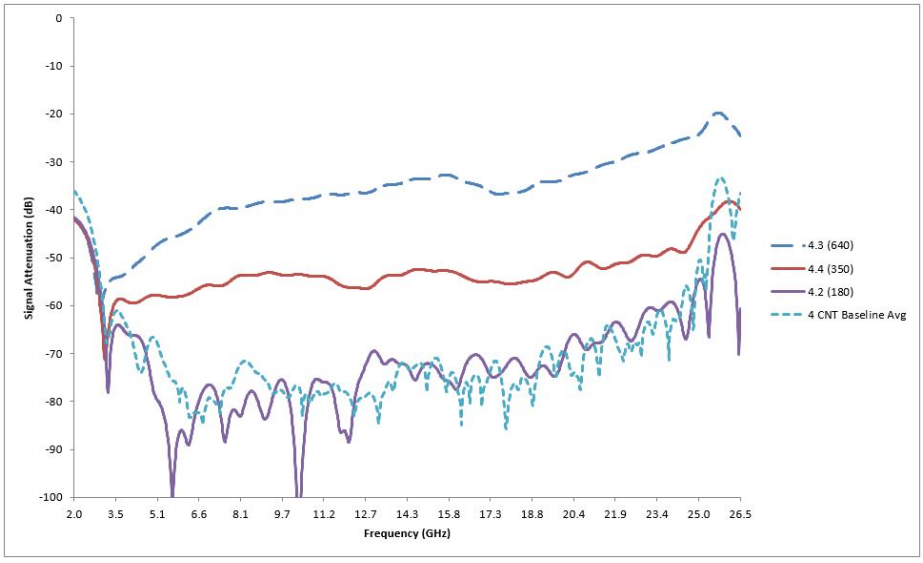

Figure 59. EMI shielding effectiveness measured by a focus beam tunnel in the range of 2.0-26.5GHz for the panels with 4 sheets of CNTs.

for continued conductivity, albeit reduced. In addition to the velocity relationships, the influence of the CNT sheets at each velocity was evaluated. Plots of the EMI shielding across the panel configurations at a constant impact velocity are presented in Figures 60, 61, and 62.

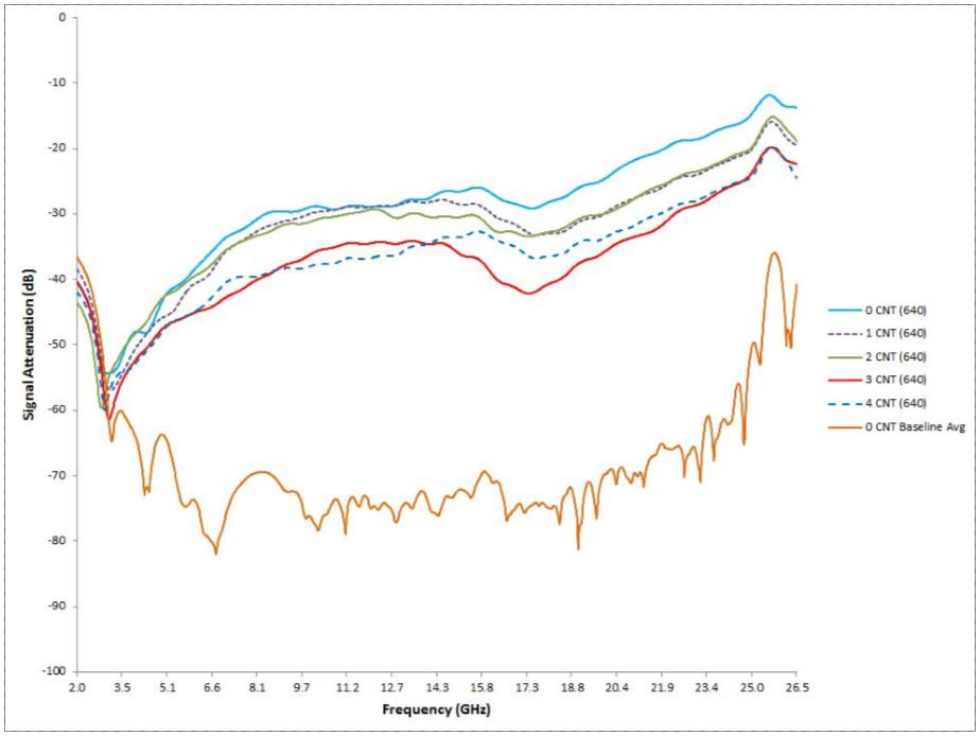

Figure 60. EMI shielding effectiveness measured by a focus beam tunnel for panels of each configuration shot at 640 ft/s.

From these plots, trends across the panel configurations and shot velocities were observed. From the panels shot at 640 ft/s it is seen that all of the panels with CNT sheets perform better than the panels with no CNTs. The trend appears to increase relative to the number of sheets of CNTs with noticeable similarity observed for the panels with one and two sheets of CNTs and for the cases of four and five CNT sheets. The maximum differences between the baseline configuration and the panels was in the frequency range of 15.6-23 GHz where the difference between no CNT sheets and four sheets exceeded 10 dB.

The panels shot at 350 ft/s demonstrated similar trends but with a much wider

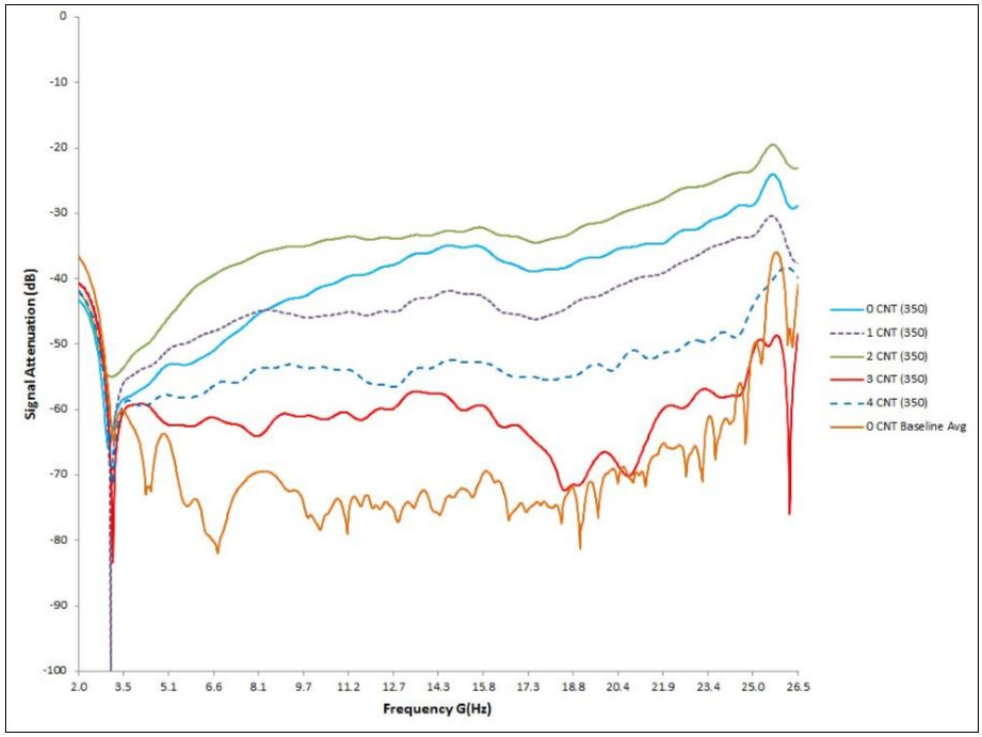

Figure 61. EMI shielding effectiveness measured by a focus beam tunnel for panels of each configuration shot at 350 ft/s

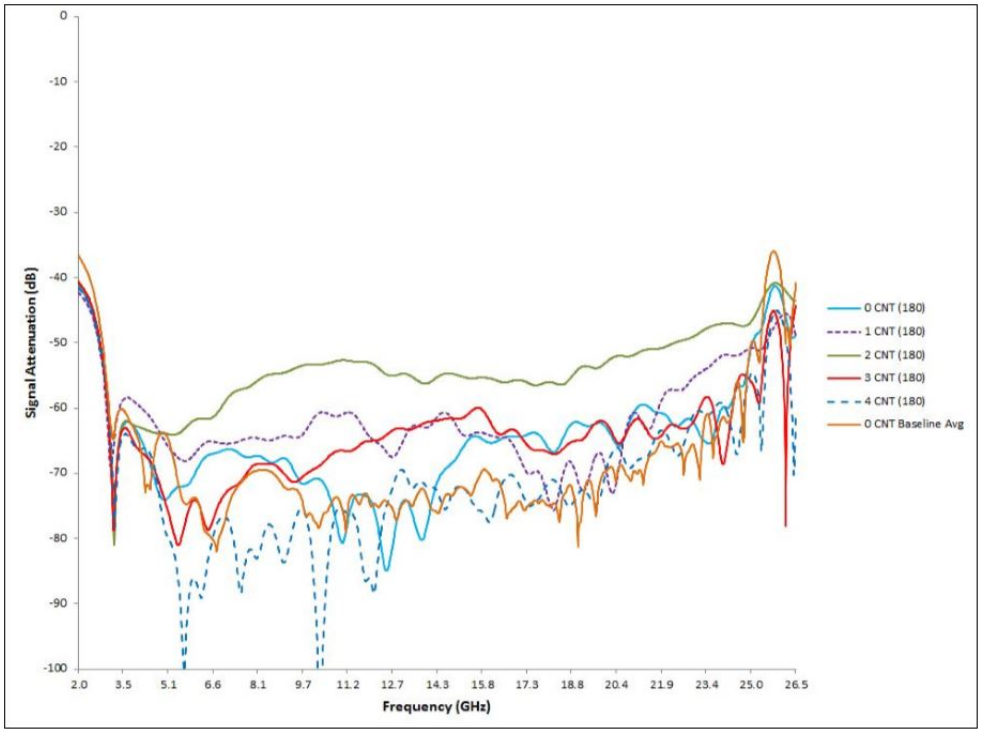

Figure 62. EMI shielding effectiveness measured by a focus beam tunnel for panels of each configuration shot at 180 ft/s

spread in attenuation values. The best performer was the panel with four sheets of CNTs which improved over the baseline panel by up to 40 dB. In this case though the panel with 2 sheets of CNTs performed worse than the all carbon fiber panel. Interestingly the test case of 2 sheets of CNTs also performed the worst in the plot of results at 180 ft/s where it trended 5-25 dB of less signal attenuation than the no CNT panel. The only configuration to noticeably outperform the all carbon fiber panel in the 180 ft/s tests was the panel with 4 CNT sheets.

The EMI measurements show that including CNT sheets in the thin carbon fiber panels improved the panel shielding effectiveness after impact. The amount of improvement increased with the number of CNT sheets and was significant for all three impact velocities. This corresponds with the finding from the C-Scans that the increased number of CNT sheets resulted in less shearing of the fibers by the projectile allowing for increased conductivity and thus shielding across the panel.

With the results of damage area inspection and EMI shielding characterization presented, all of the experimental thesis objectives were completed and studied. The research hypothesis was that the CNT sheets would positively influence the ballistic resistance of the panels and reduce impact damage to the panel in terms of damage area and EMI shielding. It was found that the CNT sheets did not influence the ballistic energy absorption of the panel significantly. In terms of damage area, the CNT sheets appeared to reduce shear by the projectile but did not change the delamination shape or size. The EMI shielding tests did show improvement in after impact shielding effectiveness with increasing CNT sheets. It is important to recall that these results were obtained for thin, eight ply thick, carbon fiber panels using a cyanate ester resin system with the CNT sheets placed at the mid-plane. The impact conditions consisted of half inch spherical steel projectiles at a velocity of 150-650 ft/s. The following chapter will summarize the results, and present final conclussions.

It will also discuss further research opportunities exposed through the experiments conducted in this thesis.

V. Summary

The purpose of this thesis was to investigate if the inclusion of CNT sheet material in a thin carbon fiber panel would enhance the ballistic properties of the panel through improving the absorption of energy from a projectile and through reducing post impact damage to the panel. The panels were produced and tested for tensile properties and constituent ratios to characterize the constructed panels. The ability of the panels to absorb energy from the projectiles was characterized through striking and residual velocity comparison, change in projectile kinetic energy, in addition to applying the data to ballistic models which predict the ballistic limit V_0 of the panel. The residual damage in the panel was characterized by delamination area and EMI shielding effectiveness. The findings from the experiments conducted to meet the objectives of this thesis will be reviewed.

5.1 Panel Development Findings

Based on the characterization work done on the constructed panels, it was determined that the combination of PMT-F6 resin, the HM-63 carbon fibers, and the Miralon CNT sheets integrated well. This was demonstrated through panel density imaging, component volume fraction determination, and tensile testing. C-Scans showed consistent panel density not varying more than 10%. Appropriate volume fractions of approximately 57 wt% fiber and 43 wt% resin were measured through an acid digestion procedure. These values are consistent with composite panel processing guidelines. The measurement of EMI shielding for the panels agreed with other works which demonstrated that the CNT sheets have good conductivity and shielding properties. The tensile testing results validated the modeling of the CNT sheet as a laminate ply as the trends followed predictions based on laminate theory.

The tensile tests show diminishing panel strength with the addition of CNT sheets. The ultimate tensile strength decreased on average 23 MPa and the elastic modulus decreased on average 2.5 GPa for each sheet of CNTs. The tensile specimens with four sheets appear to be an anomaly, showing minor improvement in these properties. After testing it was observed that the 0° and 90° plies were flipped in the ply stacking order which may have resulted in the difference in performance. In general, the trend of decreasing strength performance for 0-3 CNT sheets was as expected.

5.2 Ballistic findings

The ballistic testing simulated the impacts of high-speed debris with an aircraft. A half inch diameter steel ball bearing was fired at velocities in the hundreds of feet per second range. Three different velocities were used to construct ballistic models for the panels and to compare velocity and energy attenuation of the projectiles for the different panel configurations. Additionally V_{50} tests on three panels were conducted to try to expand the opportunity for ballistic influence from the CNT sheets to be identified. In all of these tests it was observed that only the panels with one or two CNT sheets showed some potential improvement in the energy absorbed by the composite panel. The amount of benefit was within 1 joule. This small of a difference over the range of one to four plies of CNT sheet material does not capture the ballistic potential found in CNTs at the molecular level. While CNTs have shown potential in ballistic improvement as a resin additive and in theoretical studies of CNT mats, the influence of sheet product in a thin carbon fiber composite did not demonstrate marked improvement.

5.3 Post Impact Findings

Work was conducted to identify if the CNTs sheets influenced the way ballistic impacts damaged the panels in terms of damage area and EMI shielding. C-Scans of the panels after impact did not reveal a significant difference in delamination areas due to the number of CNT sheets in the panel. It was noted that the shear plug effects in the panels were reduced as more CNT plies were included and the impact velocity was reduced. The damage mechanism appears to change from fiber shearing to more of a ripping and tearing action resulting in more frayed fibers remaining over the penetration site. This fact is probably related to the increased EMI shielding after impact observed for the panels with more CNT sheets. The higher impact velocities resulted in a greater reduction of EMI shielding performance than the lower velocity impacts. Shielding after impact differed by as much as 40 dB between the panels with no CNT sheets and the ones containing three or four CNT sheets. This finding confirms the suitability for CNTs sheets to be used in conductive applications where shielding damage resistance is desired.

5.4 Conclusions and Future Work

This thesis demonstrated that CNT sheets can be integrated well into carbon fiber laminates as a pre-preg material. It further explored the trade-space of CNT hybrid composites, showing that a couple plies of CNTs reduced the strength and modulus of the panel but the EMI shielding resilience and some additional ballistic energy absorption was gained. It also showed that while EMI shielding after damage increased with the number of CNT sheets, ballistic improvement was limited to the cases of only one or two sheets of the material being included in the carbon fiber panels.

Based on the findings of this research, potential future work is warranted. From

the ballistic testing at 180 ft/s it was seen that the panels with one or two sheets of CNTs significantly outperformed the panels with three or four sheets. Research as to why this occurred would be valuable. It may have to do with the bonding between the CNT sheets and the carbon fiber, or it may be a result of the shock wave interactions in the panel, among other theories. This research would improve understanding of the specific mechanisms which resulted in the unexpected results.

Along this vein, research with more sheets of CNTs would be valuable to further determine the shape of the trend for ballistic performance with increasing CNT sheets. Based on the experiments conducted in this thesis, the trend appears to be nonlinear due to the decreased ballistic performance in the panels with three and four CNT sheets. Knowing that around 100 plies of CNTs alone should provide significant ballistic protection, there must be some number of CNT sheets where performance increases again.

Another area of future work would be to see if a thicker host laminate would provide more detail of any ballistic strength offered by CNT sheet material. This would provide greater changes in impact and residual velocities, and allow for higher speed projectiles. The behavior of the CNT sheets in the panel may change or be easier to observe in these cases.

Future research regarding the CNT sheet location in the panel would also be of interest. While this thesis explored the thickness of the CNT sheet layer at the midplane, identifying location effects would be of value as demonstrated by Micheli *et al.* [27]. In Micheli's work the location of the CNT plies made a big difference in ballistic performance. Additionally, The influence of the CNT sheets on the impact induced compression and tension shock waves may be more evident if placed away from the midplane.

A final vector for future work would involve further evaluation of impact damage

on EMI shielding behavior. Low speed and high-speed impacts by different projectile shapes and sizes may provide additional insights into the influence of CNT sheets on signal attenuation losses due to impact damage. With this information, predictions could be made regarding shielding degradation for a given damage event.

These opportunities for future work indicate that continued research is necessary to develop understanding of CNT materials. Additional research will expand the spectrum of applications for CNTs. As developments of CNT products are made, more of the unique properties of the carbon nanotube molecule will be captured, increasing opportunities for their utilization in real-world applications.

Appendix A. Tensile Testing MATLAB Code

The MATLAB code used to predict panel properties using composite laminate theory was primarily developed by Lt O'Keefe, a fellow student at AFIT, for his work with the same carbon fiber and CNT sheet materials. Given a panel stacking sequence, it predicts the tensile and bending modulus among other properties for the panel. The code works very well with cross-ply laminates (composed of only 0/90 degree plies). It overestimated the strength of the quasi-isotropic panels used in this study as it doesn't fully account for the delamination tendencies introduced by the off axis plies. The code used was as follows:

```
%This code was developed by Lt J.C. O'Keefe for predicting the laminate
% properties of carbon fiber and CNT hybrid composites.


%% Clear Workspace
clc,clear,close all

%% Input Fiber and Matrix Values

%           - Material Matrix CNT = 1, CF = 0
MaterialMatrix = [0 0 0 0 0 0 0 0 NaN NaN NaN NaN;
            0 0 0 0 1 0 0 0 0 NaN NaN NaN;
            0 0 0 0 1 1 0 0 0 0 NaN NaN;
            0 0 0 0 1 1 1 0 0 0 0 NaN;
            0 0 0 0 1 1 1 1 0 0 0 0];
%           - Layer Fiber Orientation in Degrees
theta = [45 0 -45 90 90 -45 0 45 NaN NaN NaN NaN;
          45 0 -45 90 0 90 -45 0 45 NaN NaN NaN;
          45 0 -45 90 0 0 90 -45 0 45 NaN NaN;
          45 0 -45 90 0 90 0 90 -45 0 45 NaN;
          45 0 -45 90 0 90 90 0 90 -45 0 45];
for z = 1:length(MaterialMatrix(:,1))
    Material = MaterialMatrix(z,:);
    Material(find(isnan(Material))) = [];
    thetad = theta(z,:);
    thetad(isnan(thetad)) = [];
% Determine the Number of CNT Sheets and Number of Fiber sheets in Lami-
nate
F = 0;    %         - Pre allocate Number of Fibers
C = 0;    %         - Pre allocate Number of CNTs
for x = 1:length(Material);
        %       - NUmber Plies of CNT
    if Material(x) == 1;
```

```
        Cc = 1;
        C = C + Cc;
    else
        %       - Number Plies of Fiber
        Fc = 1;
        F = F + Fc;
    end
end

E1fiber = 441E9;       % (pa)      - Longitudinal Elastic Modulus of Fiber
(Data Sheet)
E1cnt = 27.5E9;         % (pa)      - Elastic Modulus of CNT (Data Sheet)
Em = 2.8E9;        % (pa)      - Elastic Modulus of Matrix (Self-
Deployable Joints for Ultra-Light Space Structures)
Gfiber = 114.8E9;       % (pa)      - Shear Modulus of the Fiber
Gcnt = 15E9;       % (pa)      - Shear Modulus of the CNT
Gm = 1.036E9;       % (pa)      - Shear Modulus of the Matrix
vf = 0.28;           %           - Poisson's Ratio of the Fiber
vc = 0.28;           %           - Poisson's Ratio of the CNT Sheet
vm = 0.33;          %           - Poisson's Ratio of the Matrix
df = 1830;          % (kg/m^3)  - Density of the Fiber (Data Sheet)
dc = 650;          % (kg/m^3)  - Density of the CNT (Data Sheet)
dm = 1199;          % (kg/m^3)  - Density of the Matrix (Data Sheet)
tf  = 0.00441*2.54E-2;        % (m)       - Lamina Thickness of CF (in to
m)
tc  = 0.00130*2.54E-2;        % (m)       - Lamina Thickness of CNT (in to
m)
L  = 8*2.54E-2;           % (m)       - Beam Length
b  = 1*2.54E-2;           % (m)       - Beam Width
Vf = ((F*tf)/(C*tc+F*tf))*0.65;         %           - Fiber Volume Frac-
tion
Vc = ((C*tc)/(C*tc+F*tf))*0.4;           %           - CNT Volume Fraction
Vm = 1-Vf-Vc;           %           - Matrix Volume Fraction
Vfm = .65;              %           - Fiber Volume Fraction for a fiber
```

```
lamina
Vcm = .4;                %           - CNT Volume Fraction for a CNT lamina
Vmf = 1-Vfm;             %           - Matrix Volume Fraction for a fiber
lamina
Vmc = 1-Vcm;              %           - Matrix Volume Fraction for a CNT
lamina
h = 0; %       - Pre allocate
tL = length(Material); %       - Pre allocate
    for x = 1:length(Material);
        if Material(x) == 1;
            t = tc;
        else
            t = tf;
        end
    tL(x) = t;         % (m)       - Laminate Thickness/Beam Height
    end
h = sum(tL);            %           - Laminate thickness
H = h/2;             %           - Half laminate thickness (Fig 5.2 Herako-
vich)
%%  Rule of Mixtures
% For Fiber
E1f = E1fiber*Vfm+Em*Vm; %(3.4 - Daniel - 3.23 )
E2f = 1/((Vfm/E1fiber)+((1-Vfm)/Em));    %(11.14 - Herakovich)
v12f = vf*Vfm+vm*Vmf; %(2.2.1 - Carlsson - 2.25c)
v23f = vf*Vfm+vm*(1-Vfm)*(1+vm-v12f*Em/E1fiber)/((1-vm^2)+vm*v12f*Em/
E1fiber);
G12f = Gm*(((1+Vfm)*Gfiber+Vmf*Gm)/(Vmf*Gfiber+(1+Vfm)*Gm)) %(3.6 - Daniel
- 3.53)
G13f = G12f; % (Due to 2 and 3 direction equivalent for matrix and fiber)
G23f = E2f/(2*(1+v23f));
Denf = df*Vf+dm*(1-Vfm);

% For CNT
E1c = E1cnt*Vcm+Em*Vmc; %(3.4 - Daniel - 3.23 )
```

```
E2c = E1c*0.94195;%1/((Vc/E1cnt)+((1-Vc)/Em)); %(11.14 - Herakovich)
(consider that cnt sheets are uniform in both directions E1c=E2c

v12c = vc*Vcm+vm*Vmc; %(2.2.1 - Carlsson - 2.25c)

v23c = vc*Vcm+vm*(1-Vcm)*(1+vm-v12c*Em/E1cnt)/((1-vm^2)+vm*v12c*Em/E1cnt);

G12c = Gcnt*(((1+Vmc)*Gm+Vcm*Gcnt)/(Vcm*Gm+(1+Vmc)*Gcnt));  %(3.6 - Daniel
- 3.53)

G13c = G12c; % (Due to 2 and 3 direction equivalent for matrix and fiber)

G23c = E2c/(2*(1+v23c));

Denc = dc*Vc+dm*(1-Vcm);


fprintf('Rule of Mixtures:l\n\n')

fprintf('For Carbon Fiber Lamina\n')

fprintf(' E1=%E\n E2=%E\n v12=%f\n v23=%f\n G12=%E\n G13=%E\n G23=%E\n\n',
[E1f E2f v12f v23f G12f G13f G23f])

fprintf('For Carbon Nanotube Lamina\n')

fprintf(' E1=%E\n E2=%E\n v12=%f\n v23=%f\n G12=%E\n G13=%E\n G23=%E\n\n',
[E1c E2c v12c v23c G12c G13c G23c])


%% Layer Data - For Fiber

thetad = thetad * pi / 180;     % Layer Fiber Orientation in Radians

NL = length(Material);         % Number of Layers


%% Compute Layer Height Data - For Fiber starting from the Centroid

midThicknessIdx=ceil(length(tL)/2); % Find the Center Thickness when odd/
even value


tLaminate=zeros(1,length(Material)+1); % Pre-Allocate tLaminate Matrix to
be 1+Number of Plies


% Even Number of Plies

if mod(length(tL)/2,1)== 0;

     tLaminate(midThicknessIdx+1)= 0; % Determine location of 0 ply

    fprintf('Even Number of Plies\n\n')

    % Create Thickness Matrix For Even Plies
```

```
        % Determine the thickness of each later based on position above
centriod
        a = length(tL)/2;
        ctr = 1;
        for x = a+1:length(tL);
            b = midThicknessIdx+ctr;
            tLaminate(x+1) = tLaminate(b)+tL(b);
            ctr = ctr+1;
        end
        % Determine the thickness of each later based on position below
centriod
        a = length(tL)/2;
        ctr = 0;
        for x = fliplr(2:a+1);
            b = midThicknessIdx-ctr;
            tLaminate(x-1) = tLaminate(b+1)-tL(b);
            ctr = ctr+1;
        end


% Odd Number of Plies
else
    tLaminate(midThicknessIdx)=-tL(midThicknessIdx)/2; % Calculating
poriton of middle layer below centroid
    tLaminate(midThicknessIdx+1)=tL(midThicknessIdx)/2; % Calculating
poriton of middle layer above centroid
    fprintf('Odd Number of Plies\n\n')
    % Create Thickness Matrix For Odd Plies
        [value,a]=max(tLaminate);
        ctr = 1;
        % Determine the thickness of each later based on position above
centriod
         for x = a:length(tL);
            b = midThicknessIdx+ctr;
            tLaminate(x+1) = tLaminate(b)+tL(b);
```

```
            ctr = ctr+1;
        end
        % Determine the thickness of each later based on position below
centriod
        [value,a] = min(tLaminate);
        ctr = 0;
        for x = fliplr(2:a);
            b = midThicknessIdx-ctr;
            tLaminate(x-1) = tLaminate(b)-tL(b-1);
            ctr = ctr+1;
        end
end

range = fliplr(tLaminate);  % Layer thickness decreases moving top to bot-
tom

%% Compute Qp Matrix - For Fiber
% Init A,B,D matrices
A=zeros(3,3);
B=zeros(3,3);
D=zeros(3,3);

% Q_ply and A,B,D Matrices
for x = 1:NL;
    if Material(x) == 1;
        E1 = E1c;
         E2 = E2c;
        v12 = v12c;
        G12 = G12c;
        Q11 = E1/(1-E2/E1*v12^2);
         Q22 = E2/E1*Q11;
        Q12 = v12*Q22;
        Q66 = G12;
```

```
        Q=[Q11 Q12 0;Q12 Q22 0;0 0 Q66];
    else
        E1 = E1f;
        E2 = E2f;
        v12 = v12f;
        G12 = G12f;
        Q11 = E1/(1-E2/E1*v12^2);
        Q22 = E2/E1*Q11;
        Q12 = v12*Q22;
        Q66 = G12;
        Q=[Q11 Q12 0;Q12 Q22 0;0 0 Q66];
    end
 m=cos(thetad(x));
 n=sin(thetad(x));
 T1=[m^2 n^2 2*m*n;n^2 m^2 -2*m*n;-m*n m*n m^2-n^2];
 T2=[m^2 n^2 m*n;n^2 m^2 -m*n;-2*m*n 2*m*n m^2-n^2];

 QP= T1^-1*Q*T2;
 A=A+QP*(range(x)-range(x+1));
 B=B+1/2*QP*(range(x)^2-range(x+1)^2);
 D=D+1/3*QP*(range(x)^3-range(x+1)^3);
end

%% Compute Global Laminate Properties - Bending - For Fiber
%          z
%    ______|______
%   |      |      |
% h |      |------|-----> y   (b = width)
%   |______________|          (h = height)
%          b
% X-axis is along the length of the beam
% Y-Axis is along the width of the beam
```

```
% Z-Axis is along the thickness of the beam

dstar= inv(D);                % Motavalli p101
Exb  = 12/h^3 *1/dstar(1,1); % Bending Stiffness - Motavalli p102
Eyb  = 12/h^3 *1/dstar(2,2); % Bending Stiffness - Motavalli p102
Gxyb = 12/h^3 *1/dstar(3,3); % Shear   Stiffness - Motavalli p104
fprintf('Using D Matrix for Fiber Values\n');
fprintf(' Exb=%E\n Eyb=%E\n Gxyb=%E\n\n',[Exb Eyb Gxyb]);

%% Compute Global Laminate Properties - Axial - For Fiber
astar=2*H*inv(A); %(5.80  - Herakovich)
%%
%
% $$e^{\pi i} + 1 = 0$$
%
% $$e^{\pi i} + 1 = 0$$
%
%
Ex=1/astar(1,1);  %(5.84  - Herakovich)
Ey=1/astar(2,2);  %(5.87  - Herakovich)
Vyx=-astar(1,2)/astar(1,1); % Motavalli p100
Vxy=-astar(1,2)/astar(1,1); % Motavalli p100
Gxy=1/astar(3,3); %(5.90  - Herakovich)
Gxz=Gxy;
Gyz=Ey/2*(1+v12);

fprintf('Using A Matrix for Mix\n')
fprintf(' Ex=%E\n Ey=%E\n Vxy=%f\n Vyx=%f\n Gxy=%E\n Gxz=%E\n Gyz=%
E\n\n\n',[Ex Ey Vxy Vyx Gxy Gxz Gyz])



Output(z,:) = [E1f E2f v12f v23f G12f G13f G23f E1c E2c v12c v23c G12c
G13c G23c Exb Eyb Gxyb Ex Ey Vxy Vyx Gxy Gxz Gyz];
```

```
end


Name = {'E1f' 'E2f' 'v12f' 'v23f' 'G12f' 'G13f' 'G23f' 'E1c' 'E2c' 'v12c'
'v23c' 'G12c' 'G13c' 'G23c' 'Exb' 'Eyb' 'Gxyb' 'Ex' 'Ey' 'Vxy' 'Vyx' 'Gxy'
'Gxz' 'Gyz'};
Output = [Name;num2cell(Output)];


%fprintf('Excel Results for Fiber Values\n')
%fprintf(' %E\n %E\n %E\n %E\n %E\n %E\n %E\n %E\n %E\n %f\n %f\n %E\n %
E\n %E\n\n\n',[E1 E2 v12 G12 Exb Eyb Gxyb Ex Ey Vxy Vyx Gxy Gxz Gyz])
```

Appendix B. Digital Image Correlation MATLAB Code

The following code was used to analyze the Phantom 12.1 high-speed camera video to determine the projectile velocities through digital image correlation. The code was adopted in large part from work by Captain Keane, a fellow student at AFIT.

```
%% This code  was developed by Capt Michael Keane and is used to ana-
lyze .avi files from a high speed camera in order to determine object ve-
locity through digital image correlation
close all
clear all
File='1.2_R2.avi';
vid=VideoReader(File);
n=vid.FrameRate*vid.Duration;
ftperpixel=0.001666;
fps=28000;%frames per second
scale=[0 2^vid.BitsPerPixel];
zz=26;%how many frames to jump
%% create average matrix for background subtraction
k=1;
i=1;
while i<=n
    imgavg(:,:,k)=double(readFrame(vid));
    i=i+1;
    k=k+1;
end
imginv=scale(2)-imgavg; %inverse the matrix
backgroundmean=mean(imginv,3); %average background

%%
%subtract average image from all frames

for l=1:n
    imgnew(:,:,l)=imginv(:,:,l)-backgroundmean(:,:);
    imgmax(l)=max(max(imgnew(:,:,l))); %build vector to help determine
where frag enters frame

end
 %%
```

```
 %determine when/where frag enters frame
 maxvalue=find(imgmax>mean(imgmax) & imgmax>10+max(imgmax(1:10)));
 %framestart=maxvalue(1);
 framestart=180;
 imgnew(:,:,1:framestart-1)=[]; % psy attention here!
 velsample=5;
 b=1;
for b=1:velsample+zz
[y1,x1] = find(imgnew(:,:,b) == max(max(imgnew(:,:,b))));
y(b)=y1(1);
x(b)=x1(1);
end

%create "area of interest"
x1=1;
x2=190;
y1=min(y);
y2=max(y);

y2final=round((y1+y2)/2+60);%bottom frame
y1final=round((y1+y2)/2-40); %top frame
%%

framesize=[x1, y1final, x2, y2final]; %[top left corner coords],[bottom
right coords]
%%
%image correlation and then finding peak of the difference of the two
%images to find the overall change in position. relate the peak location
to
%area of inerest to find the change in to calculate x and y velocity

for i=1:velsample
```

```
    img1=imgnew(framesize(2):framesize(4),framesize(1):framesize(3),i); %
span given coords
    img2=imgnew(framesize(2):framesize(4),framesize(1):framesize
(3),i+zz);%span given coords %%this is how to jump frames
    figure
    imshowpair(img1,img2)
   pause(1)
   close
   correlation=normxcorr2(img1,img2);
%    figure
%    surf(correlation), shading flat
%    pause(1)
%    close

[peakcoords,maxvaluepeak]=max(abs(correlation(:)));%find coordates of peak

[ypeakcoord,xpeakcoord]=ind2sub(size(correlation),maxvaluepeak(1));

output(i,:)=mydftregistration(fft2(img1),fft2(img2),20);

offset2(i,1) = output(i,4);
offset2(i,2) = output(i,3);
offset(i,1)=(framesize(3)-framesize(1))-xpeakcoord; %xoffset of peak
coords to frame coords
offset(i,2)=(framesize(4)-framesize(2))-ypeakcoord;

end

 %velo city=offset.*((spacing/pixelcal)*(1/(1/11423)));
  velocity=offset.*fps/zz*ftperpixel;%pix*1/sec*ft/px
  velocityfft=offset2.*fps/zz*ftperpixel;
  if mean(velocity(:,1))<0
      velocity1(:,1)=velocity(find(velocity(:,1)>=mean(velocity(:,1)) &
```

```
velocity(:,1)>0));
      velocity1(:,2)=velocity(find(velocity(:,1)>=100+mean(velocity(:,1))
& velocity(:,1)>0),2);
  else

    velocity1(:,1)=velocity(find(velocity(:,1)<=100+mean(velocity(:,1)) &
velocity(:,1)>0));

    velocity1(:,2)=velocity(find(velocity(:,1)<=100+mean(velocity(:,1)) &
velocity(:,1)>0),2);
  end
  velocitymag=(velocity1(:,1).^2+velocity1(:,2).^2).^.5;
  Velocitymagaverage=mean(velocitymag)
  VelocityFFTavg=mean(velocityfft(:,1))
  error1=(offset+1).*fps/zz*ftperpixel-offset.*fps/zz*ftperpixel;
  errormag=sqrt(error1(:,1).^2+error1(:,2).^2);
  errormean=mean(errormag)
```

Appendix C. Jonas-Lambert Method MATLAB Code

The following code was written to conduct the least squares fit of the striking and residual velocity pairs input by the user. It outputs the values of alpha, p, and the limit velocity estimate, V_0.

```
% Jonas-Lambert Estimate of Ballistic Limit from Striking and Residual Velocity data

%Velocity Pair Data Sets
xdata=[649.744,347.879,181.364]; %Striking Velocity
ydata=[634.667,320.833,113.344]; %Residual Velocity

%Jonas-Lambert Equation
jltheory=@(x,xdata)x(1)*(xdata.^(x(2))-x(3).^(x(2))).^(1/x(2));
lb=[0,1,0]; %Lower bounds for alpha, p, and V_0.
ub=[1,20,max(xdata)]; %Upper bounds
xo=[.9,2,150]; %Initial Guess for alpha, p, and V_0.

%Least Squares Curve Fit
[x,resnorm]=lsqcurvefit(jltheory,xo,xdata,ydata,lb,ub);

display(x)
display(resnorm)
```

Appendix D. Additional Images

4.1 Tensile Specimens Images

Presented here are the images of all 15 tensile specimens.

Figure 63. Tensile testing specimens from panel 1.1

Figure 64. Tensile testing specimens from panel 2.1

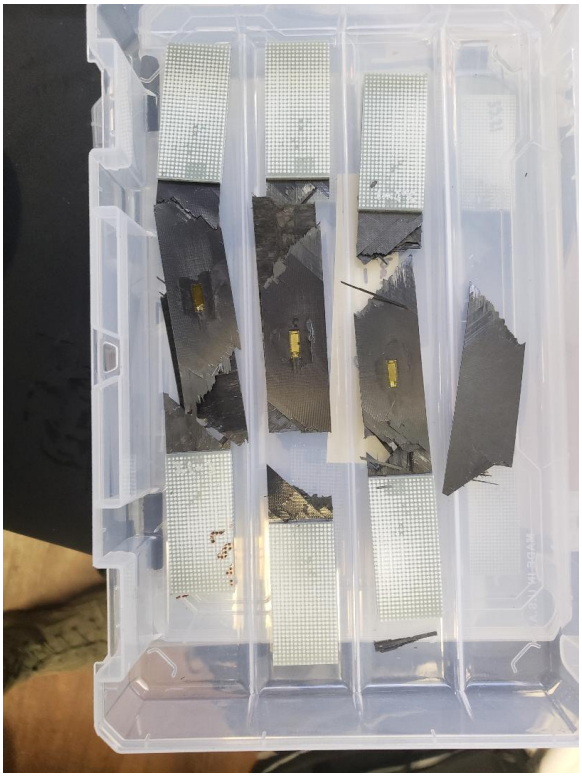

Figure 65. Tensile testing specimens from panel 3.1

Figure 66. Tensile testing specimens from panel 4.1

Figure 67. Tensile testing specimens from panel 5.1

4.2 V50 Panel Images

Presented here are the images of the back face delaminations of the panels used for V_{50} testing.

Figure 68. Back-face delaminations from V50 testing of panel 1.2

Figure 69. Back-face delaminations from V50 testing of panel 1.2

Figure 70. Back-face delaminations from V50 testing of panel 1.2

Bibliography

1. *The Resistance of Various Non-Metalic Materials To Perforation by Steel Fragments*. Technical Report, John Hopkins University, 1963.

2. ASTM International, "ASTM D3039: Standard Test Method for Tensile Properties of Polymer Matrix Composite Materials," 2017.

3. Baig, Zahid Iqbal. *Effects of ballistic impact damage on thin and thick composites*. PhD dissertation, Iowa State University, 1997.

4. Billon, H H. *A New Method for Calculating the Critical Penetration Velocity (V 0)*. Technical Report, Victoria: Austrailian Government Department of Defence: Defence Science and Technology Organization, 2007.

5. Boysen, Earl and Nancy Boysen. *Nanotechnology For Dummies* (2 Edition). Indianapolis: Wiley Publishing Inc., 2011.

6. Campbell, F. C. *Manufacturing Processes for Advanced Composites*. Oxford: Elsevier Advanced Technology, 2004.

7. Cann, Roberto J, et al. *Processing and Characterization of Carbon Nanotube Composites*. Technical Report, Hampton: NASA Langley Research Center, 2014.

8. Cheng, Qunfeng, et al. "High Mechanical Performance Composite Conductor: Multi-Walled Carbon Nanotube Sheet / Bismaleimide Composites," *Advanced Functional Materials*, *19*(20):3219–3225 (2009).

9. Citizen Armor, "Product Guide," 2016.

10. Diamond Age Corp., "Polymer Composite Armor," 2018.

11. DryWired, "DryWired Introduces NanoArmor at IACP 2014," 2014.

12. Ellis, Roger L. *Ballistic Impact Resistance Of Graphite Epoxt Composites With Shape Memory Alloy And Extended Chain Polyethylene Specra Hybrid Components*. PhD dissertation, Virginia Polytechnic Institute and State University, 1996.

13. Estrada, H., et al. "Electrical properties of fiber and carbon nanotube reinforced polymer composites." *Materials Characterization VI*. 309–320. Southampton: WIT Transactions on Engineering Sciences, 2013.

14. Fierro, John, "Amendment II Release RynoHide-The World's First Carbon Nanotube Armor for Bulletproof Vests and Other Military, Law Enforcement, and Personal Protective Tactical Gear," 2012.

15. Gina Peschel, "Carbon-Carbon Bonds: Hybridization," 2011.

16. Grujicic, Mica, et al. "Ballistic-performance optimization of a hybrid carbon-nanotube/E-glass reinforced poly-vinyl-ester-epoxy-matrix composite armor," *Journal of Materials Science* (2007).

17. Harvey, Stefanie E. "Carbon as Conductor: A Pragmatic View." *61st International Wire and Cable Symposium*. 558–562. Menlo Park: IWCS, Inc., 2012.

18. Henkel Corporation Aerospace, "LOCTITE EA 9394 AERO Epoxy Paste Adhesive (KNOWN AS Hysol EA 9394)," 2013.

19. Iijima, Sumio. "Helical microtubules of graphitic carbon," *Nature*, *354*(6348):56–58 (1991).

20. Inman, Mason, "Superstrong Carbon-Nanotube Fibers," 2007.

21. Karl Burkhart, "Making Paper That Can Stop Bullets," 2016.

22. Kinsler, R and J Collins. "Comparison of V 50 Shot Placement on Final Outcome." *Personal Armour Systems Symposium*. 17–20. Nuremburg: US Army Research Lab, 2012.

23. Lambert, J. P. and G. H. Jonas. *Towards Standardization in Terminal Ballistics Testing: Velocity Representation*. Technical Report, Aberdeen Proving Ground: USA Ballistic Research Laboratory, 1976.

24. Leghorn, Nick, "Gear Review: AR500 Armor Carbon Nanotube Soft Armor IIIA," 2013.

25. Lekawa-Raus, Agnieszka, et al. "Electrical properties of carbon nanotube based fibers and their future use in electrical wiring," *Advanced Functional Materials* (2014).

26. Loikkanen, Matti, et al. "Simulation of Ballistic Impact on Composite Panels." *10th International LS-DYNA ® Users Conference*, edited by Wayne L. Mindle. 9–1. Dearborn: Livermore Software Software Corporation, 2008.

27. Micheli, D., et al. "Ballistic and electromagnetic shielding behaviour of multifunctional Kevlar fiber reinforced epoxy composites modified by carbon nanotubes," *Carbon*, *104*:141–156 (8 2016).

28. Mylvaganam, Kausala and L C Zhang. "Ballistic resistance capacity of carbon nanotubes," *Nanotechnology*, *18* (2007).

29. Nanocomp Technologies Inc., "About Nanocomp," 2016.

30. Nanocomp Technologies Inc., "Nanotechnology," 2016.

31. Nanogloss, "The History of Carbon Nanotubes - Who Invented the Nanotube?," 2009.

32. Olster, Elliot F and Howard A Woodbury. "EVALUATION OF BALLISTIC DAMAGE RESISTANCE AID FAILURE MECHANISMS OF COMPOSITE MATERIALS,"

33. Oxford Dictionaries, "Definition of van der Waals forces in English," 2018.

34. Park, J. G., et al. "High Thermal Conductivity of Carbon Nanotube Sheet/Epoxy Composite." *18th International Conference On Composite Materials*. Jeju Island: International Commitee on Composite Materials, 2011.

35. Pineda, E, et al. "Ballistic Properties of Zylon for Application to Firearm Projectile Protection," (2003).

36. Randjbaran, Elias, et al. "The Effects of Stacking Sequence Layers of Hybrid Composite Materials in Energy Absorption under the High Velocity Ballistic Impact Conditions: An Experimental Investigation," *Journal of Material Science & Engineering*, *2*(4) (2013).

37. Resnyansky, A D and G Katselis. *Ballistic and Material Testing Procedures and Test Results for Composite Samples for the TIGER Helicopter Vulnerability Project*. Technical Report, Edinburgh: DSTO Systems Sciences Laboratory d, 2004.

38. St. Clair, Bartmoss. "Nanotechnology And Predicting The Future (Review of The Current State of Nanotechnology And Making Future Predictions With A Discussion of Forecasting Methods)," *The Amateur Academic*, (1):10 (2016).

39. Stojadinović, Saa, et al. "Prediction of flyrock launch velocity using artificial neural networks," *Neural Computing and Applications* (2016).

40. Tim Bowler. "Carbon fibre planes: Lighter and stronger by design," *BBC News* (2014).

41. U. S. Department of Defense, "MIL-STD-662F: V50 Ballistic Test For Armor," 1997.

REPORT DOCUMENTATION PAGE

Form Approved
OMB No. 0704–0188

1. REPORT DATE *(DD–MM–YYYY)*	2. REPORT TYPE	3. DATES COVERED *(From — To)*
21–03–2019	Master's Thesis	Sept 2016 — March 2019

4. TITLE AND SUBTITLE

BALLISTIC EVALUATION OF CARBON NANOTUBE SHEET MATERIAL IN MULTIFUNCTIONAL APPLICATIONS

5a. CONTRACT NUMBER

5b. GRANT NUMBER

5c. PROGRAM ELEMENT NUMBER

6. AUTHOR(S)

Keilbarth, Casey M., 1LT

5d. PROJECT NUMBER

5e. TASK NUMBER

5f. WORK UNIT NUMBER

7. PERFORMING ORGANIZATION NAME(S) AND ADDRESS(ES)

Air Force Institute of Technology
Graduate School of Engineering and Management (AFIT/EN)
2950 Hobson Way
WPAFB OH 45433-7765

8. PERFORMING ORGANIZATION REPORT NUMBER

AFIT-ENY-MS-19-M-224

9. SPONSORING / MONITORING AGENCY NAME(S) AND ADDRESS(ES)

Air Force Research Lab
2941 Hobson Way
WPAFB OH 45433-7750
DSN 255-9070, COMM 937-255-9070

10. SPONSOR/MONITOR'S ACRONYM(S)

11. SPONSOR/MONITOR'S REPORT NUMBER(S)

12. DISTRIBUTION / AVAILABILITY STATEMENT

DISTRIBUTION STATEMENT A:
APPROVED FOR PUBLIC RELEASE; DISTRIBUTION UNLIMITED.

13. SUPPLEMENTARY NOTES

14. ABSTRACT

This thesis sought to determine if the addition of commercially produced CNT sheets to thin carbon fiber panels improved the ballistic properties of the panel. The difference between 0 and 4 CNT sheets was studied. The hypothesis was that integrating CNT sheets into the laminate would increase the projectile energy absorbed by the panel and reduce the impact damage to the panel. Damage to the panel was assessed through delamination area and EMI shielding degradation. Projectile energy absorption was measured through residual velocity measurement and ballistic limit modeling. A gas gun shooting half inch steel ball bearings was used to model high speed debris impact on the panel. This study found that the addition of one or two CNT sheets provided a marginal increase of up to 0.7 joules of projectile energy reduction by the panel. In general it was not found that the CNT sheets significantly contributed to the ability of the panel to stop a projectile at the quantities studied. It was found that with four CNT sheets in the panel, the EMI shielding after impact at 350 ft/s was improved by as much as 40 dB over the panel with no CNT sheets.

15. SUBJECT TERMS

Carbon nanotube sheet material, Ballistic testing, Electromagnetic interference shielding

16. SECURITY CLASSIFICATION OF:			17. LIMITATION OF ABSTRACT	18. NUMBER OF PAGES	19a. NAME OF RESPONSIBLE PERSON
a. REPORT	b. ABSTRACT	c. THIS PAGE			Maj Andrew Lingenfelter, AFIT/ENY
U	U	U	U	143	**19b. TELEPHONE NUMBER** *(include area code)* (937) 255-3636 x6234; andrew.lingenfelter@afit.edu